W/O Emulsions:
Formulation, Characterization and Destabilization

Von der Fakultät für Umweltwissenschaften und Verfahrenstechnik
der Brandenburgischen Technischen Universität Cottbus
zur Erlangung des akademischen Grades eines Doktor-Ingenieurs
genehmigte Dissertation

vorgelegt von
MSc.-Ingenieur
Carlos Javier Morales Henríquez

aus Caracas, Venezuela

Gutachter: Prof. Dr.-Ing. Ulrich Riebel
Gutachter: Prof. Dr.-Ing. Peter Ay

Tag der mündlichen Prüfung: 23. Februar 2009

Resume

This work refers to water in oil emulsion formulation, characterization and destabilization. These topics were studied in order to generate knowledge that could be used as a base for the treatment of highly stable *W/O* emulsions. Two types of emulsions were studied: synthetics and naturals; the last ones come from the crude oil production process of different Venezuelan regions.

In this book, chapters 1 and 2 give an introduction to the research area and the theoretical background related with it, respectively.

In chapter 3, the effect of surfactant content, water content, *HLB* value, alcohol content, salinity, emulsion volume, and mixing properties on water in paraffin emulsion stability was studied. Emulsion stability was determined by the amount of water and oil separated after 30 days. After finishing the variables scans, the most appropriate formulation conditions were established, and a formulation protocol was defined. Emulsion density and apparent viscosity were measured, and viscosity was modeled by the Power Law considering both shear rate and water content.

Chapter 4 deals with emulsion characterization. Although some particle sizing devices have gained a lot of popularity, none of them is able to distinguish between drops and solids, and few are able to handle viscous oily samples. In this chapter the use of optical microscopy, enhanced by the use of digital video capabilities and image analysis software, to characterize oil production wastes is discussed.

Several thousands of particles were counted and their projected areas were measured. A discussion is given about the different corrections required in order to extract the most reliable information from the image, overcoming some of the drawbacks of this kind of measurements.

A new technique the so-called cross-linked method was developed to offer unique features like the determination of the fraction of droplets that exist in the form of non-coalesced agglomerates. When cross-linked with the results obtained by standard *ASTM* procedures, it is calculated the amount of disperse phase that exists in the form of submicron droplets or large free water drops that are usually not sampled for microscope slides.

Chapters 5 and 6 deal with emulsion destabilization. In chapter 5, a variety of materials were used to investigate their applicability as so-called collector materials, to improve the destabilization and separation of water in oil emulsions stabilized by a non-ionic surfactant. The emulsion destabilization degree was determined by the amount of water and oil separated after centrifugation. The recovery of both phases was strongly dependent on the nature of the

material, material/emulsion ratio, particle size, and contact time. By varying conditions, it was possible to increase the water separation from 0 (without material) up to 95%.

In chapter 6, the effect of a *DC* electric field on *W/O* emulsions was evaluated. Electric field magnitude, water content, cell size, electrode design, and electrode coating were considered. Emulsion destabilization was improved by combining electric field, collector material and centrifugation. A comparison is given about the emulsion characteristics in terms of microscopy between both, synthetic and crude oil emulsions.

Contents

Symbols list

Arabic symbols

A	consistency index (equation 2-3)	[cP.s^{B-1}]
A	area	[m^2]
B	Power Law index	[-]
Cc	cell characteristic constant	[m]
Cm	material content	[% w/w]
CMC	critical micelle concentration	[g/L]
Co	Octanol content	[% v/v]
Cs	surfactant content	[% v/v]
E	electric field strength	[V/m]
e	emulsion	[-]
ECN	equivalent carbon numbers	[-]
fw	water content	[-]
HLB	hydrophilic-lipophilic balance	[-]
k	emulsion conductivity	[S/m]
k_0	external/continuous phase conductivity	[S/m]
L	length	[m]
Le	distance between electrodes	[m]
m	material	[-]
N	number	[-]
p	paraffin	[-]
q_r	frequency distribution curve	[µm^{-1}]
Q_r	cumulative distribution curve	[-]
r	droplet radius	[µm]
Rp	paraffin recovery	[% v/v]
Rw	water recovery	[% v/v]
Sa	salinity	[g/dL]
Se	electrode surface area	[m^2]
SOW	surfactant-oil-water system	[-]
T	temperature	[°C]
tc	centrifugation time	[s]

t_E	Electric field time	[s]
tm	mixing time	[s]
V	volume	[m^3]
v	voltage	[V]
vc	centrifugation velocity	[s^{-1}]
V_e	emulsion volume	[m^3]
vm	mixing velocity	[s^{-1}]
V_p	paraffin volume	[m^3]
Vr	residual emulsion volume	[m^3]
V_s	separated volume	[m^3]
V_w	water volume	[m^3]
w	water	[-]
x	equivalent diameter	[m]
$\overline{x_{1,r}}$	weighted mean diameter	[m]
x_{50}	diameter, median value	[m]
x_{max}	diameter, maximum value	[m]
x_{min}	diameter, minimum value	[m]
x_{mod}	diameter, modal value	[m]
x_s	equivalent surface diameter	[m]
x_v	equivalent volume diameter	[m]

Greek symbols

γ	velocity gradient	[s^{-1}]
η	apparent viscosity	[Pa.s]
μ	viscosity	[Pa.s]
μ_c	continuous phase viscosity	[Pa.s]
τ_{yx}	shear stress	[N/m^2]

1 Introduction

During the production period of a crude oil well, the water content tends to rise. The water has to be separated, because the crude oil as selling product must not have more than 1% of water and sediments. The presence of water is not only unwanted due to its impure worthless nature, but also because it contents inorganic salts, which could provoke corrosion and obstruction damages to the refining and transport installations.

The residue of the crude oil production is a waste material composed of crude, water and sediments forming different phases including, beside the pure phases, water in oil and oil in water emulsions. This waste is normally placed in open air pools and in direct contact with the soil. These pools are known as production pitch, or macro pitch, if they have a superficial area greater than 10 hectares. With the time, the oil in water emulsions, as well as the water in oil emulsions, becomes very stable systems.

Venezuela has about 12 thousand production pitches, which hold almost 9 million barrels of oxidized crude oil, 70 million barrels of water and 50 million barrels of sediments and sludge.

In the near future new environmental laws and regulations will be in force. Therefore Venezuela has the legal compromise of establishing and applying what is required for the cleaning and recovering of the production pitches. Figure 1-1 shows several images which describe how deep the environmental problem is.

Figure 1-1. Appearance of Some Production Pitches in Venezuela

In the late years the government and the Venezuelan oil industry, "Petróleos de Venezuela" (PDVSA), have begun with a sanitation process, Figure 1-2 is a graphic example of it. The production pitches with a major content of water have been successful treated. The water was reused as service water in the oil production process, the soils could be recovered through Bioremediation (see Figure 1-3) and the sludge have been put back to the construction industry as raw material.

Figure 1-2. Sanitation Process in the Production Pitch of Puerto La Cruz Refinery

Figure 1-3. Bioremediation of a Production Pitch Soil

However, the sanitation of production pitches with crude oil as the main compound is still a challenge hard to overcome. The national and international service companies have failed when trying to recover the crude oil, because of the very different characteristics that every pitch has. Therefore, the focus on only one technique for the sanitation of all the pitches is not possible, because the pitches characteristics are so diverse that they even change inside one pitch depending on the depth.

In November 2002, in the Chemical Engineering School at the Central University of Venezuela, where I am part of the teaching staff and work as researcher, a big general meeting was realized with all the members of the school. The goal of the meeting was to define a general investigation line where all the laboratories, and existing research groups,

could participate. This new investigation line should respond the country's needs and at the same time should be the support to build a pioneer Chemical Engineering School. That is how the techniques for the proper handling of multiphase systems became the guide line of the institution and the base for the strategic plan designed afterwards. At that time the university realized the problem with the production pitches and decided to participate actively in the search for a solution. This research work comes as an answer to an urgent need of the Venezuelan oil industry: recovery and minimization of waste products from the production process.

For a proper treatment of an oil waste is necessary first a deep study of the dispersion. The proper characterization is the base to choose the right technology necessary for its separation. Then, the "what to separate" should be fixed first to be able to define the "how to separate".

In chapter 4 of this investigation, the characterization of the dispersions based on the optical microscopy is treated, as well as the combination of images analysis with the *ASTM* standard processes. The purpose of that section is to develop the digital image analysis method, taking advantage of the available image analysis program to describe with more detail the characteristics of the dispersion. This description allows determining the particle size distribution of drops and solids, as well as the quantity of water and sediments in the oil waste material. In chapter 6 these tools are once again used for the characterization of synthetic emulsions of water in paraffin.

To be able basic knowledge helpful in the solution of the pitches problem can be gained by going on deep on emulsion stability under controlled conditions. Therefore it is better to use emulsion models, which have simpler physical-chemical composition.

Chapter 3 refers to the formulation of emulsions and includes the following objectives: to determine which variables have a high impact on the stability of the water in paraffin emulsions, to find out the experimental conditions which optimize the emulsions stability and to develop a protocol to prepare stable and reproducible emulsions of water in paraffin.

To separate an emulsion implicates first to crack it or break it. For this, heat, centrifugation and electric fields can be used among other techniques. After breaking an emulsion the physical separation of the phases has to be done. Chapters 5 and 6 cover this topic and their primary objectives were: to evaluate some of the destabilization/separation techniques in order to find out the most convenient conditions for the emulsion treatment and to use the microscopy technique to characterize the coalescence phenomena comparing the achieved results with both emulsion models and crude oil emulsions.

This doctoral work was developed in the Mechanical Separation Department of the Technical University of Cottbus in cooperation with the Central University of Venezuela. It had the

financial support of the *DAAD* and two projects sponsored by the Council of Humanistic and Scientific Development (*CDCH*) from the Venezuelan universities: "*Electrostatic Destabilization and Separation of Stable Emulsions*" Project CDCH PI 08-00-6129-2005 and "*Study of the Coalescence Ways Effect in the Kinetic of the Electro-Separation in Stable Water in Oil Emulsions"* Project CDCH PI 08-00-6127-2005. The financing allowed the development of the basic infrastructure in some of the laboratories in the Chemical Engineering School at the Central University of Venezuela.

At present, the Central University of Venezuela takes part in a macro project with four more Venezuelan universities and financed by the Venezuelan Government, through the Ministry of Science and Technology. It is titled *"Development, Validation and Transfer of New Technologies for the Environmental Sanitation of Wastes from the Oil Production Activity"* and its subproject 2 titled *"Efficient Separation of Crude Oil, Water and Solids in the Oil Phase from the Production Pitches"* is conducted by the Chairman of the Chemical Engineering School Professor José Sorrentino.

The subproject 2 was just signed this year to be executed within three years with budget of 1,200,000 Euros. It suggests a systematic study which aims to understand the fundamental phenomena involves in the emulsion destabilization. Additionally, it proposes to study the acceleration of the coalescence using combined technologies to increase the separation efficiency. Thereby the applicability and continuity of the concepts developed in this doctoral work could be assured.

2 Theoretical Background

2.1 Emulsion Formulation

Macro emulsions, or simply emulsions, are liquid-in-liquid dispersions, with drop size ranging typically from 1 to 100 μm (that can be extended in special cases down to 0.5 μm or up to 500 μm). In this range, the drops are in general large enough to settle under gravity influence. Emulsions are thermodynamically unstable systems because their decay results in a decrease in free energy. However, the kinetic mechanisms involved in emulsion breaking can be so slow that the corresponding emulsion may be considered as (meta) stable as far as the application is concerned (Salager, 2000).

There are several types of emulsions depending on how the oil and water phases are located in the disperse system. The terms oil and water are used in a broad sense, i. e., the less polar and more polar of the two immiscible phases. Figure 2-1 indicates the different types of emulsions. Simple emulsions are labeled as oil-in-water (*O/W*) when they exhibit oil drops dispersed in an aqueous phase (Fig. 2-1a), or water-in-oil (*W/O*) if the opposite occurs (Fig. 2-1b), while multiple or double emulsions are symbolized either by $W_1/O/W_2$ (Fig. 2-1c) or $O_1/W/O_2$ (Fig. 2-1d). Here, *W1* (respectively O_1) and W_2 (respectively O_2) indicate the most external phase and the most internal one. Note that phases with subscript 1 and 2 may be identical or different. Biemulsions are emulsions containing two different internal phase droplets, either of the same nature but different size or of different nature, whatever the size is (Fig. 2-1e) (Salager, 2000).

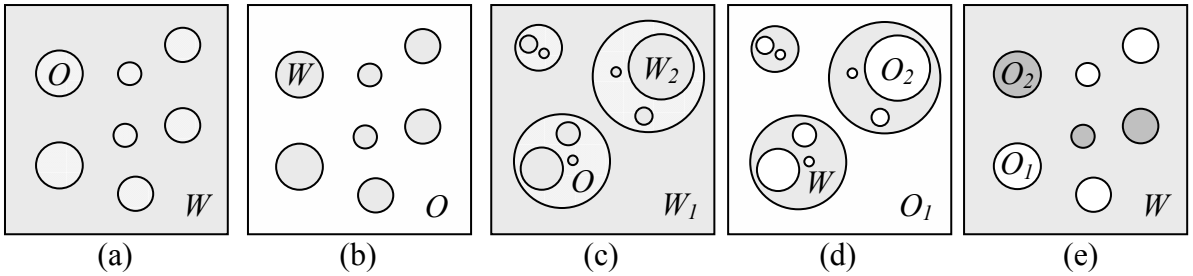

Figure 2-1. Types of Emulsions

(a) Normal or Simple Oil in Water *O/W*, (b) Normal or Simple Water in Oil *W/O*, (c) Multiple or Double $W_1/O/W_2$, (d) Multiple or Double $O_1/W/O_2$, (e) Biemulsion $O_1 + O_2/W$

Drop coalescence stability is provided by the presence of a small amount of a third component, the so-called emulsifier, which is in general a surface-active-agent or surfactant, that adsorbs at the drop interface and produces some interdrop repulsion depending on a variety of static and dynamic phenomena.

Surfactant molecules contain both a polar and a no polar group. Hence, they will not be completely at ease either in an aqueous phase or in an organic phase, since one of their groups would not get the right match with the solvent, be it aqueous or organic. For such reason, surfactant molecules exhibit a very peculiar behavior, which is inherent to their structure.

The polar group contains heteroatoms such as O, S, N, and P, as part of some functional group, i.e., carboxylate, sulfonate, sulfate, phosphate, etc. Nonionic polar groups such as -OH or -O- (ether link) are not highly polar, and thus to form a proper polar group, polyalcohol or polyether is required. The non-polar group is a hydrocarbon radical of the alkyl or alkyl-aryl kind, with typically 12 to 20 carbon atoms (Salager, 1994).

2.1.1 Types of Surfactants

In general, surfactants are classified, according to their behavior in aqueous solution, as ionic or nonionic surfactants. Those which dissociate into a surfactant negative ion (anion) and a metallic cation, the so-called counter ion, are labeled anionic surfactants. Some surfactants of this kind are Carboxylic acids and their Na or K salts, alkyl benzene sulfonates, dodecyl or lauryl sulfate, xanthates, which represent more than 50 % of the total surfactant production.

The second class in importance (40 %) gathers the nonionic surfactants, i.e., those which are not dissociated in aqueous solution. In most of these surfactants the polar group is produced by the polycondensation of ethylene oxide that results in a polyether chain. The most common surfactants are the ethoxylated alcohols, alkylphenols, acids, and esters. Nonionic surfactants are much less sensitive to electrolytes than anionic surfactants. Figure 2-2 shows the chemical structure of the nonionic surfactants Monooleate Sorbitan (top) and Nonylphenol Polyglycol Ether (4 EO) (bottom). Anionic and nonionic surfactants production reaches beyond 90 % of the total, and the remaining surfactants, e.g., cationic, amphoteric and polymeric ones, are only used for very special applications when cost is not a sensitive issue, such as in cosmetics and body care products.

In emulsion formulation, two limits for the surfactant concentration are observed. Below a concentration of the order of some thousands of ppm (0.1%), the amount of emulsifier is not sufficient to stabilize the emulsion. On the other hand, above 5% the surfactant concentration does not improve the emulsion stability. In practical applications a surfactant concentration

around 0.2-3% is used. For cost and efficiency reasons, a mixture of several surfactants is generally used as emulsifier.

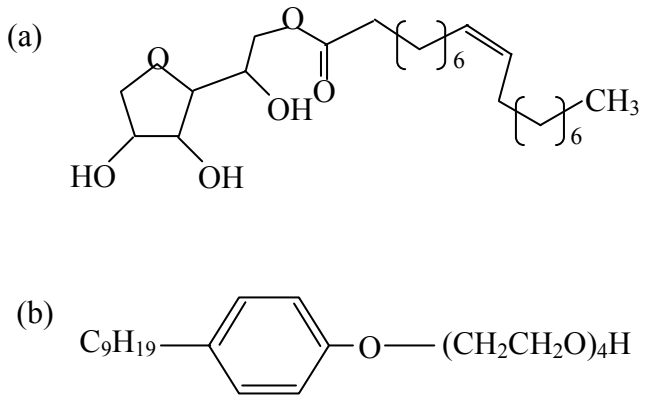

Figure 2-2. Chemical Structure of Surfactants

(a) Sorbitan Monooleate (Span 80®) and (b) Nonylphenol Polyglycol Ether (4 EO) (Arkopal N 040®)

2.1.2 Behavior of Surfactant-Water-Oil Systems

Surfactants are molecules which possess two fundamental properties. They tend to locate preferentially at the interface between a polar and a no polar phase. The phenomenon according to which a molecule comes from the bulk of a solution to place itself at the interface with some specific orientation is called adsorption (from Figure 2-3 to Figure 2-3d), and it is characteristic of the amphiphilic molecules. The adsorption is a spontaneous phenomenon, which is driven by a reduction of energy when the surfactant lipophobic group is removed from the solvent, and when one or both affinities are satisfied respectively at a surface or at an interface.

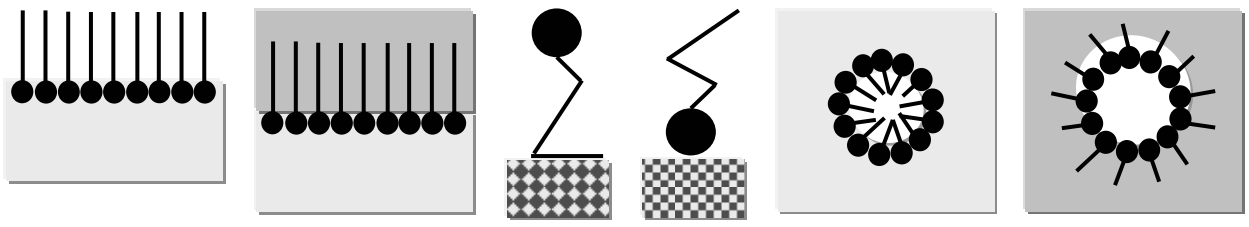

(a) (b) (c) (d) (e) (f)

Figure 2-3. Surfactants Properties

(a) Adsorption at the Water Surface, (b) Adsorption at the Water-Oil Interface, (c) Adsorption at a Nonpolar Solid Surface, (d) Adsorption at a Polar Solid Surface , (e) Spherical Micelle in Aqueous Phase, (f) Spherical Inverse Micelle in Oily Phase

At a liquid-solid interface (see Figures 2-3c and 2-3d), the relative polarity of the solid with respect to the liquid would define whether the surfactant adsorbs by the head or by the tail. When a solid is involved, other driving forces such as electrostatic attraction can play a role.

Water contains both H^+ and OH^- ions as well as other anions and cations which are likely to adsorb at a solid interface; the relative adsorption of anions and cations depends on both, the solid nature and the ionic concentrations, i.e., the pH. As a matter of fact solid surfaces are always charged when they are in contact with water, unless a very specific situation, the so-called point of zero charge or isoelectric point, is attained (Salager, 1994).

Adsorption is a dynamic phenomenon which is opposed by desorption, i.e., the transfer of a surfactant molecule to a bulk phase. Adsorption and desorption steps are often very fast; as a consequence an adsorption-desorption equilibrium is reached after some time, depending on the surfactant concentration in the bulk phase.

Since the surfactant molecule has a lower free energy when it is adsorbed at the interface than in the solvent bulk phase, the equilibrium tends toward the adsorbed state. In fact, the interface is covered very rapidly by a monolayer of surfactant molecules, where the molecules are arranged in a specific pattern which depends upon structural and geometrical characteristics. Typically a surfactant molecule requires about 30 - 50 $Å^2$ at the interface. When a monolayer is formed, everything happens as if the interface were coated with a thin layer of a new material.

The second fundamental property of surfactant molecules is their capability of self-association in aqueous or non aqueous solutions (see Figure 2-3 (e) and (f)). When the surfactant concentration increases in the aqueous phase, the surfactant molecules first saturate the interface, and then accumulate in the solution. At some point, the surfactant molecules start aggregating into the so-called micelles, a self-association structure in which the hydrophobic tail is removed from the aqueous environment.

The concentration at which the first micelles are formed is called Critical Micelle Concentration (*CMC*) (Salager, 1993). At this concentration, the factors which favor micelle formation start dominating the effects which oppose it. The *CMC* can be determined experimentally by plotting surface tension versus log of the bulk phase concentration for an aqueous solution of a surfactant. Below the *CMC*, the greater the concentration the lower the surface tension, but above the *CMC* the surface tension of the solution remains essentially constant.

One of the most important properties of surfactant solutions is that they are able to solubilize different kinds of substances. Hydrophobic substances, i.e., oils, can be solubilized inside the

micelles core, sometimes in very sizeable amounts. Some extreme cases are known in which the solubilized oil volume is actually larger than the aqueous solvent volume; for such situation to happen, the solution must contain a very large number of micelles and these must be considerably swollen. These micelles are no longer spherical, but cigar shaped or hexagonally packed, or even degraded into lamellar liquid crystals.

2.1.3 Hydrophilic-Lipophilic Balance (HLB)

Griffin (1949) introduced the Hydrophilic-Lipophilic Balance or *HLB* value, which is characteristic of the surfactant and is used as a measure of the relative affinity of the surfactant for the water and oil phases. The *HLB* measures the relative importance of the hydrophilic and the lipophilic group in the surfactant molecule.

Griffin created a continuous series of emulsifying agents, ranging from 100% oleic acid predominantly lipophilic, to 100% sodium oleate predominantly hydrophilic, by making mixtures of known composition from these two substances. A value of 1 was assigned arbitrarily to oleic acid and a value of 20 to sodium oleate, and intermediate values were based on the relative amounts of each constituent in the mixture. Each mixture was tested as emulsifier by adding to a mixture of refined white oil and water and shaking. The volume and type of stable emulsion remaining were compared (Morrison and Rose, 2002).

The method followed by Griffin serves as reference standard for commercial emulsifiers, which are tested in exactly the same way. The commercial emulsifier is assigned the *HLB* number corresponding to the reference sample.

The original method of determining *HLB* numbers is so profligate of time that shorter routes to the same end have been suggested. One example is to calculate the *HLB* number of a molecule by adding contributions from its constituent groups, using the empirical relations obtained by Davies (Davies, 1957). Also specific equations are proposed for several types of emulsifiers (Rosen, 2004). Although the *HLB* number does not take into account effects that are known to be relevant on emulsion formulation, is still used nowadays because it is based on extremely simple arithmetic (Salager, 2000).

The required *HLB* (or HLB_{req}) is an oil phase attribute, which is determined as the surfactant *HLB* that provides the best match with a given oil to produce the maximum stability of an emulsion along a surfactant *HLB* scan. For *W/O* emulsions a *HLB* between 3 and 6 is recommended.

2.1.4 Emulsion Formulation

In a broad sense, producing an emulsified system involves several choices and activities that may be classified in three categories, according to the type of variables that are dealt with.

The so-called *field* or *formulation variables* are, in addition to temperature and pressure, the intensive physicochemical variables that define the thermodynamic equilibrium conditions of the system through the equality of chemical potentials. In practical case, salinity (type of electrolyte and concentration) is used to describe the aqueous phase nature, the equivalent carbon number (*ECN*) characterizes the oil, and the hydrophilic-lipophilic balance (*HLB*) is the formulation variable that defines the surfactant. Pressure effect is generally neglected in liquid systems.

The second choice deals with the so-called *composition variables*, which define the relative amounts of the different substances involved in the system. In a surfactant-oil-water (*SOW*) ternary system, two independent composition variables are sufficient. Commonly, surfactant concentration (or proportion) and water/oil ratio (*WOR*) are the selected independent variables.

The last category involves *process variables* that allow describing the agitation process and mixing conditions, required to produce an emulsion. A variety of emulsifying devices are available, and it is often very difficult to precisely describe what exactly happens inside them when surfactants are added, but it seems that the process can be repeated and each mixing condition produces a different emulsion.

Each of the discussed variables has compensatory effects on formulation. For such reason, a one-dimensional scan is used to study the variable effect on emulsion properties.

2.2 Emulsion Characterization

2.2.1 Emulsion Properties

Type, conductivity, viscosity, drop size and stability are the most important properties of an emulsion. The two last properties are described in detail in sections 2.2.2, 2.2.3 and 2.3.

Maybe the first and most important property to be determined is the emulsion type, i. e., either oil-in-water (*O/W*) or water-in-oil (*W/O*). This is essentially equivalent to determine which the emulsion external phase is. The external phase and the emulsion exhibit similar wettability and dispersion properties. If a small amount of an *O/W* emulsion is poured in an aqueous medium its external phase would dissolve in the aqueous phase, and its oil droplets would disperse. On the contrary, a *W/O* emulsion globule would not do so (Becher, 1977).

In most cases the aqueous phase contains some electrolyte while the oil phase does not, so that the electrolytic conductivity is the property used to detect the emulsion type. Actually, the conductivity depends upon the drop size average and distribution, but it is not very sensitive, unless there are large changes in these characteristics. Emulsion conductivity typically varies with the external phase content. The variation is proportional while it is an *O/W* type and it is essentially nil (at the same scale) when it is a *W/O* emulsion, because the typical electrolytic conductivity of the oil phase is 100 or 1000 times smaller than the conductivity of the aqueous brine.

For W/O emulsions, conductivity k can be calculated as (Salager, 1999)

$$k = k_o \frac{(1+fw)\cdot(2+fw)}{(1-fw)\cdot(2-fw)} \tag{2-1}$$

Viscosity μ is a measure of the resistance of a fluid to being deformed by either shear stress or extensional stress. The fluids in which the shear stress is directly proportional to the shear rate are called Newtonian fluids. Isaac Newton postulated that, for straight, parallel and uniform flow, the shear stress τ_{yx}, between layers is proportional to the velocity gradient $\gamma = du/dy$, in the direction perpendicular to the layers (Fox and MacDonald, 2000).

$$\tau_{yx} = \mu \cdot \frac{du}{dy} \tag{2-2}$$

Newtonian fluids are those that fulfill equation (2-2). Emulsions are often non-Newtonian fluids with complex rheological behavior; most of them follow the Power Law model (Fox and MacDonald, 2000).

$$\tau_{yx} = A \cdot \gamma^B = A \cdot \gamma^{B-1} \cdot \frac{du}{dy} = \eta \cdot \frac{du}{dy} \tag{2-3}$$

Where

$$\eta = A \cdot \gamma^{B-1} \tag{2-4}$$

η is the so-called apparent viscosity that would indicate the resistance to flow under some specific conditions. A is called Consistency Index and B Power Law Index.

Dependency of emulsion viscosity upon different physical variables has been known for quite a while. It is generally written as proportional to the external phase viscosity. The ratio of the emulsion viscosity to the external phase viscosity is the relative viscosity.

The internal phase presence often has the most important influence on viscosity. The increase in viscosity due to this interaction in the case of rigid spherical drops was determined by

Albert Einstein, but his model is essentially valid up to $fw = 0.02$ (for *W/O* emulsions), where viscosity is a linear function from the internal phase content.

Emulsions are not generally monodisperse systems, but contain a distribution of drop sizes, so that small drops can enter the void space among larger drops. Moreover, liquid drops are not rigid spheres either and some deformation is likely to take place. As a consequence, fw could reach very high values.

Increase in viscosity with the internal phase proportion starts slowly, then turns faster and faster, until an almost vertical variation is registered near the emulsion inversion point in which the internal phase becomes the continuous phase and vice versa. Many studies have reported empirical relationships to describe this behavior, but none of them are valid in the general case, because many other effects, particularly the non-Newtonian behavior, have to be considered as well (Shinoda et al., 1990; Graciaa, 1984).

The third kind of variables to deal with is the drop size average value and distribution. Since the overall emulsion surface area depends on the square of the drop size, while the internal phase volume depends on the cube of the drop size, the surface-to-volume ratio changes inversely to the size. In other words, small-drop emulsions exhibit higher surface area per unit volume than big-drop emulsions. Since the interdrop friction effect is related to the drops surface area, a decrease in drop size is expected to be associated to an increase in viscosity.

Most experimental studies on monodisperse systems were carried out on solid dispersions rather than emulsions, since it is quite tedious to get a monodisperse emulsion. Experimental evidence from narrow-dispersed emulsions confirms that the viscosity increases as the average drop size decreases.

Drop size distribution also plays an important role. A polydispersed emulsion is generally less viscous than a monodisperse with the same average drop size, no matter the way the average is calculated. Also biemulsions are frequently found to be less viscous than their base emulsions, whenever the difference in average sizes or mode separation is large enough.

Other effects are likely to influence emulsion viscosity, particularly high-internal-phase-ratio emulsions in which the drops are separated by thin films. Both dynamic phenomena, such as streaming potential or interfacial viscosity retardation could take place during the drainage of these films. Electrical and steric repulsion, as well as surface hydration are probably also important in these kinds of emulsions. These phenomena that are due to the presence of adsorbed surfactant onto approaching interfaces have been studied in relation to stability problems, but not for their effect on viscosity.

As a rule of thumb, it can be said that any effect that would tend to reduce the flow of interdrop film would result in increased viscosity, or rather in impaired flowing ability.

On the other hand, the physicochemical formulation influences emulsion viscosity. The approach presented in literature is based on experimental facts because theoretical considerations are not proficient enough to give a whole comprehensive picture. For the sake of simplicity, the influence of formulation is presented on all emulsion properties simultaneously, which is the most logical way of analyzing the results since the properties are not independent, e.g., the drop size influences viscosity and stability.

2.2.2 Characterization of a Single Particle

Specification of the particle diameter x of a spherical particle allows to characterize it because all the other properties like volume, surface, specific surface and projected area, can be calculated from it. For a no spherical particle, an equivalent diameter must be specified; it is not unique, but it depends on the property that is used to define it. Thus, the equivalent diameter in volume x_v of an irregular particle is defined as the diameter of a sphere that has the same volume as the particle.

2.2.3 Characterization of a Particle System

A population of particles is described by a particle size distribution (*PSD*) that may be expressed as frequency (or density) distribution curves q_r or cumulative distributions Q_r. A particle size distribution is referred to a measured quantity M, like number ($r=0$, $M=N$), length ($r=1$, $M=L$), area ($r=2$, $M=A$), volume ($r=3$, $M=V$), etc.

Density distribution expresses the measured quantity percentage that appears in each fraction of the particle size (equation 2.5), and the cumulative function is defined as the total percentage of the particle quantity in fractions smaller than the particle size (equation 2.6).

$$q_r(x) = \frac{dM}{M \cdot dx} \tag{2.5}$$

$$Q_r(x) = \int_0^x q_r(x) \cdot dx \tag{2.6}$$

In practice, the particle size distribution is usually expressed in discrete form. In this case the cumulative size distribution can be determined as

$$Q_r(\overline{x_i}) = \sum_{j=1}^{i} q_r(\overline{x_j}) \cdot \Delta x_j \tag{2.7}$$

Some parameters like the medium value x_{50}, the modal value x_{mod}, and the weighted mean diameter $\overline{x_{1,r}}$ give important information about the dispersed system. The median value x_{50} is the particle size which divides a particle collective into two equally sized subsets; that means

$Q_r(x_{50})=0.5$. The modal value x_{mod} is the particle size where the density distribution has its maximum. A monomodal system has one modal value whereas a multimodal system has more than one. The weighted mean diameter $\overline{x_{1,r}}$, is defined as

$$\overline{x_{1,r}} = \int_0^\infty x \cdot q_r(x) \cdot dx \tag{2.8}$$

The width of the particle size distribution is usually expressed with a pair of particle sizes x_{min} and x_{max}, in which the cumulative distribution curve reaches values defined arbitrarily, but that are near and representative of the function limits 0 and 1, i.e. $Q_r(x_{min}) = 0.05$ and $Q_r(x_{max}) = 0.95$.

2.3 Emulsion Stability

The term stability, when applied to macro emulsions used for practical applications, usually refers to the resistance of emulsions to the coalescence of their dispersed droplets. The mere rising or settling of the droplets (creaming) is usually not considered instability. Neither flocculation nor coagulation of dispersed particles is considered serious signs of instability, when compared with coalescence or emulsion breaking.

The droplet coalescence rate in a macro emulsion is stated to be the only quantitative measure of its stability (Boyd, 1972). It can be measured by counting the number of droplets per emulsion unit volume as a function of time, in a haemocytometer cell under a microscope (Sherman, 1968), or by means of a Coulter centrifugal photosedimentometer (Groves, 1964; Freshwater, 1966).

2.3.1 Three Stages Mechanisms

Coalescence between drops in an immiscible liquid medium, or between a drop and its own bulk phase occurs in three stages (Sun et al., 1998 and 1999; Chen et al., 1998; Man et al., 1997). In the first stage, the drops approach each other and are separated by a film of the continuous phase. The second stage involves the thinning of this film. Thinning rate is affected by capillary pressure and disjoining pressure (Isaacs and Chow, 1992; Rommel et al., 1992) because film thinning occurs by drainage of the liquid under gravity and suction at the plateau-borders, and can be retarded due to the Marangoni effect if surfactant is present. When the film reaches a certain critical thickness (about 1000Å), other surface forces influence drainage: van der Waals attraction increases the drainage rate and double-layer repulsion decreases it (Isaacs and Chow, 1992; Vrij, 1966; Kabalnow, 1998); any significant

disturbance or instability will cause film rupture and coalescence occurs (Isaacs and Chow, 1992; Friberg and Jones, 1996).

Further thinning will cause some films to become metastable. Metastability occurs when border suction, van der Waals attraction and double-layer repulsion are balanced. Instability results when the attraction forces predominate, due to external disturbances such as thermal shocks, vibration and particles film thinning is often the overall controlling step (Eow et al., 2001).

2.3.2 Factors Determining Emulsion Stability (Rosen, 2004)

The rate at which the droplets of a macro emulsion coalesce to form larger droplets, and eventually break the emulsion, has been found to depend on a number of factors: interfacial film physical nature, existence of an electrical or steric barrier on the droplets, continuous phase viscosity, droplet size distribution, phase volume ratio, and temperature.

2.3.2.1 INTERFACIAL FILM PHYSICAL NATURE

The droplets of dispersed liquid in an emulsion are in constant motion, and therefore there are frequent collisions between them. If, on collision, the interfacial film surrounding the two colliding droplets in a macro emulsion ruptures, the two droplets will coalesce to form a larger one, since this result in a decrease in the free energy of the system. If this process continues, the dispersed phase will separate from the continuous phase, and emulsion will break. The mechanical strength of the interfacial film is therefore one of the primary factors determining macro emulsion stability.

For maximum mechanical stability, the interfacial film resulting from the adsorbed surfactants should be condensed, with strong lateral intermolecular forces, and should exhibit high film elasticity. The liquid film between two colliding droplets in an emulsion is similar to the liquid lamella between two adjacent air bubbles in foam and shows film elasticity for the same reasons (Gibbs and Marangoni effects).

The films surrounding the droplets in *W/O* macro emulsions, in particular, must be very strong, and these films are believed to be of the solid-condensed type (Schulman, 1940; Ford, 1966) characterized by very strong lateral intermolecular forces and well-developed orientation of the film with respect to the interface, which confers a good deal of rigidity to the film.

This type of film is necessary since the water droplets in a *W/O* emulsion carry little or no charge and therefore have no electrical barrier to coalescence (discussed in the following section). It is therefore mainly the mechanical strength of the interfacial film that prevents

coalescence of the droplets in *W/O* macro emulsions, and to survive under the constant bombardment by neighboring droplets, the film must have unusual strength. The great rigidity of the film in these *W/O* emulsions is evidenced by the irregular shape of the water droplets in them, in contrast to the spherical shape of oil droplets in *O/W* emulsions.

2.3.2.2 Existence of an Electrical or Steric Barrier to Coalescence on THE DISPERSED Droplets

The presence of a charge on the droplets constitutes an electrical barrier to the approach of two particles. This is believed to be a significant factor only in *O/W* emulsions. In *W/O* emulsions, there is very little charge, if any, on the dispersed particles, and experimental data indicate no correlation between stability and any charge present.

The presence of big molecular groups in the interfacial film can disable the approach of the drops, forming a steric barrier to such approach. In *W/O* emulsions, long alkyl groups extending into the oil phase from surfactants constituting the interfacial film may produce such a steric barrier.

The destabilization of an emulsion can be achieved by destroying or diminishing the repulsive field of force, or territory, created by the interfacial active solute. The preceding rationale is postulated on the assumption that electrostatic or steric stabilization lies at the root of Bancroft's rule that pointed out that, in the making of an emulsion, the liquid in which the surfactant is the more soluble becomes the continuous phase (Morrison and Ross, 2002).

2.3.2.3 Continuous Phase Viscosity

An increase in the continuous phase viscosity μ reduces the droplets diffusion coefficient *D*. As the diffusion constant is reduced, the droplets collision frequency and their coalescence rate are reduced. The external phase viscosity is increased as the suspended particles number increases, and this is one of the reasons why many emulsions are more stable in concentrated form than when diluted. The external phase viscosity in emulsions is often increased by addition of ''thickening'' agents.

2.3.2.4 Droplet Size Distribution

A factor influencing the droplet coalescence rate is the size distribution. The smaller the size range, the higher the emulsion stability. Since large particles have less interfacial surface per unit volume than small droplets, in macro emulsions they are thermodynamically more stable than the small particles, and tend to grow at the small ones expense; if this process continues, the emulsion eventually breaks. An emulsion with a fairly uniform size distribution is,

therefore, more stable than one having a wider size distribution with the same average particle size.

2.3.2.5 PHASE VOLUME RATIO

As the dispersed phase volume in a macro emulsion increases, the interfacial film surface expands further and further to surround the droplets of dispersed material, and the system instability increases. While the volume of the disperse phase increases beyond that of the continuous phase, the type of emulsion (*O/W* or *W/O*) becomes basically more unstable relative to the other emulsion type, since the interface area that is now enclosing the dispersed phase is larger than that which would be needed to enclose the continuous phase.

2.3.2.6 TEMPERATURE

A change in temperature causes changes in the following physical-chemical variables: interfacial tension between the phases, nature and viscosity of the interfacial film, emulsifying agent relative solubility in the phases, vapor pressures and viscosities of the liquid phases, and particles thermal diffusion coefficient. Therefore, temperature variations usually cause considerable changes in the emulsion stability; the emulsion may be inverted or broken.

2.3.3 Electrostatic Separation of *W/O* Emulsions

Cottrell and Speed filed the first patent on electro coalescence (1911), observing the coalescence when a high potential was applied to a pair of wire electrodes in a *W/O* emulsion. The mechanisms for this phenomenon are however not clearly understood yet (Isaacs and Chow, 1992). Dominant mechanisms should depend on factors such as fractional volumetric hold-up of dispersed phase, electrode geometry and type of electric field, although they have not been studied systematically.

2.3.3.1 FORCES ACTING UPON A WATER DROPLET IN AN ELECTRIC FIELD

A water droplet suspended between electrodes is under the effect of five forces (Draxler and Marrs, 1993). Two of these forces are gravitational and hydraulic. Gravitational force, equal to the droplet weight, acts moving the water droplet towards the bottom of the vessel. Drag forces act on the water droplet lifting it toward the oil outlet. The other forces are dipole, electrophoretic and di-electrophoretic.

Electrophoretic force

Electrophoretic force acts on charged droplets and is dependent on the field strength, droplet diameter and oil conductivity and viscosity, but is independent on droplet spacing. The

electrophoretic force has a time constant equal to the ratio of the oil dielectric constant and conductivity and will decay most rapidly in highly conductive oil (Warren et al., 1998). Therefore, the force can only be sustained by replenishing the droplet charge frequently.

Di-electrophoretic force

Di-electrophoretic force is established in a non-uniform field. The dielectrophoretic force is independent on droplet spacing, but is dependent on the droplet diameter and the change in field strength which pulls the largest droplets into the highest field gradient. This force acts to accumulate water in areas where the divergence of the electrostatic field is greatest (Warren et al., 1998).

Dipole Force

For dipole coalescence to take place droplets have to be brought together by various ways, such as Brownian motion, sedimentation, flocculation and electrophoresis, with laminar or turbulent flow mixing being generally the most important mechanisms when there is fluid flow.

Williams and Bailey (1986), Bailes and Stitt (1987) and Waterman (1965) considered this force to be the principal cause of coalescence in *AC* and *DC* electric fields. The full expression for the force between two dipoles with a distance S between their centers has been given by Pohl (1973). For the case where the dielectric constant of the disperse phase is much greater than that of the continuous phase, as in the case of *W/O* emulsions Cross gave a simplified expression (1987). The force expression assumes that drops are uncharged and of equal size. Furthermore, droplet deformation, which occurs in the presence of a strong electric field, is ignored. Dipole force is dependent on the water droplet size and the spacing among them. Assuming that water droplets are uniformly sized and homogeneously distributed, spacing is inversely proportional to the dispersed water volume. Therefore, as the dispersed water is coalesced and separated from the oil, the spacing among droplets increases and dipole forces decline rapidly; also when droplet radius increases spacing increases. Therefore, the dipole force weakens rapidly as droplets are coalesced and separated from the oil.

2.3.3.2 CHAIN FORMATION

Chain formation is influenced by a number of factors, including oil phase viscosity, disperse phase volume and the applied electric field strength (Taylor, 1991). It has been observed with both *DC* and *AC* electric fields. Chains of drops are formed by movement of single drops,

with the chains aligned in the direction of the field. Moreover, the chains do not necessarily start or finish at an electrode and may not be in contact with the electrodes (Eow et al., 2001).

The actual coalescence process depends on two factors, i.e. the breakdown of the continuous phase film between adjacent drops, and the attractive force between drops due to their potential difference. The film may be broken also by other means than electrostatic breakdown. For stationary emulsions, Taylor (1988) has shown that stable chains of drops will be created if the drops are surrounded by a rigid interfacial film, eventually leading to the bridging of the electrodes.

Taylor reports two different types of behavior. In type I, very stable droplet chains form between the electrodes, on the application of an *AC* electric field, resulting in current leakage through the chains. Drop–drop coalescence is prevented by rigid interfacial films. However, with the addition of an oil-soluble surfactant, type I characteristics transforms to type II, where rapid droplet coalescence occurs, without any chain formation, thus enhanced mobility of the interfacial film.

Without a rigid film, neighboring droplets tend to stick together and coalesce to form larger drops in an electric field. Thus, coalescence is more likely to occur in absence of chain formation where the interfacial film is not rigid. Mohammed et al. (1993) revealed that asphaltenes form solid films, retarding the film drainage rate between water drops.

2.3.3.3 FACTORS INFLUENCING ELECTROSTATIC COALESCENCE EFFICIENCY

The main factors influencing coalescence efficiency are: coalescer design, applied electric field type, applied frequency, electrode design and coating, average inlet droplet size, liquid mixture residence time, surfactant type and concentration, and dispersed phase hold-up fraction.

The efficiency of an electrostatic dehydrator is usually related to power consumption. Only a very small amount of current would be drawn for highly insulating oil. The main factors influencing power consumption will be, therefore, the continuous phase conductivity and the electrodes bridging.

The predominant coalescence mechanisms in a system depend on the nature of the applied electrostatic field. *AC*, *DC*, pulsed *DC* or combinations of them are being utilized in the separation of water-in-crude oil dispersions or emulsions. Dehydrator manufacturers rely on all fundamental types of electrostatic fields to enhance coalescence of the dispersed water droplets: *DC* fields are highly efficient, but can promote electrolytic corrosion. Therefore, they are not used in crude oil desalting applications, but only to dehydrate refined oils having low conductivity and/or in treatment of low water content refined products.

On the other hand, *AC* fields, the oldest and most common configuration, are extensively used by all manufacturers in crude oil emulsions due to their tolerance to high water cuts. Pulsed *DC* field with insulated electrodes is proposed for high water content emulsions treatment (Taylor, 1996). Finally, combined *AC/DC* fields can supply the high water tolerance of *AC* fields and the high efficiency of *DC* fields.

Generally, separation efficiency improves with increasing applied field strength (Goto et al., 1989). Nevertheless, if the field becomes too strong, various drop breakup mechanisms can occur, as the electric stress overwhelms the recovery force due to interfacial tension, depending on the physical and surface properties of the system (Williams and Bailey, 1986).

Typically, field strength of around 100 V/mm is used (Chen et al., 1994). The polarization phenomenon induced by the electric field produces dipole–dipole forces. These forces are effective over short separation distances, and significantly enhance droplet–droplet coalescence (Waterman, 1965; Chesters, 1991). The electric field effects on system performance are not always consistent, due to variations of ionic species, solvent and surfactants used.

Using *DC* voltages from 5 to 25 kV with bare electrodes, Hirato et al. (1991) showed that demulsification percentage increases linearly with time until it reaches 60–70%, with both initial rate and maximum percent of demulsification increasing with applied potential. Bailes and Larkai (1981) attributed the constant *DC* field inefficient separation to the current leakage through the insulating liquid. The problem is caused by interfacial polarization and is well described by Galvin (1986).

DC electric field is able to produce rapid electrophoretic motion of water droplets (Eow and Ghadiri, 2002). Water droplets may be charged initially by direct contact charging with the electrodes. The increased rate of droplet–droplet collision is then caused by the droplets moving rapidly between the electrodes. As a result, the rate of droplet–droplet coalescence becomes more significant, and an aqueous layer on the electrode surfaces can be formed by the droplets.

Considerations on electrode design and insulation type have been the subject of several investigations. Hsu et al. (1983) reported good coalescence with *AC* fields using insulated electrodes with a hydrophobic surface. As expected, the thinner the coating, the better is the coalescence.

Galvin (1986) dismissed claims by Bailes and Larkai (1982) regarding the use of insulated electrodes to increase separation efficiency, arguing that insulation serves just to prevent short-circuiting, and only increases the applied potential required to produce the same coalescence rate.

Galvin also recommended that if short-circuiting is a major problem, a current-limiting device should be applied so that electrode insulation is not required. However, according to Bailes and Larkai (1982) and Bailes (1992) the importance of electrode insulation is that, should bridging occur between the electrodes, the charge is only locally reduced at an insulated electrode surface. With bare electrodes, such bridging would fully discharge the capacitor, and the whole electrostatic field would break down.

3 Emulsion Formulation

The scope of chapter 3 was to develop highly stable synthetic emulsions with reproducible properties, serving as a model to study several techniques for emulsion destabilization that could be also used in crude oil emulsions. The effect of different variables was studied in one-dimensional scans and as result, emulsions with maximum stability were obtained.

3.1 Materials and Methods

For *W/O* emulsions preparation, paraffin oil and a mixture of Sorbitan Monooleate (Span 80®) and Nonylphenol Polyglycol Ether 4 EO (Arkopal N 040®) (both highly soluble in oil) surfactants were mixed. Table 3-1 shows the main physical properties of the used chemical compounds.

Table 3-1. Chemical Compounds Physical Properties

Name	Molecular Weight/ Formula	Density (kg/m^3)	Viscosity (cP)	Boiling Point (°C)	Solubility	HLB
Liquid Paraffin		900	62.3 @ 23 °C	350	Insoluble in cold water	
Water	18 / H_2O	1000	0.890 @ 25 °C	100		
Octanol	130 / $C_8H_{18}O$	829	7.21 @ 25 °C	195		
Sorbitan Monooleate	428 / $C_{24}H_{44}O_6$	1000	1100 @ 20 °C	>100	Insoluble in cold water, soluble in most oils	4.3
Nonylphenol Polyglycol Ether 4 EO	388/ HO $(C_2H_4O)_4$ $(C_6H_4)C_9H_{19}$	990-1070	160		insoluble in Water above 1%	8.6

Surfactant mixtures *HLB* values were calculated from the Span 80® and Arkopal N040® *HLB* values assuming ideal mixture behavior.

Distilled water was added slowly (using a burette) during 5 minutes, while it was mixed with a Braun stirrer model MR-5550, at 13400 rpm. After adding all the water, the components

were mixed for 5 more minutes. 100 mL of emulsion (water plus paraffin) were prepared in each run in a 600 mL beaker (see Fig. 3-1b).

Samples of 50 mL were transferred into test tubes, and monitored during 30 days. Stability of emulsions against sedimentation and coalescence was assessed altogether by the total separated volume of water plus paraffin ($Vs = Vw + Vp$) divided by the total sample volume ($V = Vw + Vp + Ve$) (see Fig. 3-1c). Emulsions with acceptable stability were defined as those in which the total separation was lower than 10% in 30 days.

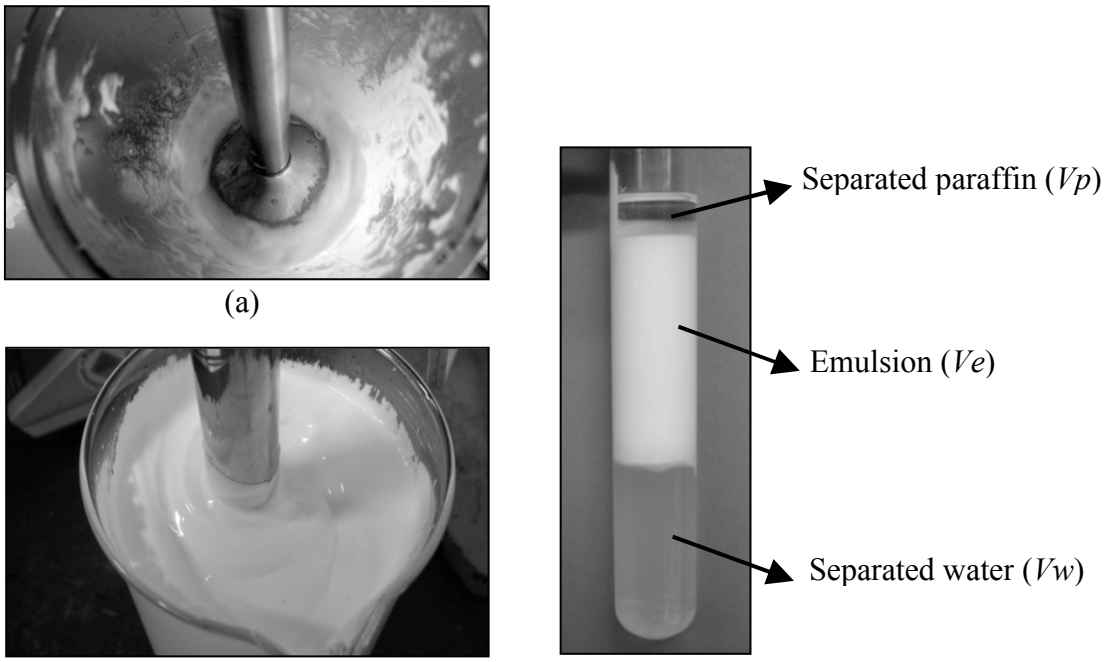

Figure 3-1. Appearance of Water-in-Oil Emulsion
Stabilized by a Mixture of Span 80® and Arkopal N 040®
Immediately after preparation ((a) 100 mL, (b) 500 mL) and 30 days later ((c) 50 mL sample in test tube). fw = 0.75, HLB = 5.5, Cs = 2% v/v, vm = 13400 rpm, tm = 5 min

After finishing the experimental tests, formulation to produce the most stable emulsions in a wide range of water content was defined. Emulsions were prepared in triplicate to validate the proposed formulation protocol reproducibility.

Emulsion density and apparent viscosity were measured. To estimate density, 30 mL of emulsion sample was placed in a 50 mL graduated cylinder. Cylinder weight with and without emulsion was measured. Density was calculated as the ratio between the emulsion weight and volume.

In order to determine the apparent viscosity a Brookfield viscometer model *LVF* was used. For viscosity measurements it was necessary to prepare batches of 500 mL emulsion (see Fig. 3-1).

Emulsion type was determined by observing what happened when a drop of each emulsion was added to a volume of either pure paraffin or pure water. Drops of *W/O* emulsion are dispersed in oil and remained as drops in water (see Figure 3-2). On the other hand, *O/W* drops emulsion are dispersed in water and remained as drops in oil.

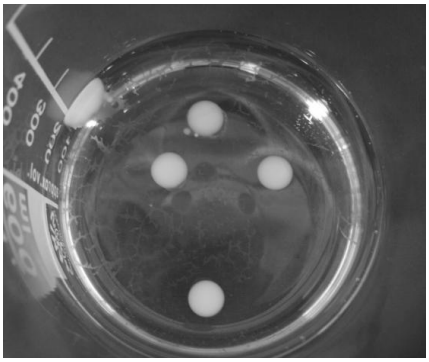

Figure 3-2. Emulsion Type Determination

Drops of *W/O* emulsion in water. External phase: paraffin. Surfactant: Mixture of Span 80® and Arkopal N40®

3.2 Experimental Plan

One-variable scans were used to study the effect of the main variables on the emulsion properties. The range of variation of each parameter was established taking into account theoretical considerations, previous experience in formulation and available capacities and resources.

The variables were: surfactant content (from 0.5 to 10% v/v), water content from 25 to 75% v/v), *HLB* value (from 4.5 to 6.5), alcohol content (Octanol from 0 to 4% v/v), water salinity (from 0 to 16 g/dL), mixing velocity (6100 to 13400 rpm), mixing time (from 5 to 20 min), mixing type (continuous or intermittent), and batch emulsion volume (from 50 to 500 mL).

All tests were carried out at room temperature (25±1 °C). *HLB* values were obtained by mixing Span 80® and Arkopal N040® according with ideal mixing rules. Surfactant and co-surfactant content are given as surfactant (or co-surfactant) volume divide by the volume of water plus paraffin. Salinity is given in terms of NaCl concentration in water. Mixing time is

defined after all water addition. Appendix A1 describes in detail the experimental conditions of each test.

3.3 Results and Discussion

3.3.1 Variables Scan

First, the effect of surfactant content on emulsion stability was evaluated. Figure 3-3 shows the results of these tests. Scan conditions are detailed in Table A1-1, appendix A1. All formulated emulsions were stable according to the defined criterion. The higher stabilities were obtained for surfactant contents above 1.5% v/v. Sedimentation was evident in all cases by the presence of a clear paraffin layer in the top of the test tubes. Coalescence was identified by the presence of separated water on the bottom, and was observed only for surfactant contents of 4.0 and 8.0 % v/v.

Although the highest stability was obtained for surfactant content of 10% v/v, the most appropriate formulation value should also take into account the costs; therefore, a surfactant content of 2% v/v was selected for the rest of the formulations. Surfactant content influence on emulsion stability is not highly significant because it is above the critical micelle concentration.

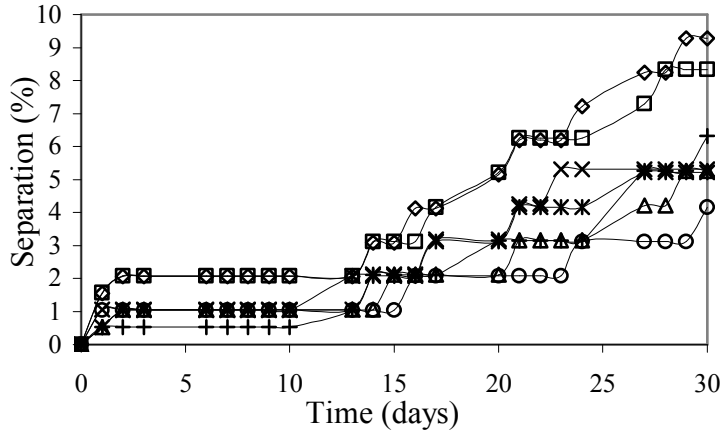

Figure 3-3. Surfactant Content Effect on Emulsion Stability

fw = 0.50, *HLB* = 5.5 with a mixture of Span 80® and Arkopal N 040®, *vm* = 13400 rpm, *tm* = 5 min, *T* = 25°C. *Cs* = 0.5-10% v/v: (◇) 0.5%, (□) 1.0%, (△) 1.5%, 2.0 (∗), (+) 4.0%, (×) 8.0%, (○) 10.0%

The second variable studied was the surfactant *HLB*. The scan conditions are detailed in Table A1-1, appendix A1. A range of *HLB* from 4.5 to 6.5 was selected. Outside this range *W/O*

emulsion stability is very low or the formulation results in an *O/W* emulsion. *HLB* describes the surfactant affinity to the water and oil phases, and its influence on emulsion stability depends strongly on the volumetric proportion of the phases. Three scans of *HLB* were made for emulsions with water contents of fw = 0.25, 0.50 and 0.75, respectively.

Figures 3-4 and 3-5 show *HLB* effect on emulsion stability. In these tests, not all the emulsions were stable enough. In some cases a separation up to 60% was obtained within 30 days after preparation.

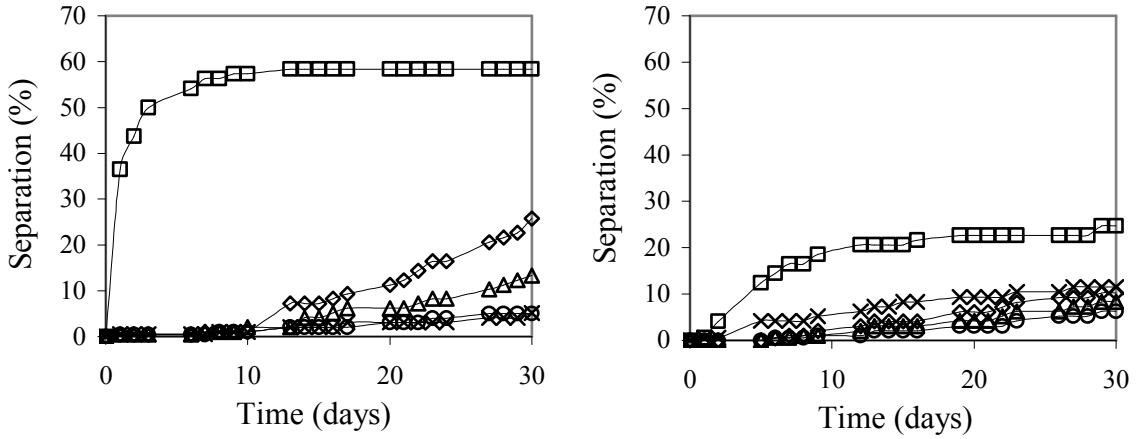

Figure 3-4. *HLB* Effect on Emulsion Stability

fw = 0.25 (left) and *fw* = 0.50 (right), *Cs* = 2% v/v, *vm* = 13400 rpm, *tm* = 5 min, *T* = 25°C. *HLB* = 4.5-6.5 with a mixture of Span 80® and Arkopal N 040®: (□) 4.5, (×) 5.0, (○) 5.5, (△) 6.0, (◇) 6.5

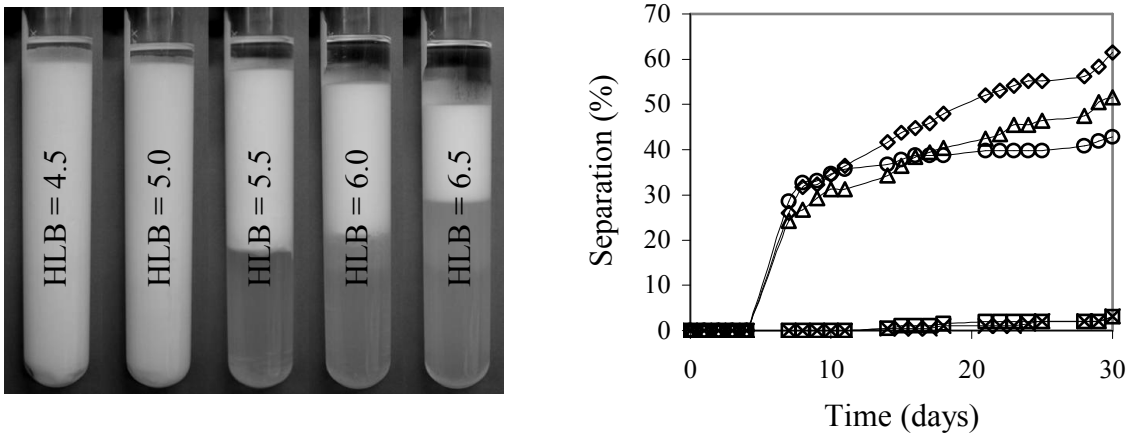

Figure 3-5. HLB Effect on Emulsion Stability

Picture (left) after 30 days. *fw* = 0.75, *Cs* = 2% v/v, *vm* = 13400 rpm, *tm* = 5 min, *T* = 25°C. *HLB* = 4.5-6.5 with a mixture of Span 80® and Arkopal N 040®: (□) 4.5, (×) 5.0, (○) 5.5, (△) 6.0, (◇) 6.5

HLB effect on stability was much more significant for emulsions with fw = 0.25 and 0.75, but in the first case separation is only due to sedimentation, which is explained by the weak interaction between the droplets. Coalescence was observed only for *fw* = 0.75. The step of droplet approach before coalescence is overcome due to the high internal phase content; drops are literally in contact and emulsion stability against coalescence decreases. The *HLB* values that yield optimum stability are 5.0 and 5.5 for *fw* = 0.25; 5.5 and 6.0 for *fw* = 0.5, and 4.5 and 5.0 for *fw* = 0.75.

With the *HLB* scan, at least one emulsion with high stability was obtained for low, medium and high water content, but the study of new variables could lead to a formula optimization and would help to understand the variables which exert higher influence on stability.

HLB scans were repeated with 2% Octanol dissolved in the paraffin before adding the water (see Table A1-3 in appendix A1). Octanol does not act as a gut co-surfactant, and in all cases the stability is reduced when alcohol is used, and both coalescence and sedimentation were observed.

Figure 3-6 is an example of these results for *fw* = 0.50. It can be observed that the best *HLB* values are between 5.5 and 6.0 (like when alcohol is not used), but in this case no formula reaches the expected stability.

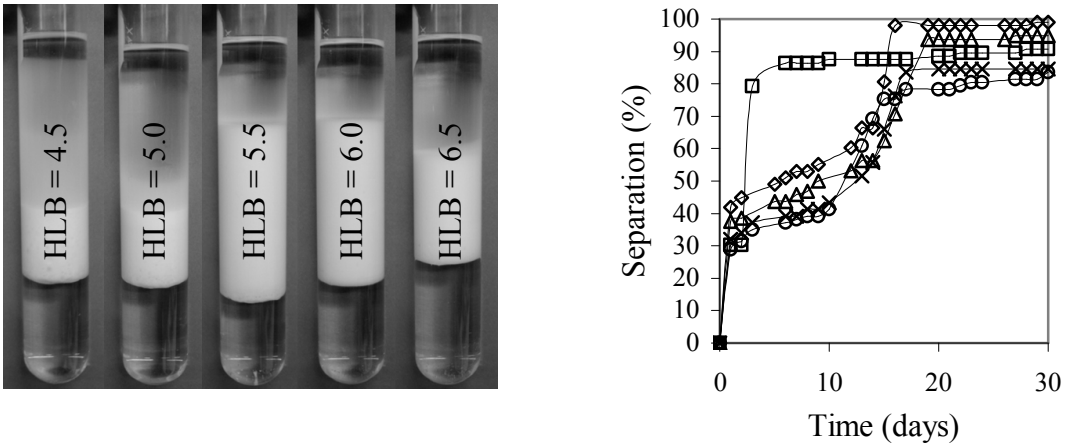

Figure 3-6. HLB Effect on Emulsion Stability with Octanol

Picture (left) after 30 days. *Co* = 2% v/v, *fw* = 0.50, *Cs* = 2% v/v, *vm* = 13400 rpm, *tm* = 5 min, *T* = 25°C. *HLB* = 4.5-6.5 with a mixture of Span 80® and Arkopal N 040®: (□) 4.5, (×) 5.0, (○) 5.5, (△) 6.0, (◇) 6.5

The Figure 3-7 summarizes the alcohol content effect on emulsion stability for *HLB* = 5.5 and *fw* = 0.25, 0.50 and 0.75. The higher the water content and/or the Octanol content, the lower the emulsion stability against coalescence.

Reduction of emulsion stability against sedimentation can be explained by a change in the required hydrophilic-lipophilic balance in presence of Octanol. The higher the *fw* the higher the octanol dissolved in the oil (for the same alcohol content on the total emulsion), that according to the Windsor concept (Salager, 2000 and Rosen, 2004) modifies the interactions between the surfactant molecules and the oil phase, which is interpreted as a variation in the required *HLB* value.

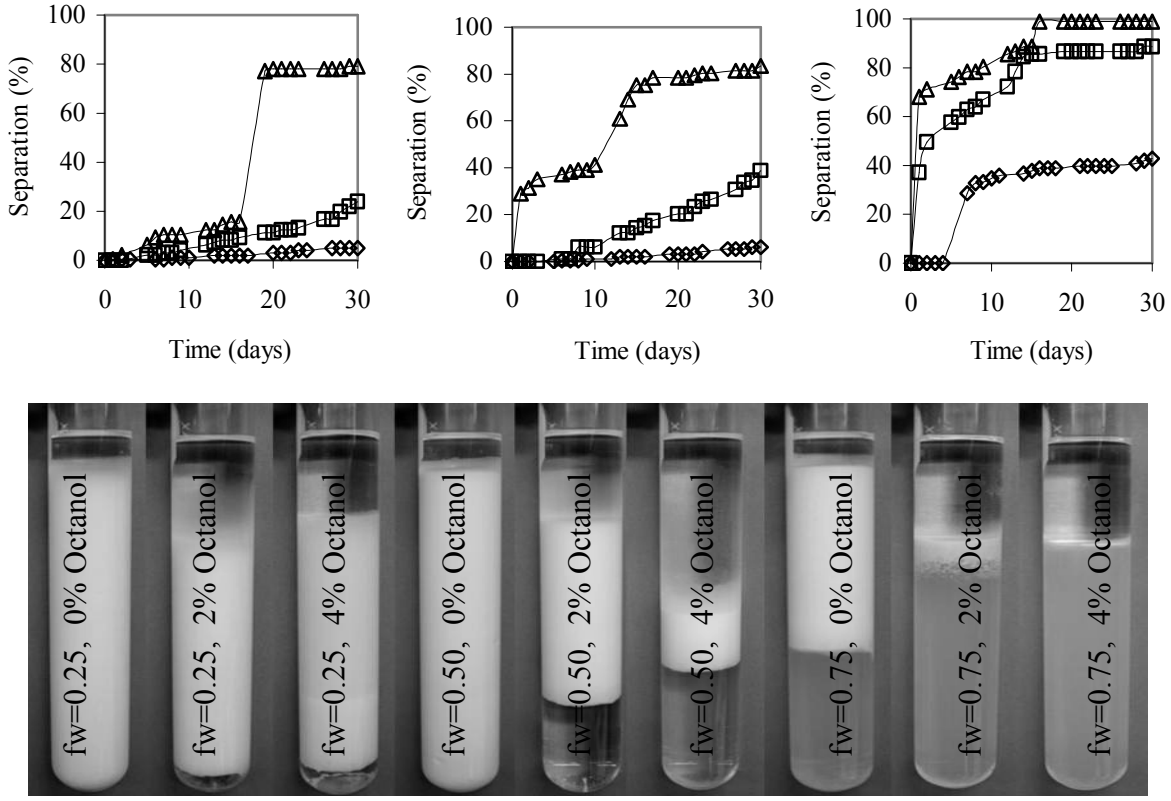

Figure 3-7. Octanol Content Effect on Emulsion Stability

fw = 0.25 (left), *fw* = 050 (middle), *fw* = 0.75 (right). *HLB* = 5.5 with a mixture of Span 80® and Arkopal N 040®, Cs = 2% v/v, *vm* = 13400 rpm, *tm* = 5 min, *T* = 25°C. *Co* = 0 - 4% v/v: (◇) 0%, (□) 2%, (△) 4%. Picture (bottom) after 30 days

As well, a water salinity scan was included in this work. The corresponding conditions are detailed in Table A1-4, appendix A1. The emulsions with the lowest separation after one month were those with a salt content of 4 and 8 g/dL (see Fig. 3-8).

For 12 and 16 g/dL of salt a second emulsion phase, somewhat translucent, was formed. In these cases, the pure paraffin layer and the translucent emulsion were measured together. Even though in some cases salinity increases the stability against sedimentation, stability does not differ significantly from the one obtained without salt. Salinity also increases the density difference; therefore, use of salt in the formulation is not justified, so it is not considered in the final protocol.

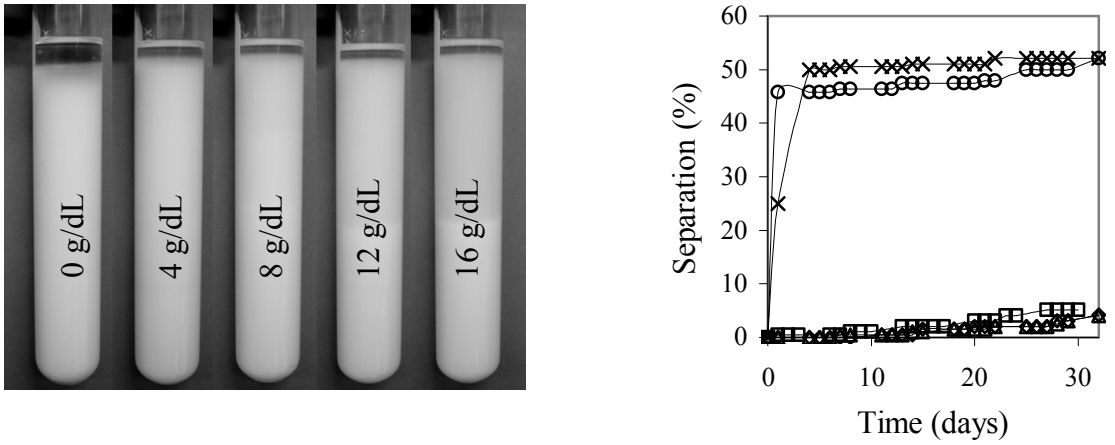

Figure 3-8. Water Salinity Effect on Emulsion Stability

Picture (left) after 30 days. *fw* = 0.25, *HLB* = 5.5 with a mixture of Span 80® and Arkopal N 040®, Cs = 2% v/v, *vm* = 13400 rpm, *tm* = 5 min, *T* = 25°C. *Sa* = 0-16g NaCl/dL Water: (□) 0 g/dL, (○) 4 g/dL, (△) 8 g/dL, (◇) 12 g/dL, (×) 16 g/dL

Figure 3-9 summarizes the effect of mixing conditions on emulsion stability. On the left (Fig. 3-9(a)) the mixing velocity effect is shown. Experimental conditions are detailed in Table A1-5, appendix A1. The selected velocities include all the stirrer operational range. The emulsions that presented the lowest separations were those obtained with 9500 and 6100 rpm. Separation decreases from 6% at 13400 rpm to 4% at 9500 rpm. Reduction in mixing velocity is favorable not only in terms of stability, but also in operational cost. Two other stirrers with velocities up to 2000 and 4000 rpm, respectively, were tested before selecting the Braun stirrer model MR-5550, but in both cases emulsion stability was not satisfactory.

Figure 3-9(b) shows the mixing time effect on emulsion stability. The scan conditions are presented in Table A1-6. The best results were obtained for 5 and 10 minutes of agitation, but for 10 minutes both coalescence and sedimentation were observed.

Figure 3-9(c) shows the mixing type effect on emulsion stability. The scan conditions are presented in Table A1-7, appendix A1. During the first 25 days, all three emulsions showed approximately the same stability; however, after 30 days, a lower separation was obtained with the intermittent mixing at variable velocity.

Comparing the three plots in Figure 3-9, it is clear that a mixing velocity reduction from 13400 rpm to 9100 rpm improves the previous result (Figure 3-9a), but a longer mixing time is not recommended (Figure 3-9b). Depending on mixing conditions, emulsion temperature varied from 31 °C at 6100 rpm and 5 minutes, to 58 °C at 13100 rpm and 20 minutes and this variation in temperature can explain the results. Even though, the changes in stability are not

demonstrated immediately also appear much later. The results on stirrer speed, mixing time and intermittent mixing indicate that low mixing temperature could favor the stability.

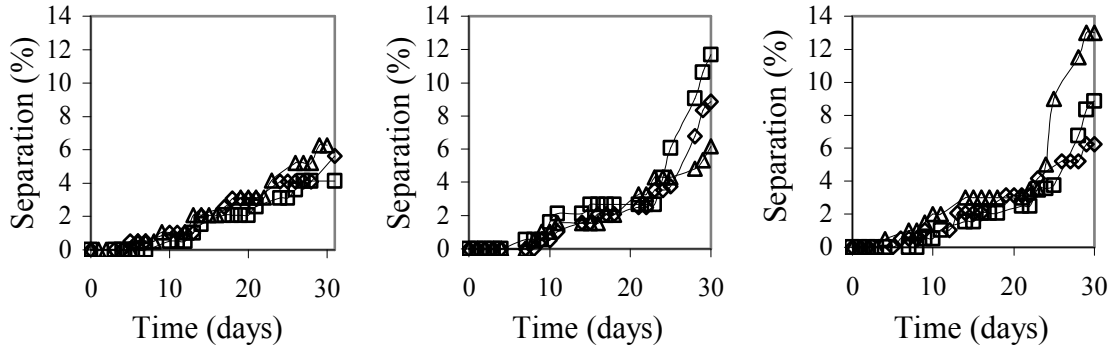

Figure 3-9. Mixing Conditions Effect on Emulsion Stability

fw = 0.50, *HLB* = 5.5 with a mixture of Span 80® and Arkopal N 040®, *Cs* = 2% v/v, *T* = 25°C. (a): Effect of mixing velocity with continuous mixing for 5 min: (◇) 6100 rpm, (□) 9500 rpm, (△) 13400 rpm. (b): Effect of mixing time with continuous mixing at 13400 rpm: (◇) 5 min, (□) 10 min, (△) 20 min. (c):[1] Effect of mixing type: (◇) continuous for 10 min. at 13400 rpm, (□) Intermittent I, (△) Intermittent II

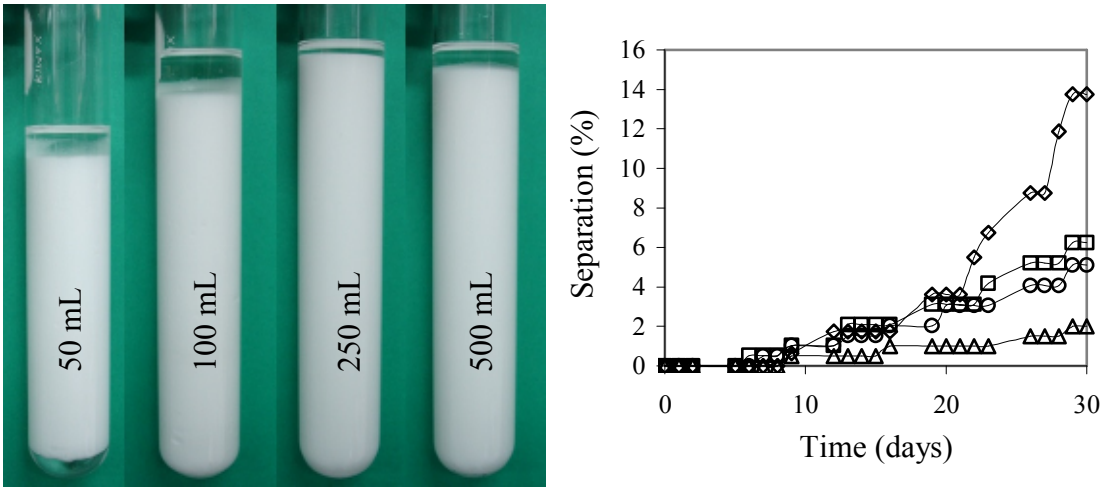

Figure 3-10. Batch Volume Effect on Emulsion Stability

Picture (left) after 30 days. *fw* = 0.50, *HLB* = 5.5 with a mixture of Span 80® and Arkopal N 040®, *Cs* = 2% v/v, *vm* = 13400 rpm, *tm* = 5 min, *T* = 25°C. Batch Volume: (◇) 50 mL, (□) 100 mL, (△) 250 mL, (○) 500 mL

[1] Intermittent I: 5 min at 13400 rpm + 5 min pause + 5 min at 13400 rpm, Intermittent II: 5 min at 8000 rpm + 5 min pause + 5 min at 13400 rpm

Figure 3-10 shows the results of batch volume scans. The experimental conditions are presented in Table A1-7, appendix A1. An emulsion stability reduction was observed when a 50 mL batch emulsion was prepared. This emulsion volume does not ensure an appropriate emulsification, because the stirrer geometry and the beaker used do not provide enough liquid height. In this case coalescence was also observed.

On the other hand, the 250 mL and the 500 mL batch volumes represent an improvement on emulsion stability compared to the results with 100 mL. For 250 mL batch volume, the separation after 30 days is only 2%. Again, an indirect influence of mixing temperature might explain this behavior.

3.3.2 Emulsification Protocol

After the scans were made, an emulsification protocol was developed. 250 mL emulsions were prepared at 9500 rpm during 5 minutes. Reproducibility and total phase separation lower than 10% was ensured.

The protocol was fixed as follows: Define the water content *fw* (0.25; 0.50 or 0.75); for this fw check the corresponding amounts of the rest of the emulsion components in Table 3-2. Add the paraffin in a 600 mL Beaker, add the surfactants (Span 80® and Arkopal N 040®) into the paraffin, stir the mixture with a glass rod, fill a burette with the required distilled water volume, begin agitation at 9500 rpm, and add the water at the specified flow rate. After adding all the water, stir 5 more minutes.

Table 3-2. Emulsification Protocol Data

fw	Paraffin (mL)	N40 (mL)	Span 80 (mL)	Water (mL)	Water Rate (mL/min)
0.25	187.5	1.3	3.7	62.5	13.0
0.50	125.0	1.3	3.7	125.0	25.0
0.75	62.5	0.8	4.2	187.5	38.0

To validate the proposed protocol each emulsion was prepared in triplicate and the stability was evaluated during a month. Average standard deviations in the separation were ±0.28, ±0.25 and ±0.14% for the samples of *fw* = 0.25, 0.50 and 0.75, respectively. Figure 3-11 shows the validation results.

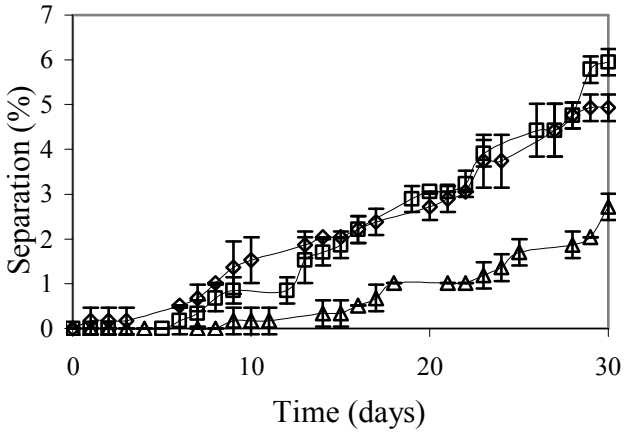

Figure 3-11. Emulsification Protocol Validation

W/O emulsions stabilized by a Span 80® and Arkopal N 040® mixture, *Cs* = 2% v/v, *vm* = 9100 rpm, *tm* = 5 min., *T* = 25°C. *fw*: (◇) 0.25, (□) 0.50, (△) 0.75

3.3.3 Emulsion Properties

All the emulsions formulated with Span 80® and Arkopal N 040® were W/O type. This behavior is in agreement with the theoretical background, since the *HLB* values used were between 4.5 and 6.5. In this case, the surfactant is highly soluble in the oil phase and this affinity favors the formation of *W/O* emulsion.

The average surface diameter of the droplets varies between 3 and 6 microns, but it could not be determined in all cases. Emulsion density was measured in all tests. The density of the pure substances is shown in Table 3-1. Density values varied from 840 to 930 kg/m^3 (measured at 38 °C), basically depending on the water content. The influence of surfactant content, *HLB*, octanol content and water salinity on density was not considerable, and mixing conditions did not affect density.

Figure 3-12 shows water content effect on emulsion viscosity. Viscosity depends on the shear rate, indicating that the emulsions are pseudoplastic fluids: the higher the shear rate, the lower the apparent viscosity. The experimental points demonstrate that increasing the water content produce a more pseudoplastic emulsion. For a constant shear rate, apparent viscosity depends strongly on the water content; for a shear rate of 0.63 s^{-1}, for example, apparent viscosity increases from 200 to 30000 cP, when water content changes from 25 to 75% v/v.

At low water content, drops are too far apart to interact among each other and the only interaction beyond the homogeneous fluid case is that of each drop with its surrounding fluid. When the number of drops increases, drop-drop interactions become predominant, and the resulting frictional effects drive the viscosity increase.

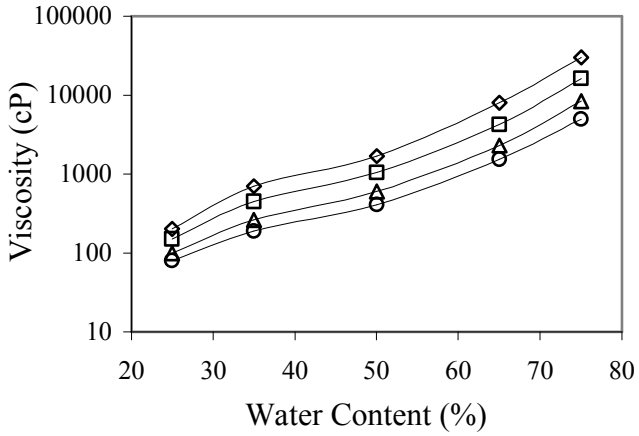

Figure 3-12. Water Content Effect on Emulsion Apparent Viscosity

W/O Emulsions Stabilized by a mixture of Span 80® and Arkopal N 040®. *HLB* = 5.5, *Cs* = 2% v/v, *vm* = 13400 rpm, *tm* = 5 min, *T* = 25°C. Shear Rate γ: (◇) 0.63 s^{-1}, (□) 1.26 s^{-1}, (△) 3.14 s^{-1}, (○) 6.28 s^{-1}

Apparent viscosity was fitted by the power law (equation 2-4). Consistency index $A\ [cP.s^{B-1}]$ and Power Law Index *B* was calculated for each emulsion at different water content values. The results are presented in Table 3-3.

Table 3-3. Power Law Constants for water-in-oil emulsion Stabilized by Span 80® and Arkopal N 040®

Water Content *fw*	**Consistency Index** $A[cP.s^{B-1}]$	**Power Law Index** *B*
0.25	164.26	0.595
0.35	522.62	0.429
0.50	1243.2	0.383
0.65	5391.1	0.293
0.75	20300	0.226

Our results agree with the experience that demonstrates that the emulsion viscosity increases with the internal phase content. Although many empirical relations have been proposed, their precision cannot be determined since these equations do not take into account the pseudoplastic behavior of the emulsion which can be very significant for high *fw* values (Salager, 1999).

Consistency and Power Law Index values shown in Table 3-3 depend on the emulsion water content. For this reason, a polynomial adjustment of A *[cP.s^{B-1}]* and B *[dimensionless]* constants based on the internal phase content is proposed (as shown in equations 3-1 and 3-2),

$$A = 1691505.33fw^4 - 2781930.33fw^3 + 1673741.30fw^2 - 430342.25fw + 40001.21 \quad (3\text{-}1)$$

$$B = 35.691fw^4 - 78.541fw^3 + 62.487fw^2 - 21.719fw + 3.2082 \quad (3\text{-}2)$$

Thus, the apparent viscosity of fresh emulsion can be determined with a model that simultaneously includes the internal phase content effect and the emulsion pseudoplastic behavior.

Figure 3-13 shows shear rate effect on apparent viscosity. Experimental and modeled values are presented together. Modeled values were obtained from the power law, and Consistency Index A *[cP.s^{B-1}]* and Power Law Index B were calculated from equations 3-1 and 3-2, respectively.

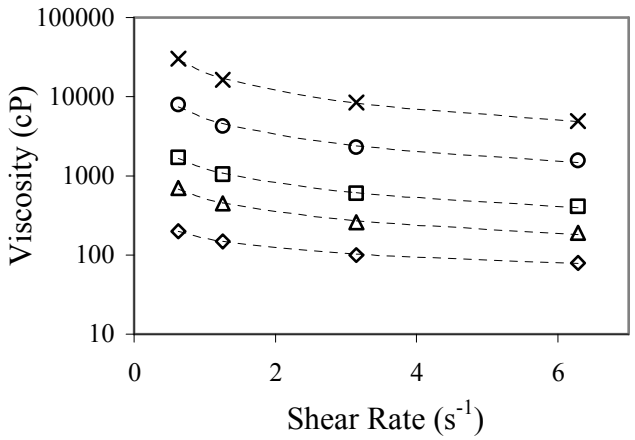

Figure 3-13. Effect of Shear Rate on Apparent Viscosity

W/O Emulsions Stabilized by a Mixture of Span 80® and Arkopal N 040®. *HLB* = 5.5, *Cs* = 2% v/v, *vm* = 13400 rpm, *tm* = 5 min, *T* = 25°C. Symbols correspond to the experimental values and lines correspond to the modeled ones, *fw*: (◇) 0.25, (△) 0.35, (□) 0.50, (○) 0.65, (×) 0.75

Figure 3-14 compares both experimental and modeled apparent viscosity values in a parity diagram. Average error was 0% and the standard deviation was 4%. The viscosity of the external phase has a remarkable influence on the emulsion viscosity; therefore, the proposed model is only valid for oil water emulsions where the external phase viscosity is similar to that of the used paraffin.

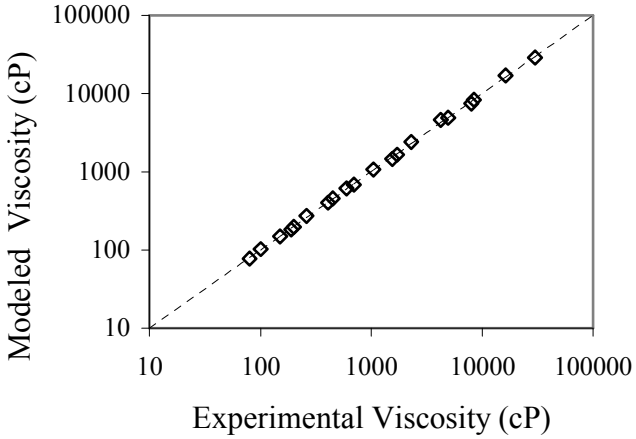

Figure 3-14. Comparison between Modeled and Measured Apparent Viscosity W/O Emulsions Stabilized by a Mixture of Span 80® and Arkopal N 040®. *HLB* = 5.5, *Cs* = 2% v/v, *vm* = 13400 rpm, *tm* = 5 min, *T* = 25°C, *fw*: 0.25-0.75, γ: 0.63-6.28 s^{-1}

Octanol content and water salinity effect on apparent viscosity was also measured. Results are shown in Figures 3-15 and 3-16, respectively. The higher the alcohol content, the lower the apparent viscosity. The Octanol effect on emulsion viscosity can be explained by a reduction in the external phase viscosity. The opposite effect is obtained for the water salinity, where the salinity effect is much stronger: the higher the water salinity, the higher the apparent viscosity. Although in this experiment the droplet size could not be measured regularly for all salt concentrations, a decrease in the average surface diameter x_s from 5 microns to no detectable values was demonstrated. The reduction in droplet size and a probably narrow size distribution explain the increase in viscosity.

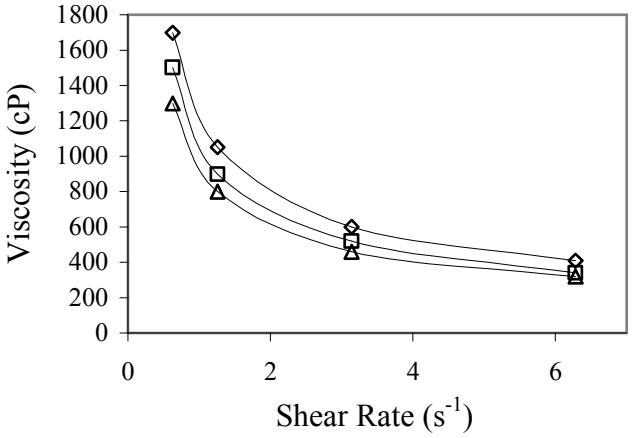

Figure 3-15. Octanol Content Effect on Emulsion Apparent Viscosity W/O Emulsions Stabilized by a mixture of Span 80® and Arkopal N 040®. *HLB* = 5.5, *Cs* = 2% v/v, *fw* = 0.50, *vm* = 13400 rpm, *tm* = 5 min, *T* = 25°C, *Co*: (◇) 0%, (□) 2%, (△) 4%

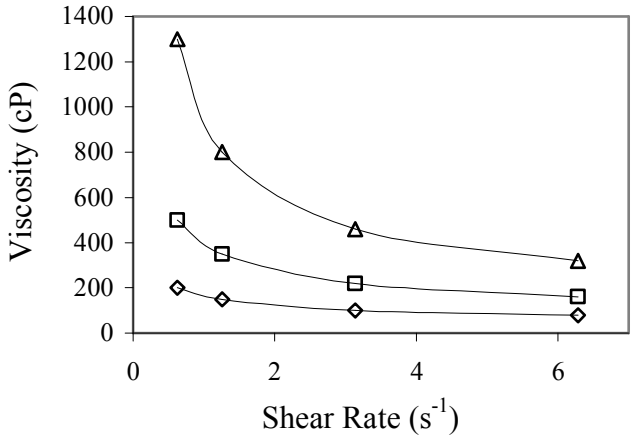

Figure 3-16. Water Salinity Effect on Emulsion Apparent Viscosity

W/O Emulsions Stabilized by a mixture of Span 80® and Arkopal N 040®. *HLB* = 5.5, *Cs* = 2% v/v, *fw* = 0.25, *vm* = 13400 rpm, *tm* = 5 min, *T* = 25°C, *Sa*: (◇) 0 g/dL, (□) 8 g/dL, (△) 16 g/dL

In Figure 3-15, for a shear rate of 0.63 s^{-1}, viscosity decreases by 200 cP when octanol content increases from 2 to 4%, but when water salinity increases from 8 to 16 g/dL (see Fig. 3-16) viscosity increases by 800 cP.

3.4 Conclusions and Recommendations

- Span 80 and Arkopal N40 mixtures stabilize water in paraffin emulsions in a wide range of water content. A validated protocol shows maximal standard deviations of ±0.28% in emulsion stability reproducibility and, in all cases, water plus paraffin separation was lower than 6% v/v.
- The *HLB* required to produce a most stable emulsion depends on the emulsion water content; therefore, a *HLB* scan is recommended when nonionic surfactants are used. Mixing velocity and emulsion batch scans can optimize the emulsion stability.
- Surfactant content and water salinity do not influence significantly on stability of water in paraffin emulsions stabilized by Span 80® and Arkopal N040® mixtures. In contrast, octanol presence harms the stability of such emulsions.
- Water in paraffin emulsions stabilized by Span 80® and Arkopal N040® mixtures show a pseudoplastic rheological behavior at both low and high internal phase content. A model based on power law, which takes into account the water content, reproduces

very well the experimental viscosity values. Water salinity increases remarkably the emulsion viscosity.

4 Emulsion Characterization

Before testing an emulsion separation technique, a characterization is required. The complete characterization of an emulsion involves a detailed chemical and physical analysis of all of its components, as well as any bulk property that might be of interest. Waste oil emulsion characterization is studied in this chapter. In order to characterize an emulsion, it is necessary to determine the amount of each phase present, the nature of the dispersed and continuous phases, and the disperse phase size distribution.

Accurate determination of oil, water and solids content is one of the most important aspects of emulsion characterization (Mikula, 1992). A large number of techniques like near infrared spectroscopy (Orr, 1988; Gossen et al., 1993; Santos et al., 1998; Hallevik et al., 2000), X-ray, light and neutron scattering (Kaler et al., 1983; Münch et al., 1993; Caldwell et al., 1989) based on widely different scientific principles have found use in the measurement of droplet size, but microscopy is often the last word in size distribution determination of dispersed systems (Mikula, 1992; Kano et al., 1984). Therefore, microscopy (Ebert et al., 1983; Bradbury, 1990; Drelich et al., 1992) and photomicrography (Mason et al., 1995; Garti, 1997) have been extensively used for these purposes.

4.1 Experiments and Handling of Data

Heavy and medium oil samples from six different pits of production were analyzed: Acema 100, Guara 2. Merey 31, Fosa 1, Fosa 2 and Orocual. All samples were tested four times. Viscosity varies from 100 to 1500 cSt. Characterization was made in two stages. In the first stage water and solids content were determined by Distillation (*ASTM D-4006*) and Extraction (*ASTM D-473*), respectively.

The distillation apparatus, shown in Figure 4-1, consists of a glass distillation flask, a condenser, a graduated glass trap and a heater. The sample is heated under reflux conditions with a water immiscible solvent (Xylene) which co-distills with the water in the sample. Condensed solvent and water are continuously separated in a trap; the water settles in the graduated section of the trap, and the solvent returns to the distillation flask.

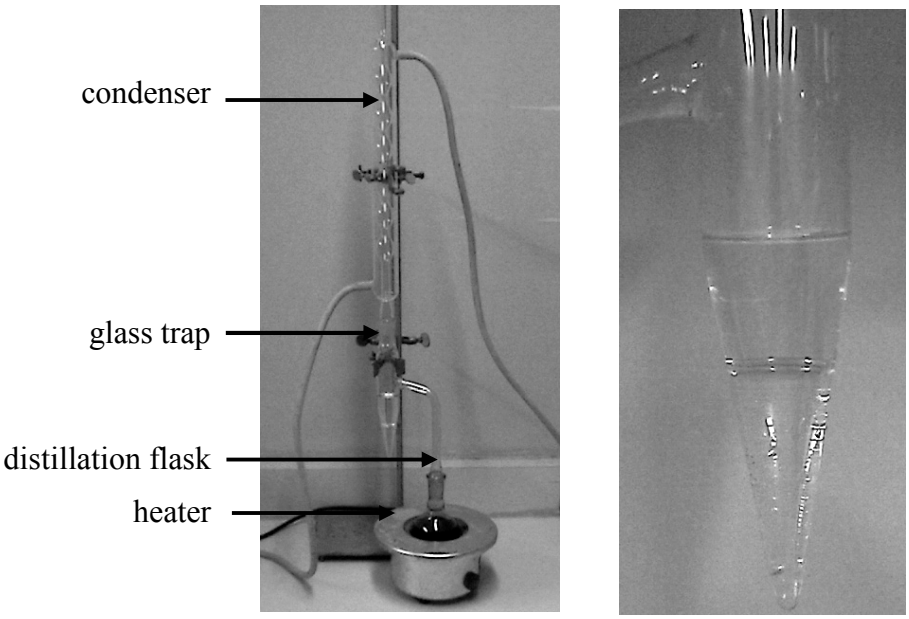

Figure 4-1. Distillation Apparatus for *ASTM D4006* Test

(a) General view, (b) glass trap detail

The extraction apparatus, shown in Figure 4-2, consists of a soxhlet extractor, an extractor flask, a condenser, an extraction thimble and a heater. The oil sample, contained in the filter case, is extracted with hot toluene until the residue reaches constant mass. The mass of residue, calculated as a percentage, is reported as sediment by extraction.

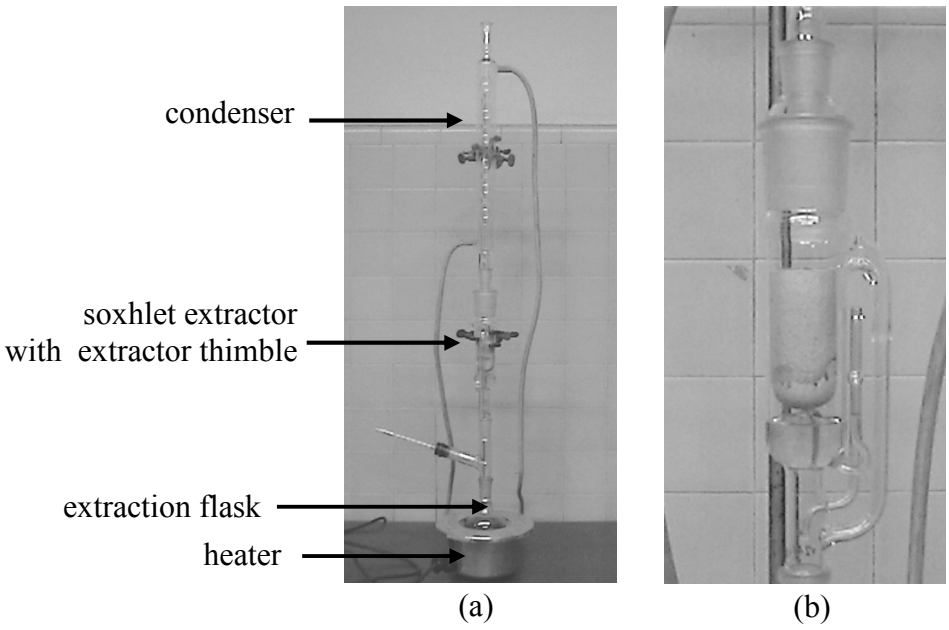

Figure 4-2. Extraction Apparatus for *ASTM D473* Test

(a) General view, (b) soxhlet extractor detail

For particle size determination, an optical microscope Nikon *MED-600* (see Fig. 4-3) with camera and the image analysis software Image Pro Plus 4.0 from Media Cybernetics were used.

Samples were prepared by placing a drop on the microscope slide with a fine needle, spreading it in order to provide a thin layer that lets pass the light. Dilution with xylene was tested, but it changed drastically the particle size distribution of the emulsions within seconds and therefore, it was not used. The microscope technique used was brigthfield with transmitted light. Magnifications of 5X, 10X and 20X were included for all samples; for Fosa 1, 50X was also utilized.

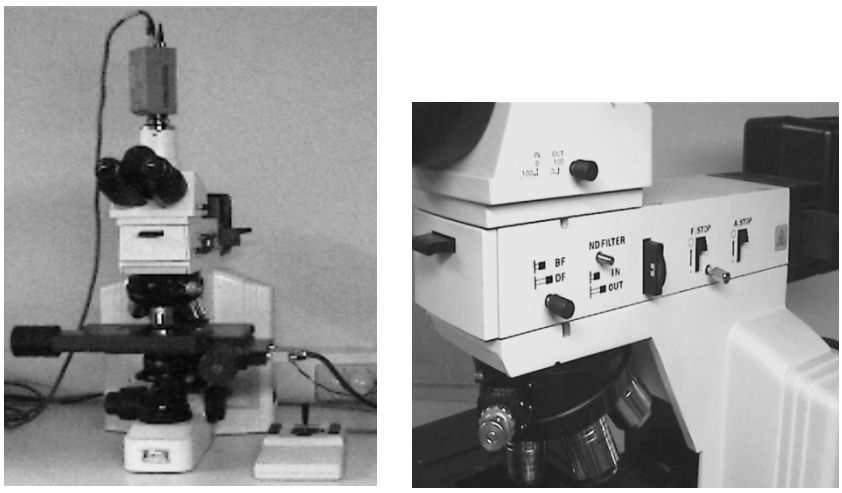

(a) (b)

Figure 4-3. Microscope Nikon *MED-600*

(a) General view, (b) functions detail

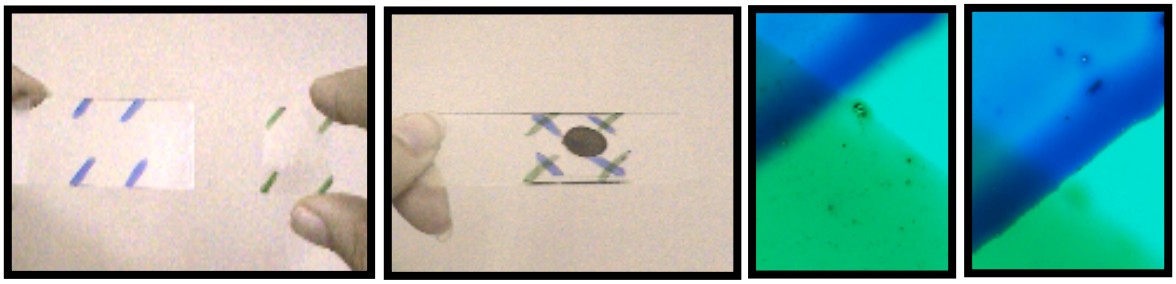

(a) (b) (c) (d)

Figure 4-4. Thickness Sample Determination

(a) Slide and cover glass marks, (b) sample with marks, (c) cover focal point, (d) slide focal point

The sample thickness was measured microscopically by drawing marks on the internal faces (towards the sample) of both the microscope slide and the cover glass (see Figure 4-4a and 4-4b), and checking the travel in mm of the fine adjustment knob from the focal point of the cover green mark (Fig. 4-4c) to the focal point of the slide blue mark (Fig. 4-4d).

Before characterizing the system, water drops and solids were identified and discriminated by using a color mask: The drops of water (white in Figure 4-5a) were colored in blue and the solid particles (black in Figure 4-5a) were colored in green. Solids were differentiated from droplets by their opaque character, whereas droplets let pass the light through them. The particle analysis of drops and solids is made separately. Figure 4-5 shows the use of the color masks.

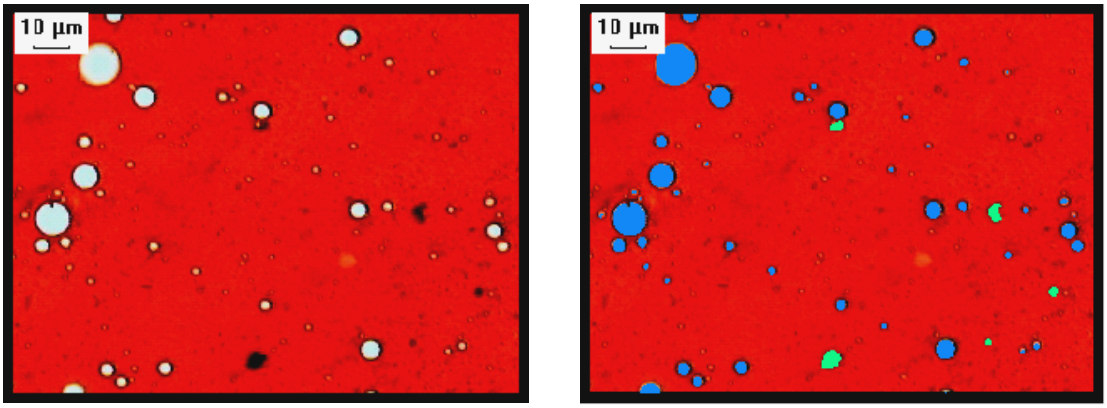

(a) (b)

Figure 4-5. Use of the Color Mask to Discriminate Droplets from Solids
(a) Original picture, (b) picture with blue mask for droplets and green mask for solids

Three counts on each sample were made for characterization of water: in the first and second counts the drops and solids in contact with the borders of the pictures were excluded. The first count was based on the differentiation of the drop color from the crude continuous phase dark color; for this reason the agglomerated drops were counted like a single drop as shown in droplet number 20 in Figure 4-6b.

In the second count the separation of the drops that were agglomerated in the first count was made, based on the slight change of colors appreciated in the edges of the drops, as well as in the change of the curvature of agglomerate drops. Figure 4-6(c) is an example of the second count. Droplet number 20 in Figure 4-6b is separated in droplets number 7, 21, 28, 34 and 40. The combination of the first and second count allowed identifying the agglomerate drops by means of comparison the coordinates of the center of mass. Coordinates from nonagglomerate particles appear in both counts, coordinates that appear only in the first count are from

agglomerate, and coordinates that appear only in the second count correspond to the discrimination of the agglomerate as separate drops. Both counts were used to determine the particle size distribution.

The third count included also the droplets and solids in contact with the borders of the pictures for calculation of the phase ratio. Figure 4-6(d) is an example of the third count. There, the droplet number 5 that does not appear in the first and second count is also identified with the blue mask and included. The actual particle size of the droplets in contact with the borders can not be accurately calculated and, therefore, these particles are not taken into account for particle size distribution purpose, but only for water volume estimation. For solids, only the first and the third counts were made because of the solids irregular shape.

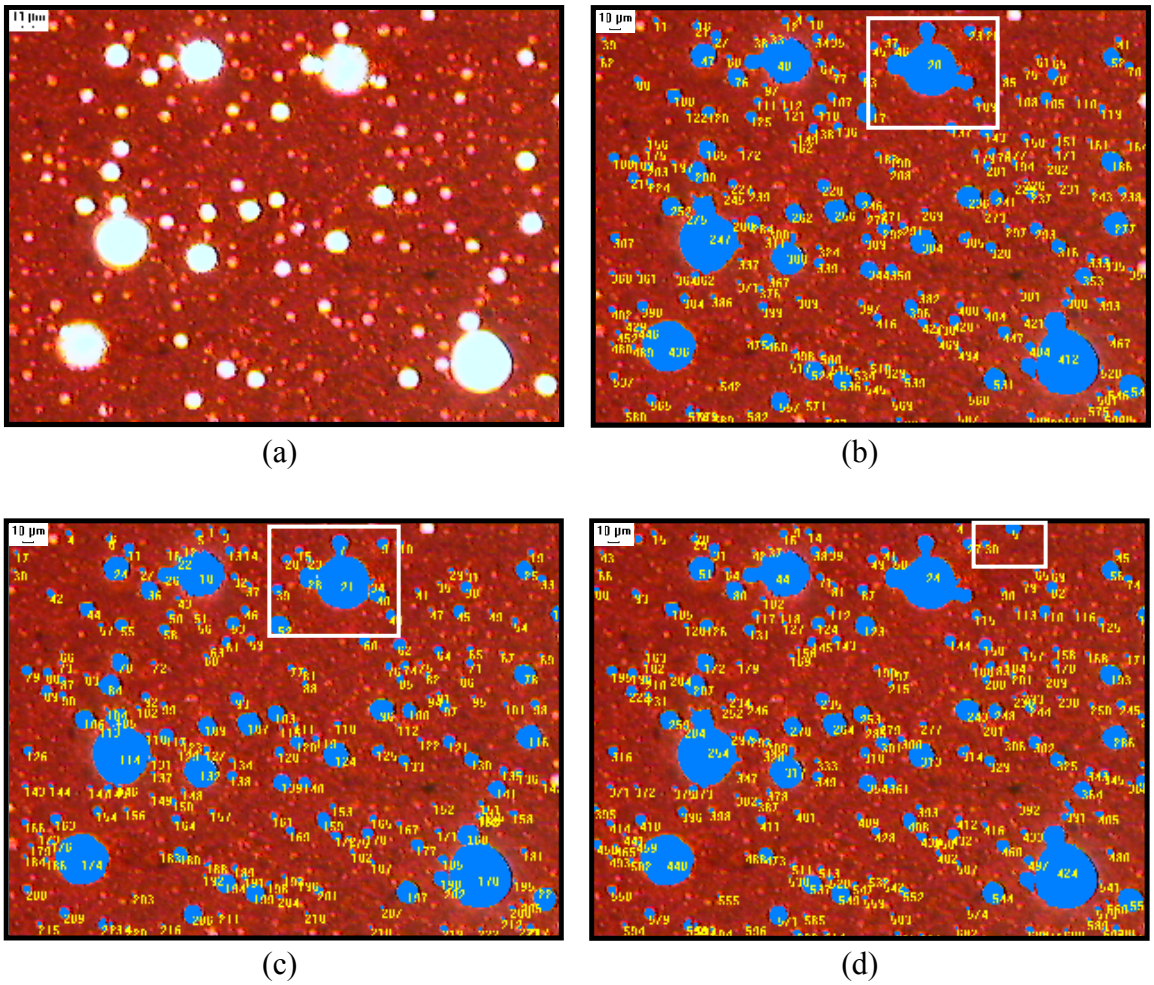

Figure 4-6. Droplet Counts

(a) Original picture, (b) first count for droplets: without borders and without agglomerate discrimination, (c) second count for droplets: without borders and with agglomerate discrimination, (d) third count for droplets: with borders and without agglomerate discrimination

In each count the number of particles, projected area and coordinates of mass center of each one was determined. These data were manipulated in order to calculate the particle size distribution for solids and water, equivalent diameters, water content, solid content, and percentage of agglomerated water. Figure 4-7 shows the four test results for Acema 100 sample.

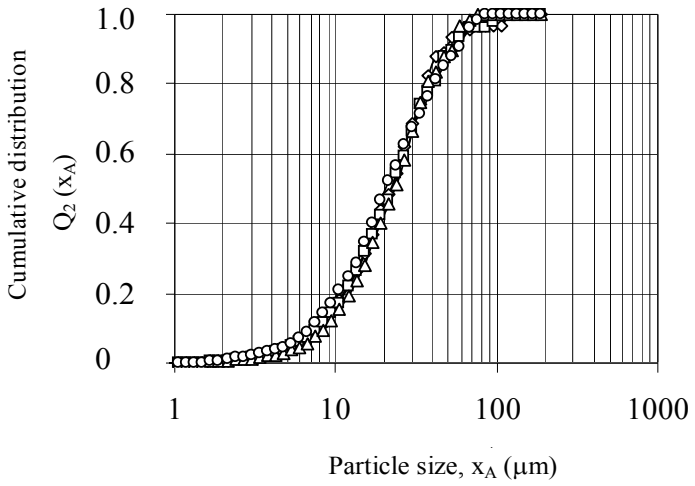

Figure 4-7. Reproducibility of Droplet Size Distribution Q_2 (x_A)
Determined by Optical Microscopy

Sample Acema 100. Magnification used: 20X. Sample thickness: 29.5 μm. Droplets in contact with the borders of the pictures were excluded. Number of particles counted in test 1: 6175, number of particles counted in test 2: 5944, number of particles counted in test 3: 6221, number of particles counted in test 4: 5832. (◇) test 1, (□) test 2, (△) test 3, (○) test 4

4.2 Corrections for Image Analysis

Because each sample was analyzed with three different magnifications, the observed differences for a sample are due to the capacity of a given magnification to distinguish particles in a certain size range. The proper combination of several magnifications leads to a more reliable result. Drops were counted, measured and classified into different groups according to their sizes. A combined magnification curve was built selecting for every size range the magnification for which the greatest number of particles was observed. This criterion allows including in the combined distribution all the particles of each size that were detected by any one of the used magnifications. If a particle was detected at least by one magnification it is because it exists, because the sample area is the same, and the combined distribution is always a more reliable result than the one obtained with a single magnification.

Figure 4-8 shows an example of the combined magnification effect on the particle size distribution.

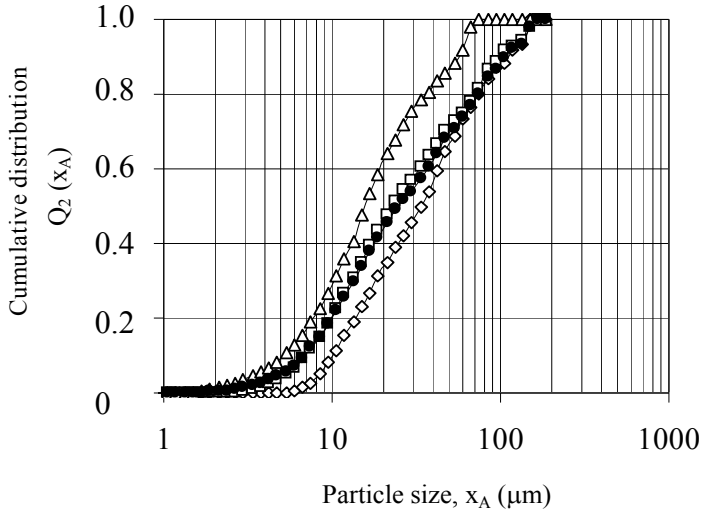

Figure 4-8. Effect of the Used Magnification on the Droplet Size Distribution Q_2 (x_A) Sample Guara 2. Sample thickness: 30.2 μm. Droplets in contact with the borders of the pictures were excluded. Number of particles counted at 5X: 4308, number of particles counted at 10X: 9368, number of particles counted at 20X: 9109, and number of particles counted with the combined magnification: 13350. (◇) 5X magnification, (□) 10X magnification (△) 20X magnification, (●) combined magnification

An important amount of drops is present as agglomerates and could be analyzed as single drops, generating errors in the results. In order to identify the agglomerated drops, the centers of mass location for each "particle" obtained by the first and the second count were compared. The coordinates that appear just in one count correspond to droplet agglomerates in the first count which are separated in the second one. Differences up to 50% were observed in the average size by the separation of agglomerate drops.

A correction was also made in the calculation of the diameter for "deformed" drops. These drops were identified as those with an equivalent diameter greater than the thickness of the film of the sample under study. With solids this correction was unnecessary because all particles were smaller than the film thickness. Figure 4-9 shows that for big particles, the volume is overestimated if they are considered like spheres because the droplets are squashed. The deformed drops actual diameters were recalculated considering them as cylinders with the base equal to the projected area and the height equal to the film thickness. Considering squashed drops as cylinders reduce the overestimation in volume.

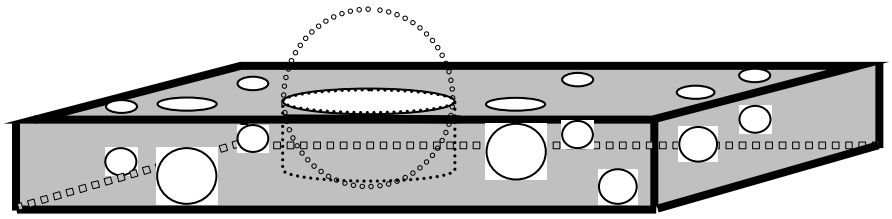

Figure 4-9. Droplet Volume Estimation

Projected area is used to calculate the droplet volume. Small droplets are assumed to be spherical but squashed droplets are estimated as cylinders

Not always it is possible to visualize in the microscope simultaneously all the particles that are distributed along the thickness of the sample. For this reason it was necessary to calculate the focal depth for all of the samples. For droplets, the focal depth was defined as the range of visibility of selected droplets of about 10 μm diameter. Here however, the total film thickness of all samples was smaller than the focal depth. At the focal point, the greatest number of particles was observed, and when moving away from it, the number of visible droplets was always smaller. No new droplets did appear indicating that the thickness of the sample was smaller than the focal depth, and all the droplets that could be distinguished were observed at the focal point.

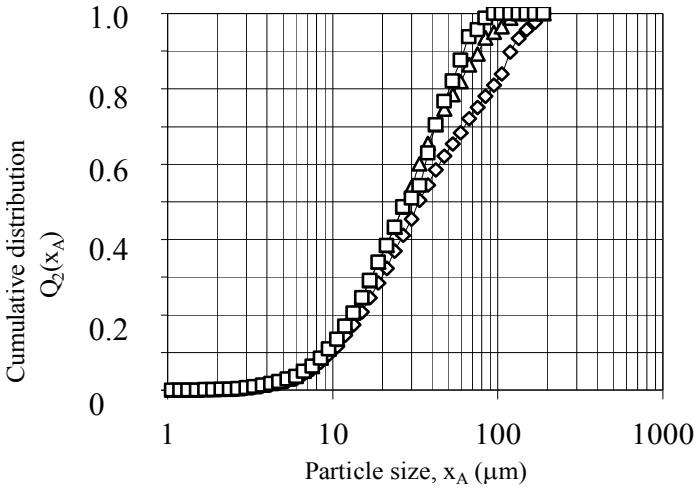

Figure 4-10. Effect of All Corrections on Droplet Size Distribution Q_2 (x_A)

Sample Acema 100. Sample thickness: 29.5 μm. Droplets in contact with the borders of the pictures were excluded. Number of particles counted: 18689. Combined magnification 5X+10X+20X. (◇) original, (△) with agglomerates discrimination, (□) with agglomerates discrimination and deformation correction

On the other hand, the opaque appearance of the solid particles also allowed their analysis in all the thickness of the sample. Figure 4-10 demonstrates how the particle size distribution of a sample is varied when applying the different corrections.

4.3 Results and Discussion

Cumulative and density distributions and equivalent diameters in number, area and volume were determined on all samples for both solids and water droplets. Number and area distribution are direct results of the image analysis, whereas the volume distribution was calculated assuming that particles were spheres, although for solids this is not true because the shape factor is not considered. However, this calculation allows the comparison with *ASTM* analysis which is in volume, and allows inferring certain characteristics of the dispersion that otherwise cannot be detected.

Figure 4-11 is an example of size distributions for solids particles of Merey 31 sample. Solids are in the range from 1 to 30 μm, whereas water droplets vary from 1 to 95 μm.

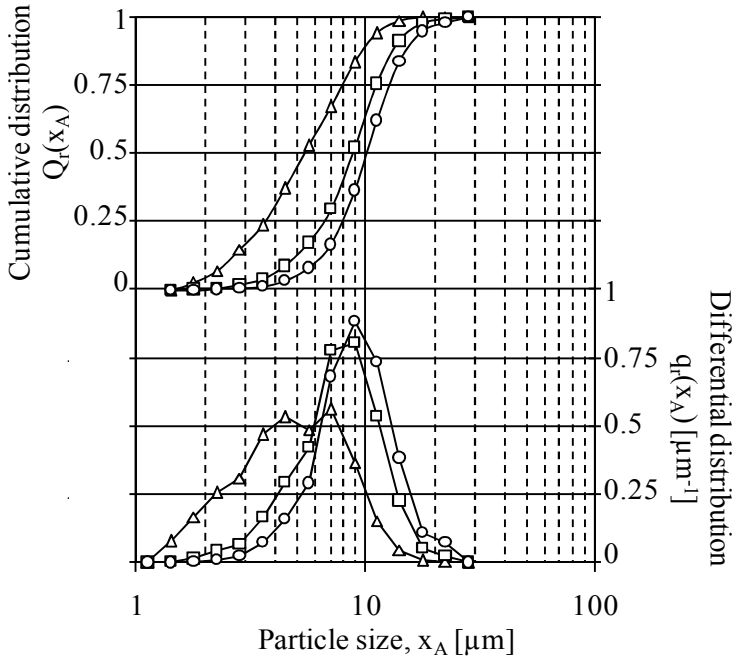

Figure 4-11. Cumulative (top) $Q_r(x_A)$ and density size distribution (bottom) $q_r(x_A)$ for solids determined by optical microscopy

Sample Merey 31. Sample thickness: 36.38 ± 4.94 μm Solids in contact with the borders of the pictures were excluded. Number of particles counted: 2020. Combined magnification 5X+10X+20X. (△) number: r = 0, (□) area: r = 2, (○) volume: r = 3

Minimum size is limited by the observation capacity that can be reached and was 1 μm for 20X magnification, and 0.45 μm when a 50X magnification was included. Only for Guara-2 sample a maximum limit of 115 μm was obtained, while for the other samples the biggest particle was smaller than this size. Size distributions for water and solids of all tested emulsions are presented in appendix A2.

Figures 4-12 and 4-13 show some results of the characterization performed for the Merey 31 sample. The combined distribution that includes all the used magnifications was manipulated to calculate the water content. The reported values are the average of four measurements and the maximum standard deviation in total water content between 6 tested emulsions was 2%.
In Figure 4-12 the effect of different corrections on water content is shown. When the agglomerated drops are discriminated, the water content decreases. The most significant difference is observed when the drop size is corrected according to the analyzed sample thickness. This correction implies to discriminate the squashed drops and to calculate their volume from the projected area considering that it does not correspond with the volume of a sphere. Without this correction the volume of the large drops is overestimated and these drops have the stronger influence in volume estimation.

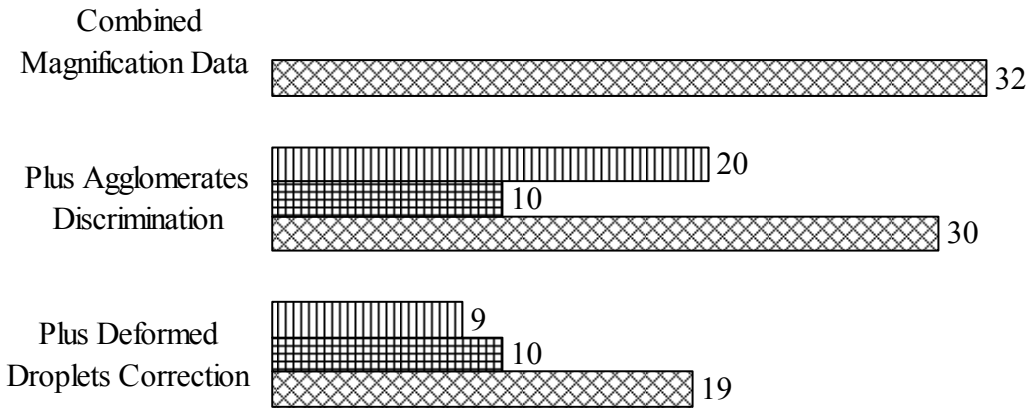

Figure 4-12. Effect of Each Correction on Water Content (%)
Determined by Optical Microscopy
Sample Merey 31. Sample thickness: 36.38 μm. Droplets in contact with the borders of the pictures were included. Combined magnification 5X+10X+20X. (▨) total water content, (▦) agglomerated water, (▥) non agglomerated water

In Figure 4-13, the diagram on the top summarizes the results obtained by optical microscopy after all corrections, while the diagram on the bottom shows water and solids contents obtained by distillation and extraction, respectively. Continuous phase content (oil) was always calculated by difference.

ASTM analysis does not give information about the state of agglomeration of the drops as it can be obtained by microscopy, and in some cases water content obtained by microscopy is lower than *ASTM* result. Part of the difference can be explained by the fact that by microscopy, drops out of the detection range are not counted, and because free water existing in large droplets or "water pockets" is excluded when samples for microscopy are prepared. In the case of solids there are also differences that are explained by non-detected particles and because volume is calculated from the weight using a general density value according with the *ASTM* standard.

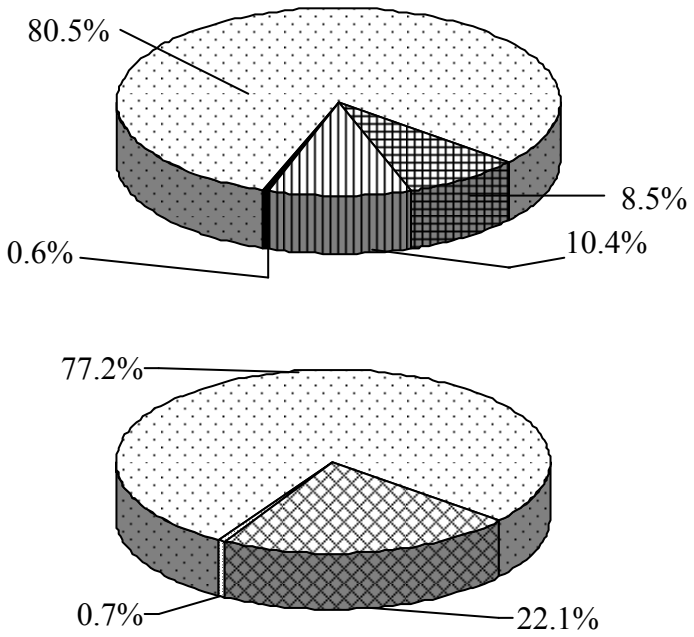

Figure 4-13. Water and solids content (%) determination:
Comparison between ASTM (bottom) and microscopy (top) results

Sample Merey 31. *ASTM*: water content by distillation *ASTM D-4006* and solids content by extraction *ASTM D-473*. Microscopy: droplets and solids in contact with the borders of the pictures were included, combined magnification 5X+10X+20X, sample thickness: 36.38 ± 4.94 μm, water content determination include agglomerate discrimination and thickness correction. (▨) total water, (▮) solids, (□) crude oil, (▤) non agglomerated water, (▥) agglomerated water

Finally, microscopy results can suffer from sampling errors due to the restricted sample size, when compared with *ASTM* results. The separate analysis of both methods, *ASTM* Standards and Microscopy, does not show relevant information about the dispersion state. A more complete picture can be obtained by comparison of the *ASTM* and microscopy results.

The cross-linked method is a new correction by normalization based on the statement that the actual water and solids contents are those measured by the standard techniques. So in fact, the correction shows the water undetected by microscopy. Application of this method shows that, for example, the emulsion Guara 2 (Figure 4-14) has 2.0 % v/v water that is present in the form of free water or as droplets out of the observation range, plus 20.1 % v/v of water in form of drops and 18.0 % v/v water in form of agglomerates, last both in the range between 1 and 90 μm. The total water content is then the same as obtained by *ASTM* procedures.
On the other hand, solids can be distinguished in two groups: 1.4% v/v are particles between 1 and 25 μm and 0.3% are particles smaller than 1 μm. The same analysis correction was applied to the 5 remaining samples and the results are reported in Appendix A4.

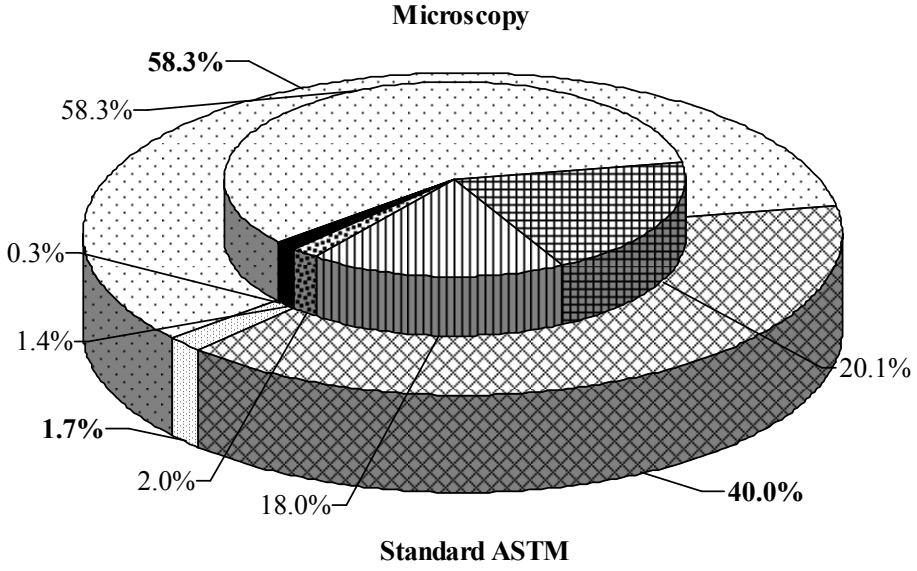

Figure 4-14. Water, oil and solid phase volume ratio determined by cross-linked method Sample Guara 2. Microscopy (top): combined magnification 5X+10X+20X, sample thickness: 61.38 ± 18.44 μm. *ASTM* (bottom): water content by distillation *ASTM D-4006* and solids content by extraction *ASTM D-473*. (▨) total water, (■) solids, (□) crude oil, (▦) non agglomerated water, (▥) agglomerated water, (▩) non detected water, (▫) non detected solids

4.4 Conclusions

- Optical microscopy allows characterizing complex systems of oil, water and solids differentiating all the phases even for dark and highly viscous samples and giving droplet and solids size distributions.
- Knowing the particle size distribution of droplets and solids allows a more detailed analysis of the dispersion and even making some inferences about its stability.
- A new handling procedure for the image analysis results of water and solid in oil mixtures has been proposed, including some new features:

  The use of combined magnifications allows correcting the original data in such a way that all particle size ranges are included and a more reliable particle size distribution is generated.

  Additional corrections to the original data are needed in order to recalculate the drop size of those droplets that are deformed by the sample preparation and in order to estimate the additional amount of small droplets that are not counted due to the small focus depth.

  The use of the image analysis software capabilities allows differentiating between isolated and agglomerated drops of water.
- Phase concentration obtained by microscopy differs significantly from the values obtained by standard *ASTM* techniques, while microscopy provides additional valuable information about the dispersion state. Therefore, the cross-linked method was developed whereby the phase concentrations from microscopy are re-normalized to the *ASTM* data.

5 Emulsion Separation: The Collector Material Concept

Packings can improve the physical separation of immiscible phases according with its capacity to provide interfacial contact area and its preferential affinity for one of the phases. The wetting concept has been used in the last years to increase the separation in different processes involving emulsions.

Dezhi et al. (1999) studied demulsification of water-in-oil droplets with wetting coalescence materials using conventional stirred and packed columns. They tested four kinds of natural fibers and two kinds of inorganic materials, obtaining that natural fiber A, selected from shaves of wood showed the best performance in demulsification. The packed column showed much better performance in terms of demulsification efficiency and repeated use of the recovered oil phase for extracting cadmium in a simulated wastewater.

Ito et al. (2002) studied the rapid separation of *n*-decane oil droplets in the presence of sodium dodecyl sulfate (SDS) by a packed bed column with fibrous ferro-nickel slag (FS); the results were discussed in terms of electric interfacial interaction of both an *n*-decane droplet and a collector medium. They suggested that separation using surface characteristics is a promising method for the recovery of stable emulsified oil droplets.

Shin and Chase (2004) determined the wettability effect on the coalescence mechanism in fibrous filters. Experimental results from tests on coated glass rods were presented and flow of water-in-oil emulsion around the glass rods was observed. When the rod surface is wetting, the disperse phase coats the rod, whereas when the surface is non-wetting drops neither stick easily to the surface nor coat it, but slide around to the downstream side, where they are dragged off the rod.

Kapilashrami et al. (2004) investigated the substrates effect of the hydrophobic/hydrophilic character on the drying behavior of dilute silicone oil-in-water emulsions by light microscopy and ellipsometry, and showed that emulsion droplets do not adsorb to the hydrophilic substrate. The hydrophobic substrate, on the other hand, destabilizes emulsion and increases coalescence rate. They suggested that destabilization is promoted by the strong interaction between the emulsion droplets and the hydrophobic substrate.

In this work, the effect of packing material on centrifugal separation of highly stable water-in-oil emulsions is studied. A fundamental characteristic of surfactants is their tendency to adsorb at interfaces in an oriented manner. Surfactant orientation and packing at the interface

determines how the interface will be affected by the adsorption, i.e., whether it will become more hydrophilic or more hydrophobic (Rosen, 2004).

The contact angle of a water drop placed on the solid surface can be used to determine the predominant orientation of the adsorbed surfactant molecules. The greater the contact angle, the higher the surface hydrophobicity.

The contact angle can not be quantified when the solid is formed by finely divided particles. In this case, if surfactant adsorption turns the solid more hydrophilic, it will disperse better in water after adsorption; but hydrophobic particles will either float or settle down of the water faster after surfactant adsorption. Alternatively, the particles may be shaken with a mixture of equal volumes of water and a no polar solvent (e.g., hexane). If the particles have become more hydrophobic by surfactant adsorption, they will disperse better in the no polar phase than before; but if they have become more hydrophilic, they will disperse better in the aqueous phase (Rosen, 2004).

5.1 Experiments and Results

5.1.1 Emulsion Formulation

Stable synthetic water-in-oil emulsions with 25, 50, 75 and 80% v/v water, and 2% v/v surfactant were prepared on the basis of the protocol described in Section 3.2.2. 500 mL of emulsion (water plus paraffin) was prepared in each run and the *HLB* value was 4.3 corresponding to Sorbitan Monooleate pure.

5.1.2 Materials Preselection and Preliminary Tests

Solids with different hydrophobicities were preselected by a study of Zavarce (2006) and are described on Table 5-1.

Hydrophobicities were estimated from the wettability observed when droplets of water and paraffin were placed on the material surface. Void fraction was calculated as the ratio between the free volume of 10g of material (measured with water) and the measurable volume of the material in a graduated conic test tube of 15 mL volume.

Table 5-1. Characteristics of preselected materials

Material		Behavior	Void Fraction
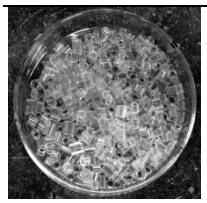	Glass	hydrophilic	0.69
	Polypropylene	lipophilic	0.37
	PVC	lipophilic	0.71
	Metal	dual	0.72
	Cedar Wood	lipophilic	0.62
	Saman Wood	lipophilic	0.63
	Peanut Shell	lipophilic	0.75

Figure 5-1 shows the peanut shell apparent wettability by water (top) and paraffin (bottom). It can be observed that the water droplet keeps its shape while the paraffin droplet spreads on the peanut shell surface, indicating that the material is preferentially wetted by paraffin; therefore, it can be defined as lipophilic. A hydrophilic material is defined as well wetted only by water, and dual material refers to the one that is wetted by both water and paraffin.

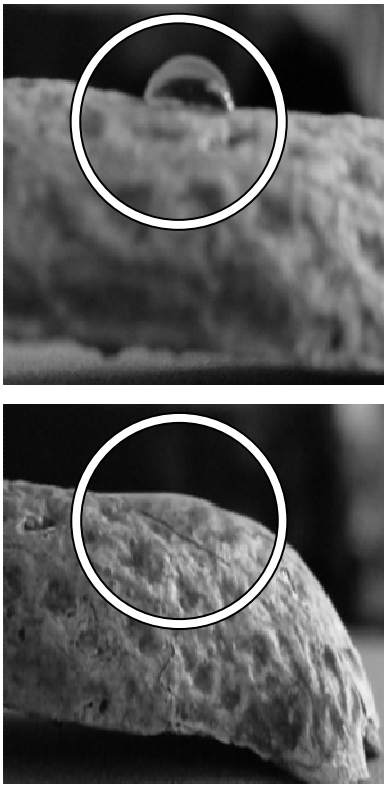

Figure 5-1. Water/ Peanut Shell (top) and Paraffin/ Peanut Shell (bottom) Wettability

Figure 5.2 shows an example of the distribution oh the phases on a sample. Samples with 9 g of emulsion (e) and 1 g of material (m) were mixed with a glass rod in a centrifuge test tube for some seconds and were centrifuged at 2600 rpm. Water-in-oil emulsion stability against both clarification and coalescence was measured as a function of centrifugation time.

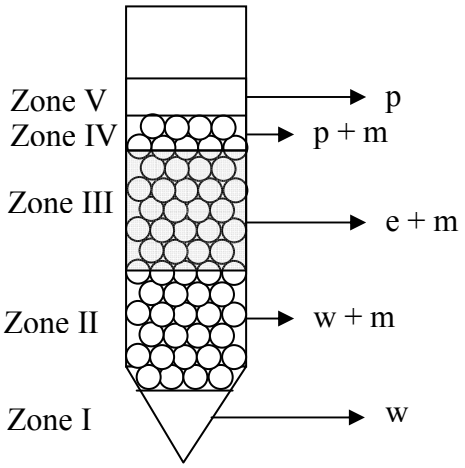

Figure 5-2. Example of the Phases Distribution on a Sample

Clarification is defined as the recovered paraffin volume (p) because the water droplets move to the bottom leaving clarified paraffin on the top. Coalescence is given as the recovered water volume (w). In the most general case, water is recovered in zones I and II, whereas paraffin is recovered in zones IV and V. For liquid phase volume determination in zones II and IV it is necessary to consider the material void fraction.

The kinetics of water and paraffin separation in preliminary tests is shown in Figures 5-3 and 5-4, respectively. Two statements are obtained from these results: (1) for some materials it is possible to increase the water and paraffin recovered percentage in comparison with the absence of material; (2) there is a big difference between Cedar wood and Saman wood curves for both water and paraffin recovery. Differences can also be observed, in the case of polypropylene and *PVC* curves.

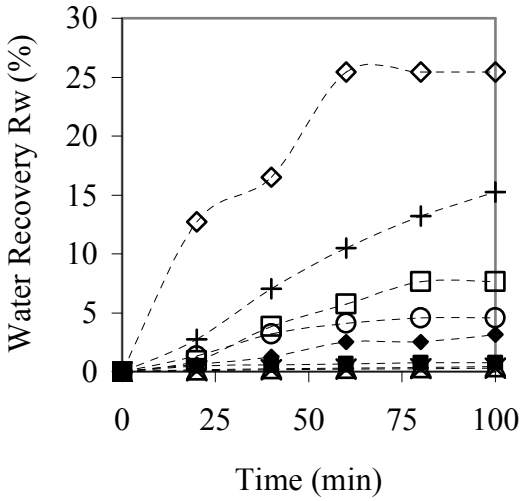

Figure 5-3. Effect of Centrifugation Time on Water Recovery in Preliminary Tests *Cm* = 10% w/w, *vc* 2600 rpm. Emulsion formulation: *fw* = 0.80, *Cs* = 2% v/v, *vm* = 13400 rpm. (◇) Cedar wood, (+) peanut shell, (□) polypropylene, (○) glass, (◆) Saman wood, (■) PVC, (×) metal, (△) without material

Comparing Figures 5-3 and 5-4 it can be noticed that there is a stronger material influence on the coalescence process (Fig. 5-3) than on the clarification process (Fig. 5-4). Clarification (or sedimentation without coalescence) occurs even in absence of packing material, but a constant volume of paraffin recovered is not reached in the studied time.

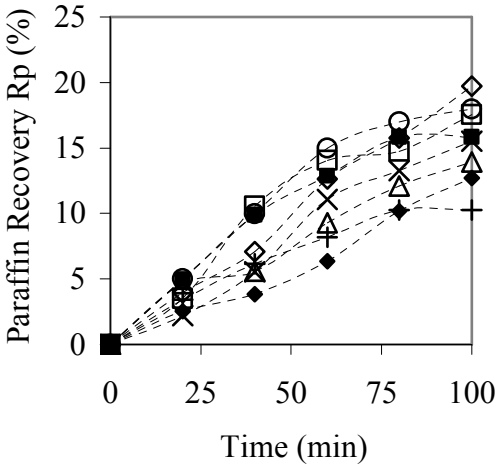

Figure 5-4. Effect of Centrifugation Time on Paraffin Recovery in Preliminary Tests *Cm* = 10% w/w, *vc* = 2600 rpm. Emulsion Formulation: *fw* = 0.80, *Cs* = 2% v/v, *vm* 13400 rpm. (◇) Cedar wood, (+) peanut shell, (□) polypropylene, (○) glass, (◆) Saman wood, (■) PVC, (×) metal, (△) without material

Glass (highly hydrophilic) and peanut shell (highly lipophilic) were selected for the main tests, in order to understand the influence of type and size of material on emulsion stability.

5.1.3 Effect of Material Type on Phases Recovery

Crushed glass and peanut shell were sieved and particles smaller than 0.89 mm were used. Samples with 9 g of emulsion and 1 g of material previously mixed with a glass rod were centrifuged at 2600 rpm for 2 hours. Water and paraffin recovery were evaluated as a function of time. Each test was repeated three times and the average values and standard deviations were calculated to evaluate the repeatability.

The effect of using collector materials on water coalescence is reported in Figure 5-5. As it is shown, both materials, the hydrophilic (glass) and the hydrophobic (peanut shell), improve coalescence in comparison with the absence of collector materials; therefore, for this particle size and material ratio, peanut shell can be defined as a "good collector material" where water recovery reaches 86±5%. In contrast, glass is a "poor collector material" with a water recovery of only 11±2%.

In Figure 5-5, glass and peanut shell particles were smaller than in the preliminary test, detecting faster coalescence for both materials. In this case, separation occurs above 30 minutes; but for larger particles (see Fig. 5-3) more time is required to reach the maximum

recovery: 80 min for glass and more than 100 min for peanut shell. The particle size influences not only the coalescence rate but also the maximum amount of separated water, because for larger particles (see Fig. 5-3), the water recovery is hardly 15 % and 5% for peanut shell and glass, respectively. Besides the differences on wettability between both materials, the glass also settles more quickly than the peanut shell, which means a less effective contact between the material and the emulsion.

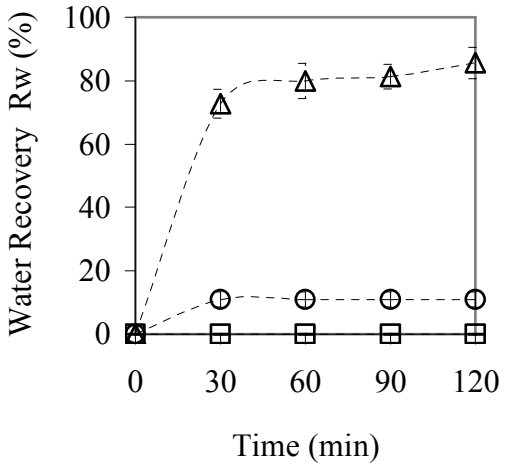

Figure 5-5. Effect of Material Type on Average Water Recovery *Rw*
Cm = 10% w/w, *x* < 0.89 mm, *vc* = 2600 rpm. Emulsion formulation: *fw* = 0.80, *Cs* = 2% v/v, *vm* = 13400 rpm. (△) peanut shell, (○) glass, (□) without material

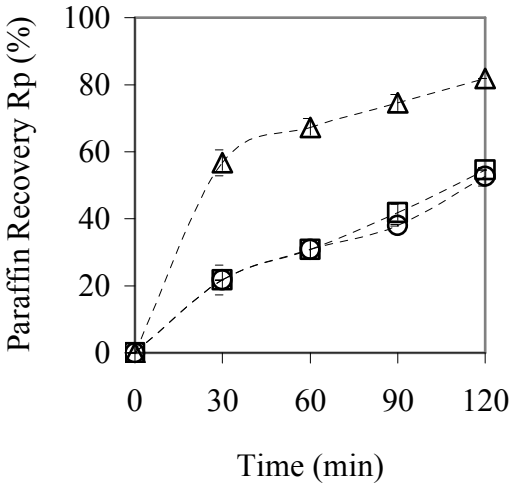

Figure 5-6. Effect of Material Type on Average Paraffin Recovery *Rp*
Cm 10% w/w, *x* < 0.89 mm. *vc* = 2600 rpm. Emulsion formulation: *fw* = 0.80, *Cs* = 2% v/v, *vm* = 13400 rpm. (△) peanut shell, (○) glass, (□) without material

Results obtained for paraffin recovery are shown in Figure 5-6. Only the lipophilic material promotes clarification by sedimentation itself, and 82% of paraffin is recovered in comparison with 54% for the hydrophilic material and without material. Clarification requires more time than coalescence, therefore no maximum values are reached in 120 minutes. Observing clarification kinetics, two steps are present: a faster one, approximately during the first 30 minutes, that is controlled by the nature of the material (it is here where the material hydrophobicity is important). The second step is slower, and the rate of clarification is practically independent on the material nature.

5.1.4 Effect of Collector Material Particle Size on Phases Recovery

To go on deep into the effect of collector material particle size on separation observed in Figures 5-3 and 5-5, peanut shell was ground and sifted through sieves of 0.89 and 2.38 mm. Four sizes were used including the half cuts (see Figure 5-7).

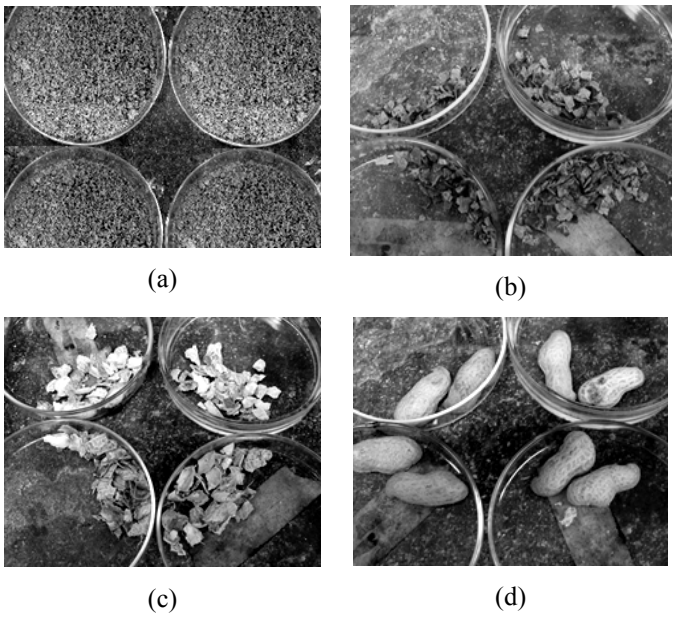

Figure 5-7. Peanut Shell Particle Sizes

(a) Particles smaller than 0.89 mm, (b) particles between 0.89 and 2.38 mm, (c) particles larger than 2.38mm, (d) half peanut shell

Samples of emulsion with 10% w/w of material were centrifuged up to 30 minutes, corresponding to the first kinetic step, at 2600 rpm. Volume of separated water was measured every 10 minutes and water recovery was calculated and reported in Figure 5-8.

Coalescence is strongly governed by material size, and a critical size from which the water recovery is drastically increased has been found. For sizes bigger than 0.89 mm the water recovery is lower than or equal to 8%, whereas with particles smaller than 0.89 mm the water recovery reaches 71%, which is over 8 times higher.

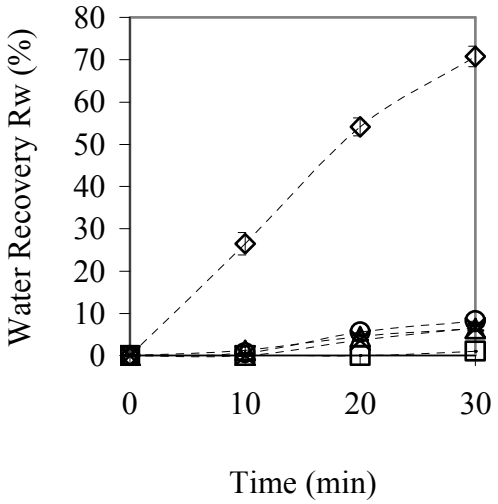

Figure 5-8. Effect of Particle Size on Average Water Recovery *Rw*

Material: peanut shell. *vc* = 2600 rpm. Emulsion formulation: *fw* = 0.80, *Cs* = 2% v/v, *vm* = 13400 rpm. (◇) $x < 0.89$ mm, (△) 0.89 mm $< x <$ 2.38 mm, (○) $x >$ 2.38 mm, (×) half shell, (□) without peanut shell

5.1.5 Emulsion Type and Collector Material Efficiency

W/O and *O/W* emulsions with 30% v/v water and 70% v/v paraffin were prepared using a surfactant mixture with 85% v/v of Sorbitan Monooleate (span 80) and 15% v/v of nonil phenol ethoxylated (N150) to provide high stability (see Table 3-1 for physical properties). Only the mixing array was changed to produce both emulsion types: for *W/O* emulsion, water was added to paraffin and for *O/W* emulsion, paraffin was added to water.

Two particle sizes were selected: fine particles smaller than 0.2 mm and coarse particles bigger than 0.8 mm. Samples with 1.5g of peanut shell of each size were prepared in test tubes, 30mL of *W/O* emulsion was added to each tube. An equivalent set was prepared with *O/W* emulsion. All tubes were centrifuged three times for 20 minutes, and after the third centrifugation they were monitored for 3 weeks. Tubes with pure emulsions were centrifuged to demonstrate the emulsions stability.

Figure 5-9 shows the results after the third centrifugation. Between the second and the third

centrifugation no changes were observed. Three weeks later, slight changes in sedimentation and coalescence were observed. The collector material effect is independent on the emulsion nature because there is an equivalent separation between tests with *O/W* emulsions (from (a) to (c) in Figure 5-9) and the *W/O* emulsions (from (d) to (f) in Figure 5-9). Once again, fine particles (tubes (a) and (d)) promote both sedimentation and coalescence better than the coarse particles (tubes (b) and (e)).

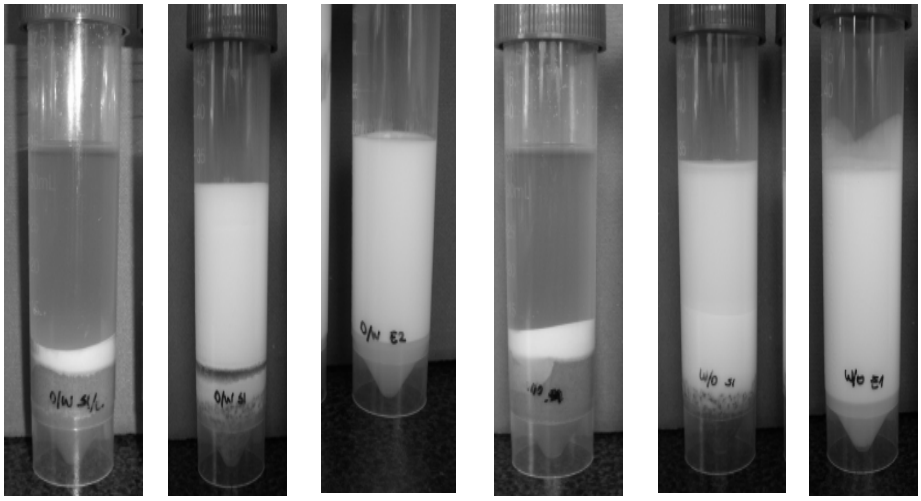

(a) (b) (c) (d) (e) (f)

Figure 5-9. Effect of Emulsion Type on Collector Material Efficiency
(a) *O/W* emulsion and fine dry peanut shell, (b) *O/W* emulsion and coarse dry peanut shell, (c) pure *O/W* emulsion, (d) *W/O* emulsion and fine dry peanut shell, (e) *W/O* emulsion and coarse dry peanut shell, (f) pure *W/O* emulsion

5.1.6 Effect of Collector Material Contact Time on Phases Recovery

Water droplets were observed one day later of the centrifugation on the walls of some test tubes. It was decided to evaluate the effect of the material contact time. Two cases were studied: in the first case, the samples were centrifuged for 20 minutes immediately after their preparation; in the second case, the samples were also centrifuged for 20 minutes but 24 hours later. In both cases, centrifugation was set at 2600 rpm. Results are presented in Figure 5-10.
Water recovery is strongly influenced by the collector material particle size; the smaller the particle size, the greater its effect on the coalescence process for both operational modes. Water recovery changes from 0 to 54% in the first operational mode, and from 0 to 72% in the second one. The same behavior is observed on paraffin, but only in the first operational

mode (paraffin recovery changes from 7 to 21%); nevertheless, when the centrifugation is made a day after the sample preparation, the paraffin recovery does not show an important variation (from 21 to 27%), and the amount of separated paraffin for all material sizes practically agrees with the experiments in which no material is used.

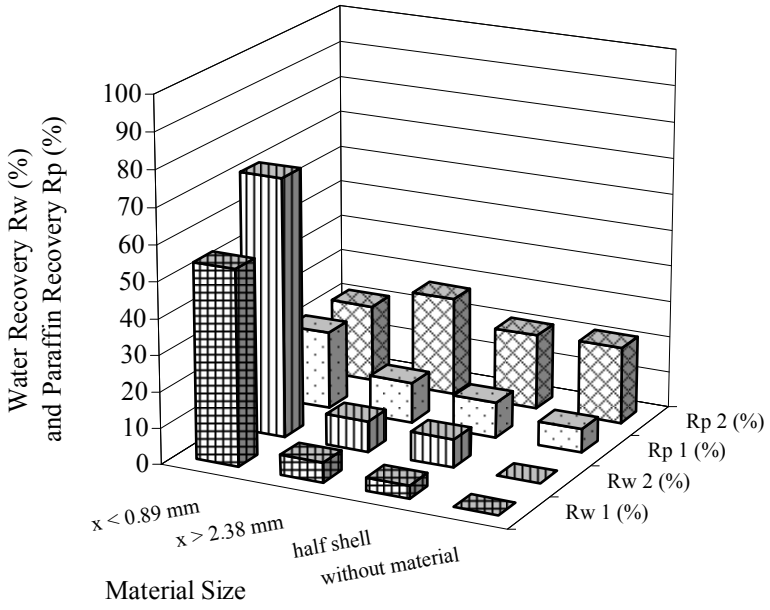

Figure 5-10. Effect of Material Contact Time
on Average Water Recovery *Rw* (%) and Paraffin Recovery *Rp* (%)

Material: peanut shell. Centrifugation conditions: *vc* = 2600 rpm, *tc* = 20 min. Emulsion formulation: *fw* = 0.80, *Cs* = 2% v/v, *vm* = 13400 rpm. (▦) *Rw 1* (%): water recovery when centrifugation is carried out immediately after sample preparation; (▥) *Rw 2* (%): water recovery when centrifugation is carried out 24 hours after sample preparation; (□) *Rp 1* (%): paraffin recovery when centrifugation is carried out immediately after sample preparation; (▨) *Rp 2* (%): paraffin recovery when centrifugation is carried out 24 hours after sample preparation

In order to find the maximum recovery, another test was carried out following the procedure previously described as "the second case", but repeating the cycle during several days. These results are shown in Figures 5-11 and 5-12.

The water and paraffin recovery is increased up to 96 and 82%, respectively, when the smallest collector material size is used (x < 0.89 mm). Separation kinetics is similar as described in Figures 5-6 and 5-7. For water, the rate of separation is increased when the size of the collector material diminish. For paraffin the same behavior occurs, but only after the first operational cycle (day 2), because for the first day the influence of the material size in the

paraffin recovery is not verified.

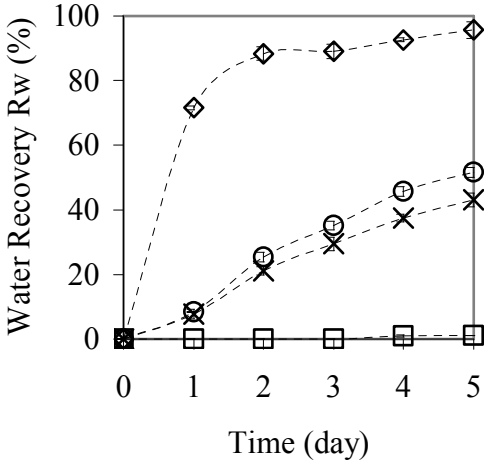

Figure 5-11. Effect of Particle Size on Average Water Recovery *Rw*

Material: peanut shell, *Cm* = 10% w/w, *vc* = 2600 rpm, *tc* = 20 min/day. Emulsion formulation: *fw* = 0.80, *Cs* = 2% v/v, *vm* = 13400 rpm. Particle Size: (◇) *x* < 0.89 mm, (○) *x* > 2.38 mm, (×) half shell, (□) without peanut shell

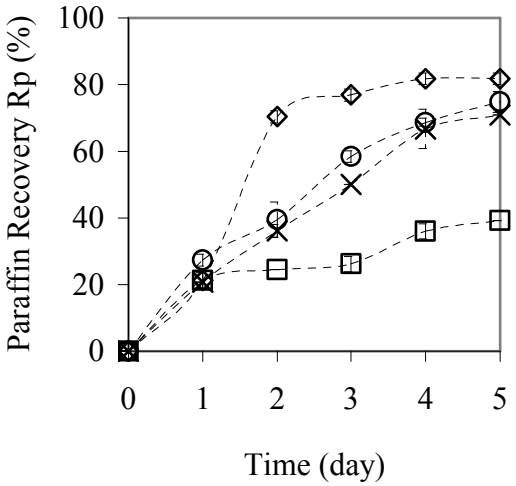

Figure 5-12. Effect of Particle Size on Average Paraffin Recovery *Rp*

Material: peanut shell, *Cm* = 10% w/w, *vc* = 2600 rpm, *tc* = 20 min/day. Emulsion formulation: *fw* = 0.80, *Cs* = 2% v/v, *vm* = 13400 rpm. Particle Size: (◇) *x* < 0.89 mm, (○) *x* > 2.38 mm, (×) half shell, (□) without peanut shell

To evaluate the contribution of daily centrifugation and contact time, a sample with the finest material was prepared and centrifuged for 20 minutes at 2600 rpm, only the first and last day. For comparison, Figure 5-13 shows the case when daily centrifugation was made. Contact time is responsible of emulsion destabilization, and centrifugation only helps to the physical separation of the phases. At the last day, both samples (with and without daily centrifugation)

shows the same separation of water and paraffin. Also, when centrifugation could help destabilizing the emulsion, it is clear that the contact time is the parameter that takes the control of the total effect.

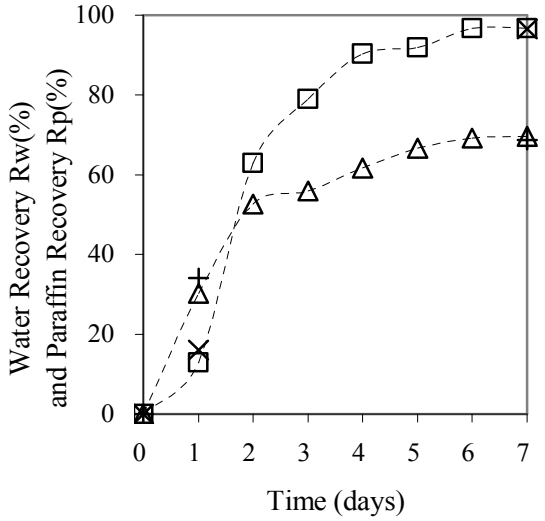

Figure 5-13. Effect of Contact Time on Average Water and Paraffin Recovery

Material: peanut shell, *Cm* = 5% w/w, *vc* = 2600 rpm, *tc* = 20 min/day, *x* < 0.89 mm. Emulsion formulation: *fw* = 0.75, *Cs* = 2% v/v, *vm* = 13400 rpm. Water and Paraffin Recovery[2]: (△) *Rw 1*, (+) *Rw 2*, (□) *Rp 1*, (×) *Rp 2*

5.1.7 Emulsion Water Content and Collector Material Effectiveness

W/O emulsions with *fw* = 0.25, 0.50 and 0.75 were prepared and stabilized with span 80®. The emulsifier content was the same for the three formulated emulsions. Suspensions with 90% w/w of water-in-oil emulsion and 10% w/w of collector material (peanut shell) in size smaller than 0.89 mm were centrifuged at rpm 2600 until the recovered amount of both phases was constant. The tests were repeated three times, and the standard deviation was calculated and reported. Results are shown in Figures 5-14 and 5-15.

An emulsion with low disperse phase content tends to be, by nature, more stable than an emulsion with high disperse phase content. In these experiments, the highest water recovery (*Rw* = 65%) is reached for *fw* = 0.50, whereas the smallest value was obtained for *fw* = 0.25 (*Rw* = 37%).

The results are attributed to differences in *HLB* required because all the emulsions were formulated at *HLB* constant. It seems to be that, for a given particle size, there is an amount of peanut shell that optimizes the water recovery, and that depends on the emulsion water

[2] *Rw 1* and *Rp 1*: daily centrifugation, *Rw 2* and *Rp 2*: centrifugation at the first and at the last day

content. In terms of separation rate, the process becomes slower when the water content of the emulsion increases, but it is in general faster than the clarification process. The paraffin recovery diminishes when the emulsion water content increases, and values of 92, 88 and 82% v/v are obtained for *fw* = 0.25, 0.50 and 0.75, respectively.

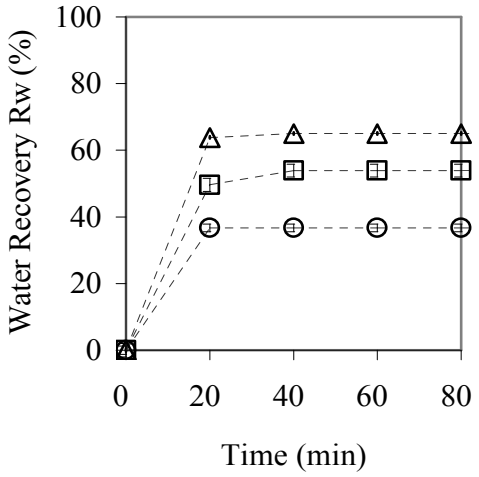

Figure 5-14. Effect of Emulsion Water Content
on Collector Material Effectiveness to Promote Coalescence
Material: peanut shell, *Cm* = 10% w/w, *x* < 0.89 mm, *vc* = 2600 rpm. Emulsion formulation: *Cs* = 2% v/v, *vm* = 13400 rpm. (□) *fw* = 0.75, (△) *fw* = 0.50, (○) *fw* = 0.25

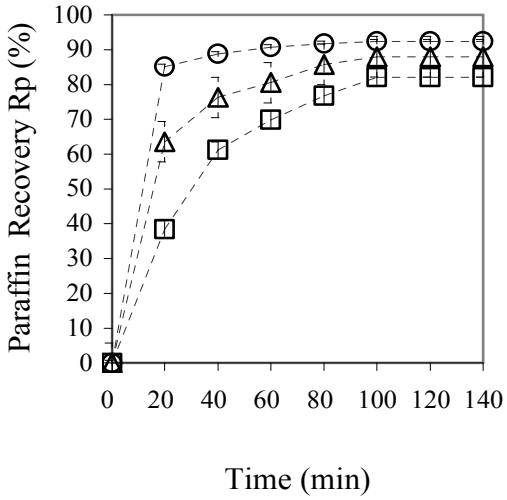

Figure 5-15. Effect of Emulsion Water Content
on Collector Material Effectiveness to Promote Clarification
Material: peanut shell, *Cm* = 10% w/w, *x* < 0.89 mm, *vc* = 2600 rpm. Emulsion formulation: *Cs* = 2% v/v, *vm* = 13400 rpm. (□) *fw* = 0.75, (△) *fw* = 0.50, (○) *fw* = 0.25

Separation as a function of emulsion water content and collector material amount is compared

in Figures 5-16 and 5-17. Tests at 0, 5 and 10% w/w of collector material were made. The samples were centrifuged per consecutive 20 minutes periods, and the separation of water and paraffin was registered until the last 3 values were constant for each case.

Figure 5-16 shows that there is no water separation in the absence of collector material, and when the emulsion concentration increases, more collector material is required: when 5% w/w of material is used, water recovery is 67% v/v for the emulsion with 25% of water, but to obtain a similar recovery (65% v/v) in a more concentrated emulsion (with 50% of water), 10% w/w of material is required. In clarification case (corresponding to Figure 5-17), the same tendency is observed, but clarification occurs spontaneously in all cases, including also those without collector material.

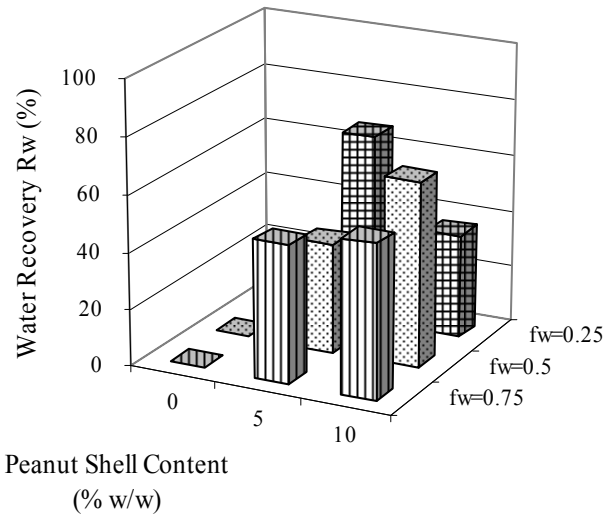

Figure 5-16. Effect of Collector Material Content on Coalescence

Material: peanut shell, *Cm* = 0, 5 and 10% w/w, *x* < 0.89 mm, *vc* = 2600 rpm, the samples were centrifuged until water recovery was constant. Emulsion formulation: *Cs* = 2% v/v, *vm* = 13400 rpm. (▥) *fw* = 0.75, (▨) *fw* = 0.50, (▤) *fw* = 0.25

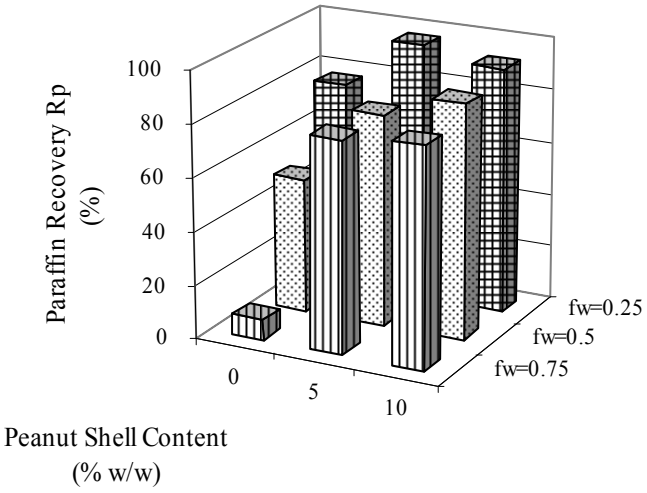

Figure 5-17. Effect of Collector Material Content on Clarification

Material: peanut shell, *Cm* = 0, 5 and 10% w/w, *x* < 0.89 mm, *vc* = 2600 rpm, the samples were centrifuged until paraffin recovery was constant. Emulsion formulation: *Cs* = 2% v/v, *vm* = 13400 rpm. (▥) *fw* = 0.75, (□) *fw* = 0.50, (▦) *fw* = 0.25

5.1.8 Proposed Mechanism

It seems that the collector material does not only help on the physical separation of the phases, but also promotes emulsion destabilization: the surfactant finds a new state of balance and leaves the water-oil surface, allowing coalescence of water droplets. The new state also must satisfy the surfactant double affinity which is preferentially soluble in oil.

Theory of the surfactant-water-oil (*SWO*) systems behavior leads us to formulate a hypothesis: the surfactant leaves the water-oil surface and is adsorbed on the solid surface by the tail side because its affinity to lipophilic surfaces. When the emulsion is broken, water can coalescence and settle. The surfactant leaves the head in contact with the free water that is within the collector material at the bottom of the test tubes satisfying its amphiphilic character. Thus, destabilization would occur if there is enough interface area to allow the adsorption of all the surfactant.

To support the proposed mechanism, complementary tests were made with particles smaller than 0.71 mm. Three samples with 1.5 g of peanut shell were prepared in test tubes; and two samples of these were submerged in water and water plus 8% v/v surfactant Span 80® (previously mixed), respectively, for 10 days. After that, the excess of liquid was removed

with absorbent paper from the so-called "wetted peanut shell". The material that was not submerged in liquid is called "dry peanut shell". The water as well the surfactant could be adsorbed in the peanut shell; in which case, the capacity of the peanut shell to break the emulsion would have to fall when it is compared with the result reached with dry shell.

W/O emulsion with 80% v/v water and 20% v/v paraffin were prepared using Sorbitan Monooleate (span 80) to provide high stability. 40mL of *W/O* emulsion was added to test tubes with peanut shell (wetted with water, wetted with water/surfactant, and dry). After 10 days, all tubes were centrifuged at 2600 rpm for 5 minutes.

Figure 5-18 shows the samples appearance after the centrifugation. Dry particles (Fig. 5-18c) promote separation significantly better than those that previously were submerged in water/surfactant mixture (Fig. 5-18a) indicating a partial exhaustion of the peanut shell in this case; but when water wetted peanut shell is used (Fig. 5-18b), there is no significant differences in water recovery in comparison with the dry peanut shell sample result. The hypothesis of partial saturation of the solid via surfactant adsorption is supported and although the water could also be adsorbed, it is clear that the surfactant adsorption occurs and is the one which promotes emulsion destabilization.

(a) (b) (c)

Figure 5-18. Evidence of Surfactant adsorption

Material: peanut shell, $x < 0.71$ mm, vc = 2600 rpm, tc = 5 min (after 10 days). Emulsion formulation: Cs = 2% v/v, vm = 13400 rpm, fw = 0.80. (a) Peanut shell was previously submerged in water/surfactant mixture 8% v/v, (b) peanut shell was previously submerged in water, (c) with dry peanut shell

Surfactant adsorption occurs only in presence of water, because when peanut shell previously wetted with pure Span 80® was tested in a similar experiment, water recovery did not

diminish in comparison with the case when dry peanut shell was used. In presence of water, surfactant can satisfy its double affinity by adsorption on the solid surface that is lipophilic.

From figure 5-3 it is understood that it is not sufficient that a material is lipophilic so that it can act as good collector material. Brown coal was tested as collector material, because it is commonly used in separation processes as adsorption, absorption and filtration.

W/O emulsion with 80% v/v water and 20% v/v paraffin were prepared using Sorbitan Monooleate (span 80®) to provide high stability. 40mL of *W/O* emulsion was added into test tubes within 1.5 g of brown coal particles smaller than 0.71 mm. After 10 days, the tubes were centrifuged at 2600 rpm for 30 minutes.

The Figure 5-19 shows that brown coal could be used as collector material. The average water recovery was 38% v/v (Fig. 5-19a) in comparison with 0% when no material was used (Fig. 5-19b). It is recommendable to make more tests in order to find the operational conditions (particle size, material content and contact time) that optimize the brown coal collector material effect.

(a) (b)

Figure 5-19. Coal as collector material

Material: brown coal, $x < 0.71$ mm, $vc = 2600$ rpm, $tc = 30$ min (after 10 days). Emulsion formulation: $Cs = 2\%$ v/v, $vm = 13400$ rpm, $fw = 0.80$. (a) sample with brown coal, (b) sample without brown coal

5.2 Conclusions

- In absence of the collector material, the clarification process remarkably depends on emulsion water content, and concentrated emulsions are much more stable against

clarification. When the collector material is used, clarification is increased for all water contents range and paraffin recovery is independent of water content.

- Hydrophilic and hydrophobic materials can improve the coalescence of water in *W/O* emulsions, but when hydrophobic materials are used, the effect is more significant.
- A collector material not only helps on the physical separation of the phases but also promotes coalescence.
- Effect of collector materials on coalescence depends on the particle size. Both, rate of coalescence and amount of separated water increase when the collector material particle size is reduced.
- The optimal amount of collector material for improving emulsion destabilization depends on the emulsion water content.
- Concentrated emulsions required more collector material than the diluted ones.
- The effect of collector materials is independent of the emulsion type and can destabilize both: *W/O* and *O/W* emulsions.
- A suggested mechanism that could explain the collector material effect, is considering that coalescence occurs because the surfactant finds a new state of balance in which it leaves the water-oil surface and is adsorbed on the solid surface by the tail side, leaving the head in contact with the formed free water and satisfying its double affinity. At the end of the process the collector material settles and stays in the aqueous phase.
- It is recommendable to make more tests in order to find the operational conditions (particle size, material content and contact time) that optimize the coal effect as collector material.

6 DC Electric Field and Emulsion Destabilization

The main factors influencing electrostatic coalescence efficiency are: coalescer design, applied electric field type, applied frequency, electrode design and coating, average inlet droplet size, liquid mixture residence time, surfactant type and concentration, and dispersed phase hold-up fraction. Some of them are studied in this chapter. The efficiency of electrical process is usually related to power consumption. A very small amount of current would be drawn for completely insulating oil. The main factors influencing power consumption will be, therefore, the continuous phase conductivity and the electrodes bridging.

6.1 Materials and Equipment

In order to evaluate the *DC* electric field effect on paraffin in water emulsion dehydration, a 20 mL glass cell (Cell A), provided with a thermocouple and two copper electrodes (0.50 x 2.50 cm^2) was designed. The cell characteristic constant *Cc*, defined as the surface area of one electrode *Se* divided by the distance *Le* between them was 0.49 cm. Figure 6.1 describes the cell.

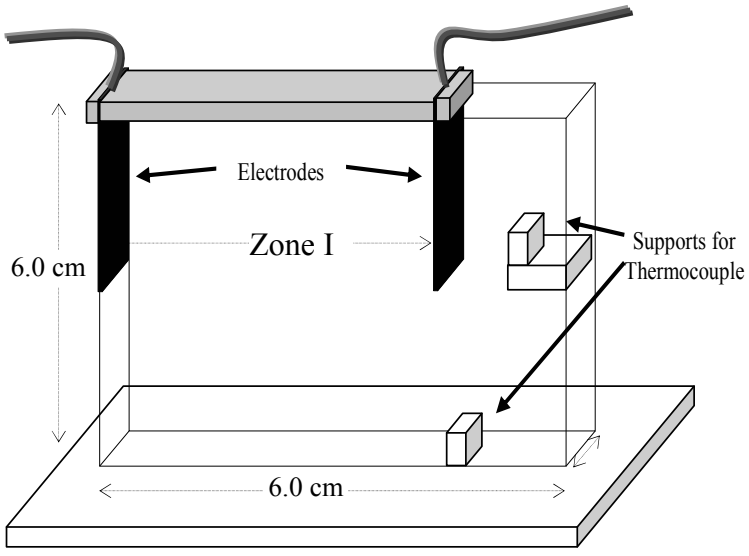

Figure 6-1. Glass Cell for Emulsion Electrostatic Dehydration

Two power supplies were tested: a 2000 V and maximum 2 mA made in the Physics Laboratory from Universidad Central de Venezuela and a 10000 V and maximum 0.5 mA model 13670.93 supplied by PHYWE.

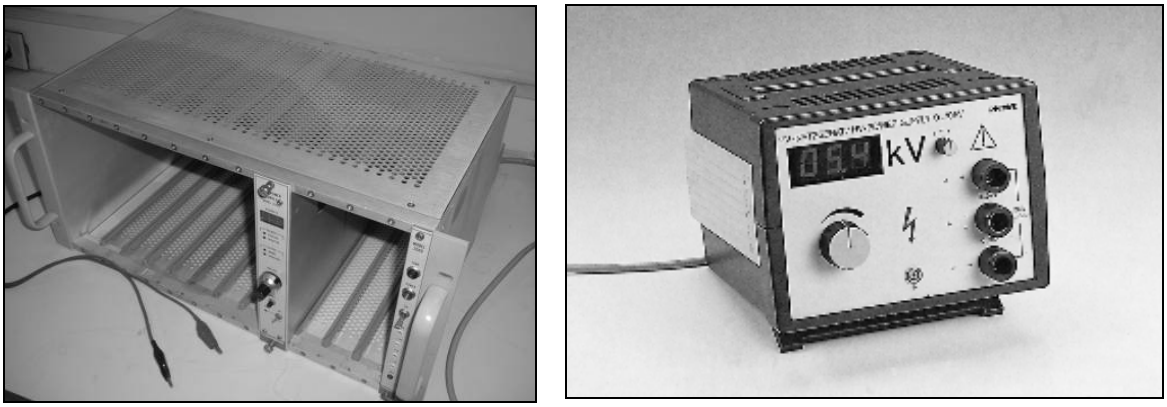

(a) (b)

Figure 6-2. DC Power Supplies

(a) 2000 V and 2 mA, (b) 10000 V and 0.5 mA

A second cell (Cell B) with adjustable and movable electrodes in a separation range from 0 to 2 cm was designed in order to observe the emulsion coalescence in a microscope. Although this cell was used only for monitoring coalescence, and no measurements were made, it has allowed understanding some of the difficulties to overcome when an electric field is applied to stable and highly viscous crude emulsions. In this case, a 25000 V and 0.5 mA PHYWE power supply was used with a video camera. Figure 6.3 shows a scheme of the cell.

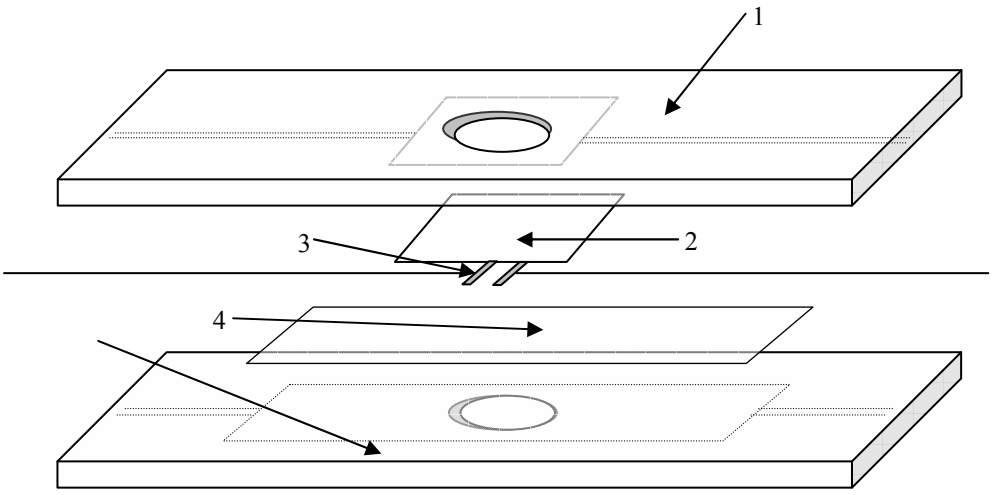

Figure 6-3. Cell for Microscopic Observation

(1) *PVC* plates (120 mm x 40 mm x 3 mm), (2) Cover (20 mm x 20 mm), (3) adjustable electrodes (L=5 mm) with cable, (4) microscope slide (76 mm x 26 mm x 1 mm)

6.2 Experiments and Results

6.2.1 DC Electric Field Effect on Emulsion Destabilization

Stable synthetic water in paraffin emulsion with 50 % v/v water and 1 % v/v Span 80® and N40® surfactant mixture with *HLB* = 5.4 were prepared at 13000 rpm. In order to discriminate between the phases, a red colorant soluble in oil was added, after verifying there was no influence on emulsion stability. The emulsion stability was monitored during 30 days and the total separation (water plus paraffin) was 8 % v/v.

To evaluate the *DC* electric field effect on the emulsion stability, several tests were made from 0.5 to 2 kV, in the glass cell with 20 mL of fresh emulsion, and water separation was monitored as a function of time. Each test was made in triplicate to ensure the repeatability. The Power Supply is shown in Figure 6-2a.

In preliminary tests, water accumulation was observed in the positive electrode. Quickly, water chains were formed between both electrodes causing short circuiting. For this reason, it was necessary to cover the electrodes with a zinc anticorrosive paint which is, in essence, a hydrophobic film able to repel the water. The coating promotes the fast displacement of water droplets to the cell bottom, avoiding bridging between the electrodes. Figure 6-4 shows the DC electric field effect on water recovery.

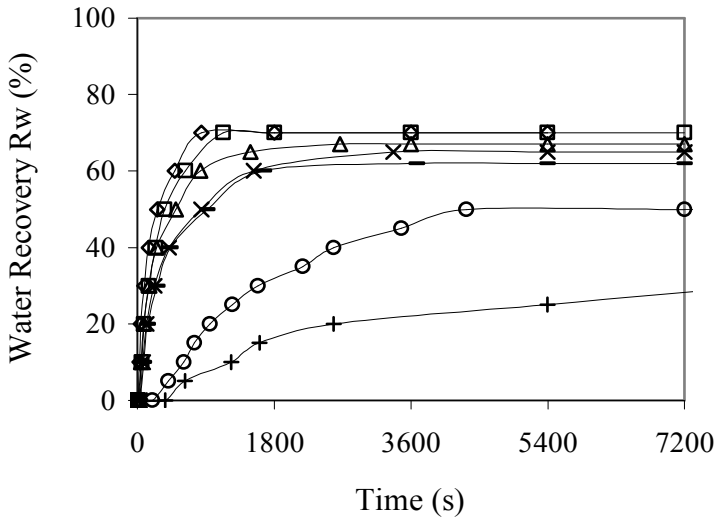

Figure 6-4. DC Electrostatic Field Effect on Water Recovery

Water in Paraffin Emulsion, Surfactant: Span 80® and N 040® Mixture, *HLB* = 5.4, *vm* = 13000 rpm, *tm* = 5 min, *fw* = 0.50. *E*: (+) 90 V/cm, (○) 130 V/cm, (—), 180 V/cm, (×) 220 V/cm, (△) 270 V/cm, (□) 310 V/cm, (◇) 350 V/cm

Temperature was monitored in all tests. It varied from 22 to 24 °C. Initially, demulsification percentage increases linearly with time. Initial rate (represented by the slope of the curves) and the maximum percentage of water recovery, increase with the applied potential, but only up to 1750 V corresponding to 310 V/cm. As it is shown in Figure 6-4, above this voltage, a higher water recovery is not reached. Maximum Standard deviation at maximum water recovery was lower than 2 %.

Also it is observed that, as the electric field is increased, the proportion between obtained separation and applied electric field is reduced, since for 130 V/cm the separation is 50 %, and for 310 V/cm the water recovery is only 70 %. The inefficient separation of water can be explained, because if the field becomes too strong, various droplet break up mechanisms could occur, counteracting coalescence.

Emulsion half life time, define as the time required to separate 50% of one of the phases, was measured on water. Results are shown in Figure 6-5. For 90 V/cm the half life time could not be measured. Variation of the emulsion half life time shows an asymptotic behavior for low values of electric field. From 180 V/cm, the emulsion half life time is reduced significantly, thus it can be said that a dehydration process in these conditions would be more appropriate in terms of energy saving, although it represents a reduction in water recovery from 70 % at 310 V/cm to 62 % at 180 V/cm.

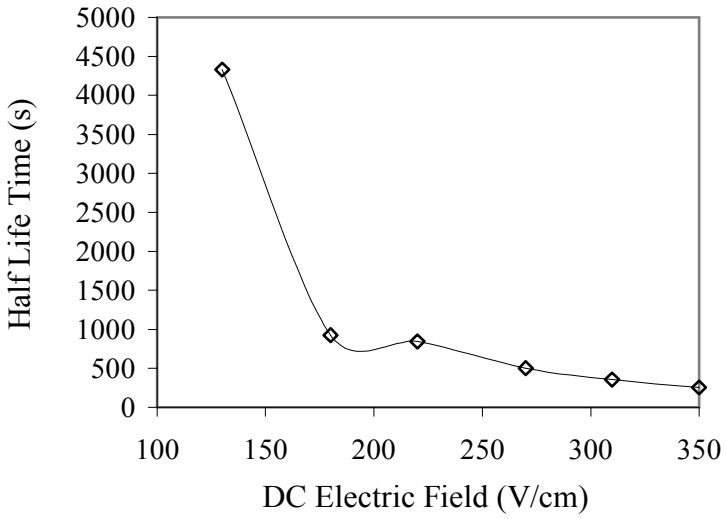

Figure 6-5. DC Electric Field Effect on Emulsion Half Life Time

Water in Paraffin Emulsion, Surfactant: Span 80® and N 040® Mixture, *HLB* = 5.4, *vm* = 13000 rpm, *tm* = 5 min, *fw* = 0.50

The power supply shown in Figure 6-2b was also tested, but with this device it was not possible to maintain a high potential difference value. This is due to the maximum current limit of this equipment that is only 0.5 mA, which is not enough to deal with an

emulsion of 50 % v/v water at high potential difference. However, when the emulsion water content is reduced, the resistance to the current increases. Then it is possible to reach more and more high potential differences as the coalescences process occurs.

A test was performed at *DC* variable electric field. For that, the device was set up at 10000 V, but due to the current limit, a maximum voltage of 320 V, corresponding to 56 V/cm electric field, was reached at the beginning.

Time, water separation and voltage were monitored; the results are shown in Figure 6-6. The voltage increased gradually up to 2730 V, corresponding to 485 V/cm. A variation in the temperature of up to 2 °F was observed. A maximum water recovery of 80 % v/v was reached in 3350 seconds, which is 10 % more than in the case in which the constant voltage device was used. A vertical asymptote in the graph of reached electric field as a function of separated water also demonstrates the separation limit. Dehydration efficiency is improved by using a variable electric field, because 70 % of water recovery is reached with a maximum potential difference of 290 V/cm in 1556 s in comparison with 310 V/cm required in 1130 at constant electric field operation.

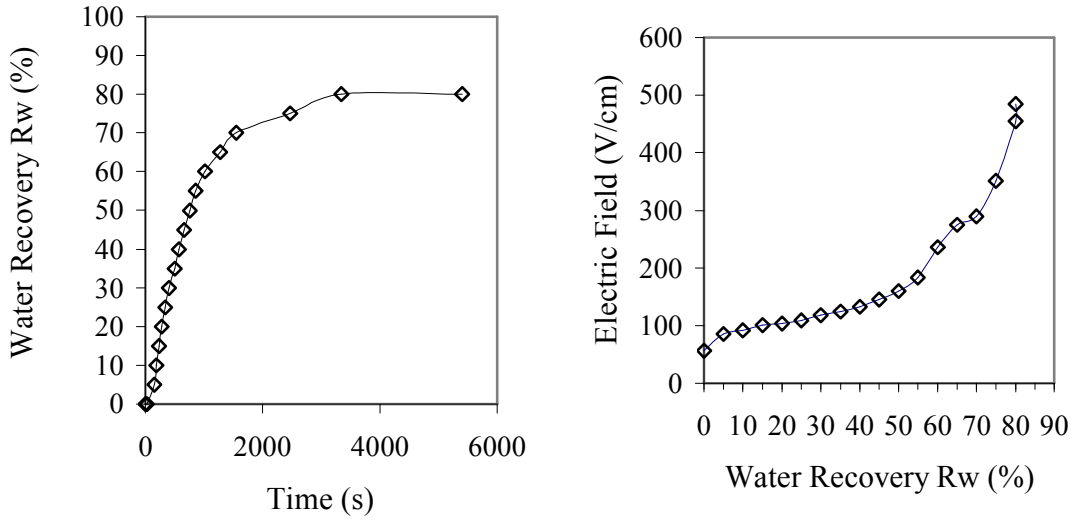

Figure 6-6. Variable DC Electric Field Effect on Water Recovery

Water in Paraffin Emulsion, Surfactant: Span 80® and N 040® Mixture, *HLB* = 5.4, *vm* = 13000 rpm, *tm* = 5 min, *fw* = 0.50

In order to evaluate the water content effect on the electric emulsion dehydration, a water content scan was made. Water in paraffin emulsions with 30, 40, 50 and 60 % water content were prepared. The *HLB* of all of the emulsions was 5.9 and it was achieved with a Span 80® (*HLB* = 4.3) and Arkopal N 100® (*HLB* = 13.0) mixture. The power supply shown in Figure 6-2a was used, and the experiments were made at a maximum voltage of 2000 V (350 V/cm). This

voltage was not reached for 60 % of water content emulsion, so this emulsion could not be studied.

Dehydration results are shown in Figure 6-7. Maximum water separation of 25, 38 and 52 % v/v for 30, 50 and 40 % water content emulsions were reached, respectively. This result can be explained based on chapter 3 discussion, where it was concluded that the required *HLB* to obtain a maximum of stability in an emulsion depends strongly on the water content. Here, all the emulsions were formulated at constant *HLB*. For this reason the original stability already is different, independently of the electric field application. Whereas at low dispersed phase content, interactions between drops are weak and the contact and coalescence probability is small, something that contributes to the stability, it is important to emphasize that with a high internal phase content, drops can be literally in contact, and in this case it is the magnitude of the different attractive and repulsive forces what defines the stability. These forces are influenced by the emulsion formulation.

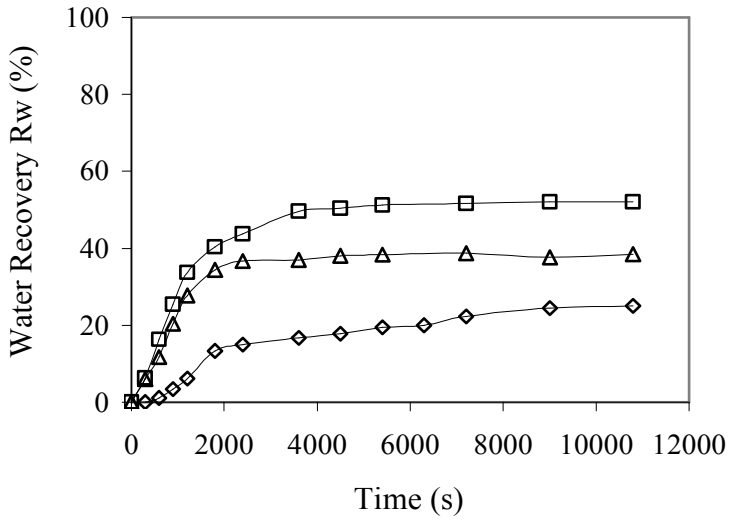

Figure 6-7. Water Content Effect on Water Recovery

Water in Paraffin Emulsion, Surfactant: Span 80® and Arkopal N 100® Mixture, *HLB* = 5.9, *vm* = 13400 rpm, *E* = 350 V/cm. Water Content: (◇) *fw* = 0.30, (□) *fw* = 0.40, (△) *fw* = 0.50

6.2.2 Electrodes Design and Dehydration Efficiency

A 100 mL glass graduated cylinder was used as dehydration cell. For this, a pair of copper electrodes were integrated in the cell and connected to a 25000 V and 0.5 mA power supply (see Figure 6-2b). Two types of electrode geometry were designed, flat parallel plates and concentric cylinders, as they are described in Figure 6-8; corresponding dimensions are detailed in Table 6-1. Two pairs of flat electrodes were made varying the cell constant

(electrodes *A* and *B* in Table 6-1). The cylindrical electrode pair was evaluated in two ways: using the external cylinder as positive electrode and the internal cylinder as negative electrode (electrode *C*, Table 6-1) and vice versa (electrode *D*, table 6-1).

Table 6-1. Electrodes description. For a 100 mL graduate cylinder, 22 cm length

Electrode Name	Electrode Type	Dimensions (cm)	Cell Constant *Cc* (cm)	Notes
A	parallel flat plates	S_1=11.80, S_2=2.10, S_3=0.70	35.40	
B	parallel flat plates	S_1=11.38, S_2=1.50, S_3=1.64	10.41	
C	concentric cylinders	D_i=0.23, D_e=1.92, S_4=11.27	70.82	Internal cylinder (-)
D	concentric cylinders	D_i=0.23, D_e=1.92, S_4=11.27	70.82	Internal cylinder (+)

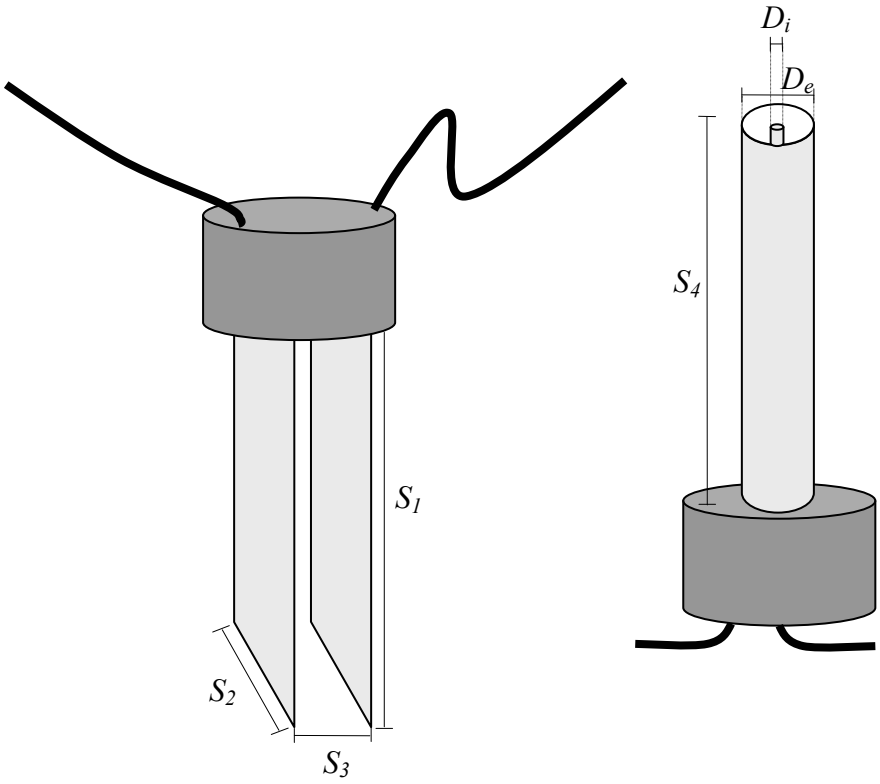

Figure 6-8. Electrodes description

(a) Parallel Flat Plate, (b) Concentric Cylinders

Water in paraffin emulsion stabilized with a Span 80® and Arkopal N 100® mixture was prepared and used in dehydration tests. Surfactant concentration and *HLB* was 2.5 % v/v and 5, respectively, water content was 20 and 30 % v/v. The cell constant effect on emulsion

destabilization is shown in Figure 6-9. Water recovery is 52 % when the electrode *A* is used, whereas with electrode *B*, separation was hardly 13 %.

In both cases 2000 V voltage was applied, and although the superficial area of electrode *B* is a little smaller than the one of electrode *A*, the basic difference is the distance between the electrodes. The cell constant (defined in section 6.1) for electrode *A* is three times higher and the associated electric field is approximately double; as a result, a better water separation with the electrode *A* is obtained.

Cell constant influence on emulsion clarification showed the same tendency, but the paraffin recovery values were higher in both cases: with electrode *A* was 81 %, and with electrode *B* was 62 %. Although the original interest of this part of the study was promoting electrical coalescence of water, the results obtained in terms of clear phases contribute to the final goal of this research which is to obtain clean oil.

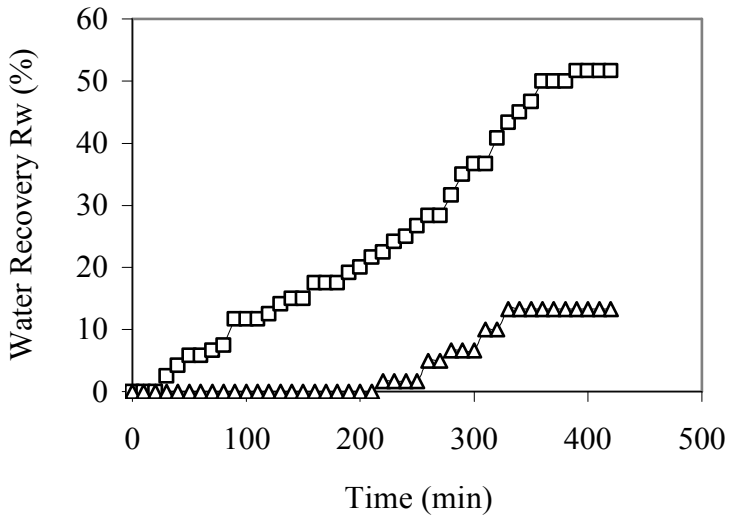

Figure 6-9. Cell Constant Effect on Emulsion Dehydration

Water in Paraffin Emulsion, *fw* = 0.30, Surfactant: Span 80® and N 100® Mixture, *Cs* = 2.5%, *HLB* = 5.0, *vm* = 13400 rpm, *v* = 2000 V. Parallel Flat Plate Electrodes, Cell Constant *Cc*: (△) 10.41 cm, (□) 35.40 cm

In Figure 6-10 two different electrode geometries are compared: flat plates versus concentric cylinders. The voltage applied in both cases was 6000 V, and the treated emulsion had 20 % of water. Additionally, the effect of a change of polarity, as it is described in the table 6-1, was evaluated.

Paraffin and water recovery was higher when plate electrodes were used, even though the cylindrical electrodes cell constant was higher. Once more, the applied electric field was more

efficient to promote paraffin clarification than water coalescence. For plate electrodes, for example, water recovery was only 32 %, but paraffin recovery was 90 %.

In all tests, a layer of a viscous emulsion was accumulated in the negative electrode and the cell walls; whereas the positive electrode was wetted by water and surrounded by clear paraffin. This situation demonstrates the migration of water droplets towards the positive electrode surface. The electric field promotes the droplets movement to the positive electrode and subsequent coalesce; then, the water slips down on the positive electrode surface and it is accumulated on the cell bottom.

On the other hand, Figure 6-10 also shows that the polarity change of the cylindrical electrodes does not affect the paraffin recovery but the water coalescence. Water recovery is favored when the internal cylinder acts as negative electrode, perhaps because in this case water droplets migrate from the internal cylinder towards the external cylinder where the superficial area is bigger and the water finds fewer impediments to move.

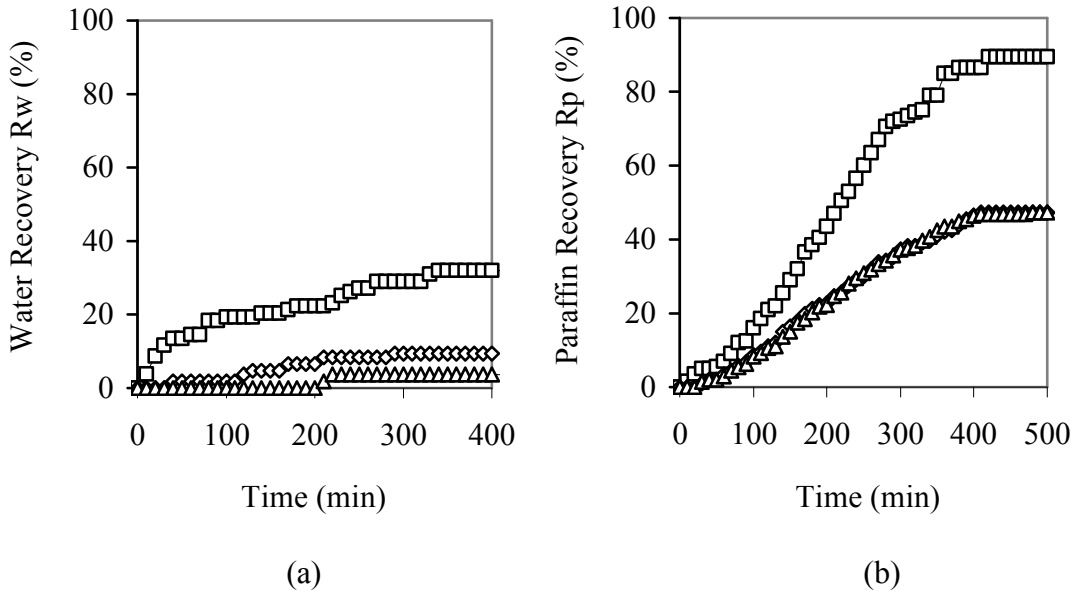

Figure 6-10. Electrodes Geometry Effect on Emulsion Destabilization

(a) Water Recovery, (c) Paraffin Recovery. Water in Paraffin Emulsion, fw = 0.20, Surfactant: Span 80® and N 100® Mixture, Cs = 2.5 %, HLB = 5.0, vm = 13400 rpm, v = 6000 V. Electrode Type: (△) D, (◇) C, (□) A

Figure 6-11 shows pictures of the emulsion film on the negative electrode surface and the cell wall near the negative electrode side where the emulsion film is located.

When experiments in the 20 mL electrostatic cell (cell *A*) were made, it was necessary to cover the electrodes with an anticorrosive paint, a hydrophobic film able to repel the water

and avoid bridging of the electrodes. Nevertheless, when the 100 mL cell was used it was not necessary, and the tests were made with bare electrodes.

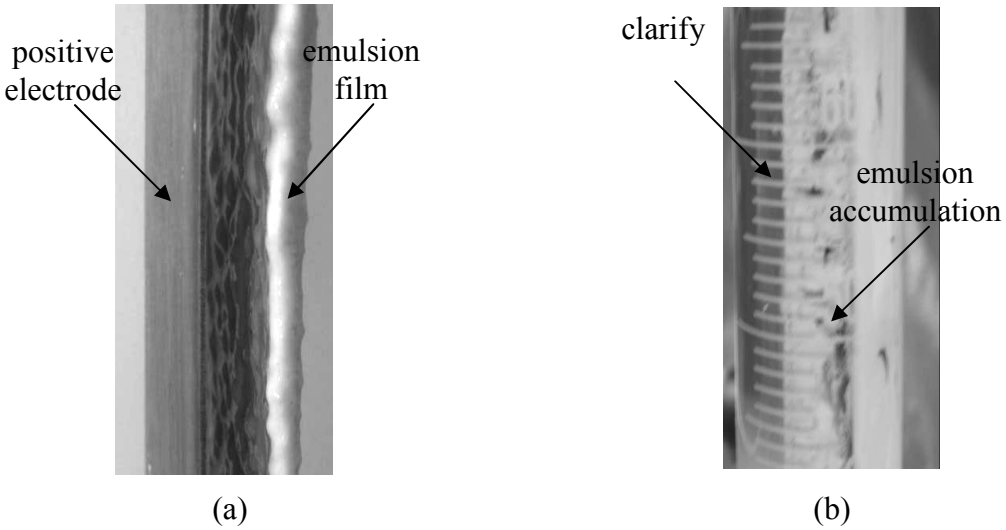

Figure 6-11. Emulsion accumulation after the Dehydration Process
(a) On the negative electrode surface, (b) on the cell wall

To compare the effect of coated electrodes on dehydration efficiency, a test was made with type *A* electrodes using the anticorrosive paint. The results are shown in Figure 6-12.

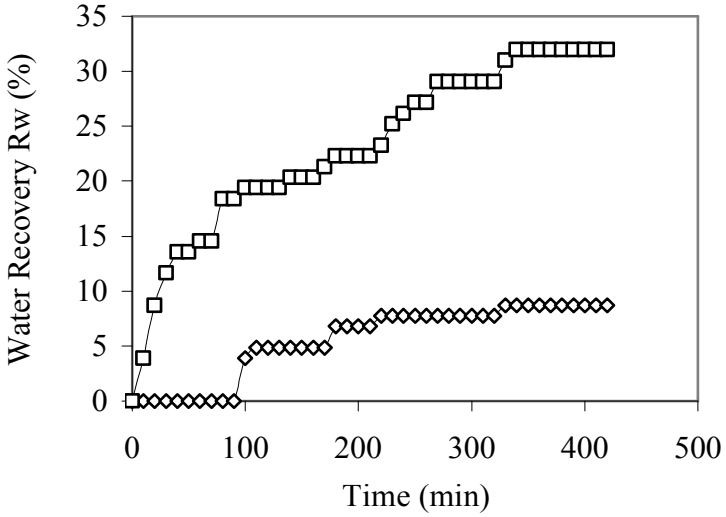

Figure 6-12. Electrodes Coating Effect on Emulsion Dehydration
Water in Paraffin Emulsion, *fw* = 0.20, Surfactant: Span 80® and N 100® Mixture, *Cs* = 2.5 %, *HLB* = 5.0, *vm* = 13400 rpm, *v* = 2000 V. Parallel Flat Plate Electrodes, Electrodes Type *A*, Cell Constant *Cc* = 35.40 cm. (◇) with coating, (□) without coating

Water recovery was considerably smaller when covering was used, indicating that coating just prevents short-circuiting and increases the applied potential required to get the same coalescence rate. These results disagree with Bailes and Larkai (1982) and Bailes (1992), regarding the use of coated electrodes to increase the separation efficiency, and are consistent with Galvin (1986).

6.2.3 Separation Process Integration for Emulsion Destabilization

To combine the collector material and electric field effect on water in oil emulsion destabilization, new copper electrodes were designed. They can be inserted directly to the centrifuge test tubes. The cell constant was 1.6 cm. Figure 6-13 shows the electrode scheme. The effective electrode length is 8 cm, they are 0.2 cm wide and the distance between them is 1 cm.

Stable synthetic water in paraffin emulsions with 25 % v/v water and 2 % v/v Span 80® were prepared on the basis of the protocol described in Section 3.2.2.

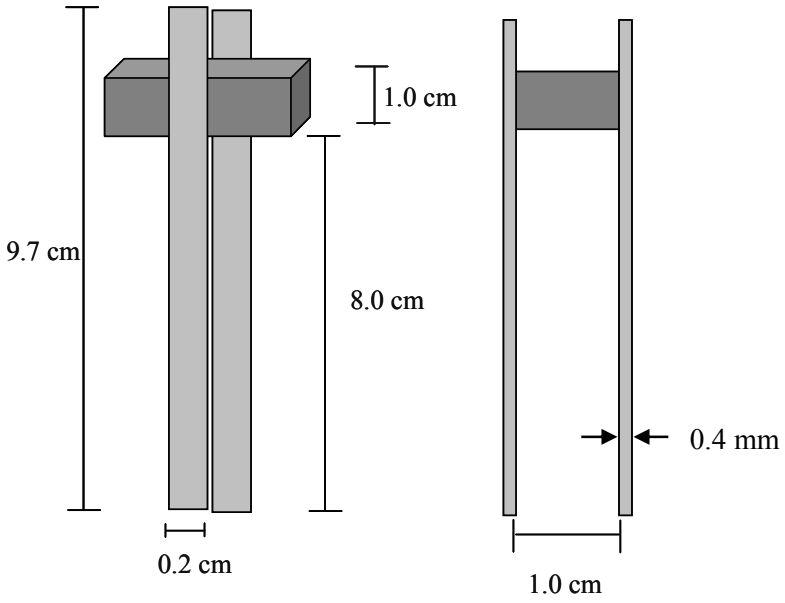

Figure 6-13. Electrodes for Centrifuge Test Tubes

Material: copper. *Cc* = 1.6 cm

In the integration test 1, 10 g of fresh emulsion was centrifuged for 20 min at 2600 rpm. In test 2, 5 % w/w peanut shell (x < 0.89 mm) was added and mixed with a glass rod before centrifugation. In test 3 collector material was not used; however, an electric field of 700 V/cm was applied for 5 min before centrifugation. In test 4, the emulsion was tried at 700

V/cm for 5 min, after that, 5 % w/w of collector material was added and finally the sample was centrifuged. In test 5 the collector material was added before applying the electric field and centrifugation, but in this case voltage was stable only up to 400 V; therefore, an electric field of 400 V/cm was used.

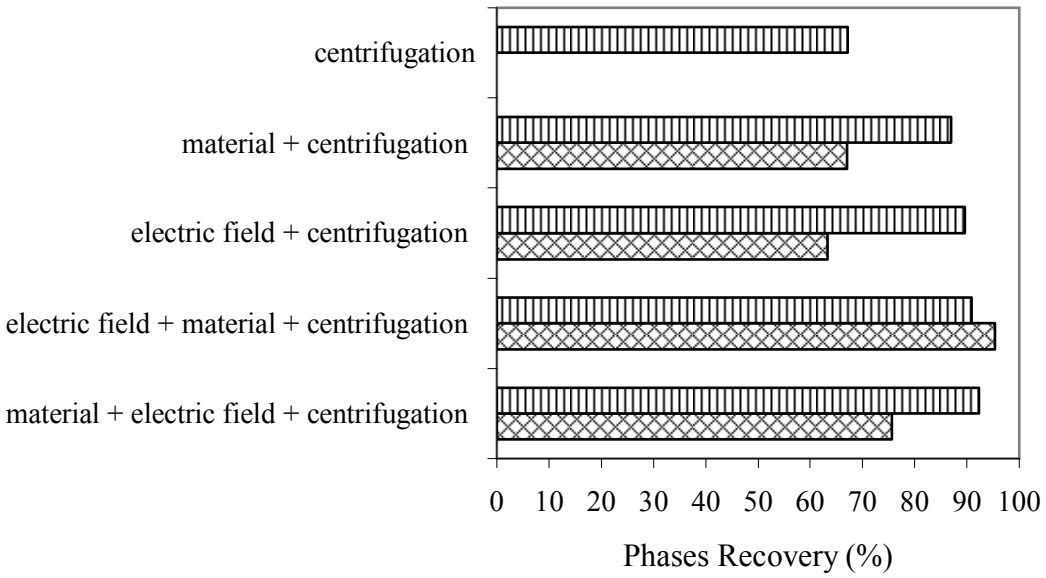

Figure 6-14. Combined Techniques Effect on Water and Paraffin Recovery
Water in Paraffin Emulsion, Surfactant: Span 80®, *HLB* = 4.3, *Cs* = 2 % v/v, *vm* = 13400 rpm, t_E = 5 min, *tc* = 20 min, *vc* = 2600 rpm, *Cm* = 5 % w/w, *x* < 0.89 mm. Recovery: (▨) Water (▥) Paraffin

Although indeed some configurations improved the clarification process, important changes were observed in the water coalescence since the water recovery varied from 0 % in test 1 to over 95 % in test 4. Paraffin recovery, however, varied from 67 % in test 1 to 91 and 92 % in tests 4 and 5, respectively.

It seems that peanut shell presence increases the conductivity of the emulsion continuous phase, reducing its tolerance to *DC* electric field. When acting separately, electric field and collector material improve coalescence, but when they are combined, the effect is stronger and higher coalescence is reached.

6.2.4 Microscopic Approach on Emulsion Electrostatic Dehydration

In this section, characterization by microscopy of water in paraffin synthetic emulsions and water in crude oil emulsions is compared. The characterization was made before and after the application of an electric field. Therefore, samples of the original and the residual emulsion

were analyzed in the microscope according to the procedure developed in chapter 4. Additionally, the coalescence in crude oil emulsions under electrostatic field at microscopic scale was monitored and documented by means of videos and photography.

Direct Microscopic Observation of Coalescence in Water in Oil Emulsions

The electrical cell described in figure 6-3 was used to observe the phenomenon of coalescence of water in crude oil emulsions which are residues of the production process with high stability. Figure 6-15 shows a photo sequence from the initial state of the emulsion up to 1 minute of 1000 V/cm electric field application. The Figure refers to Fosa Acema 100, which has a water content of fw = 0.471 and a particle average size of x_s =15.4 μm. The time of application of electric field appear below each picture.

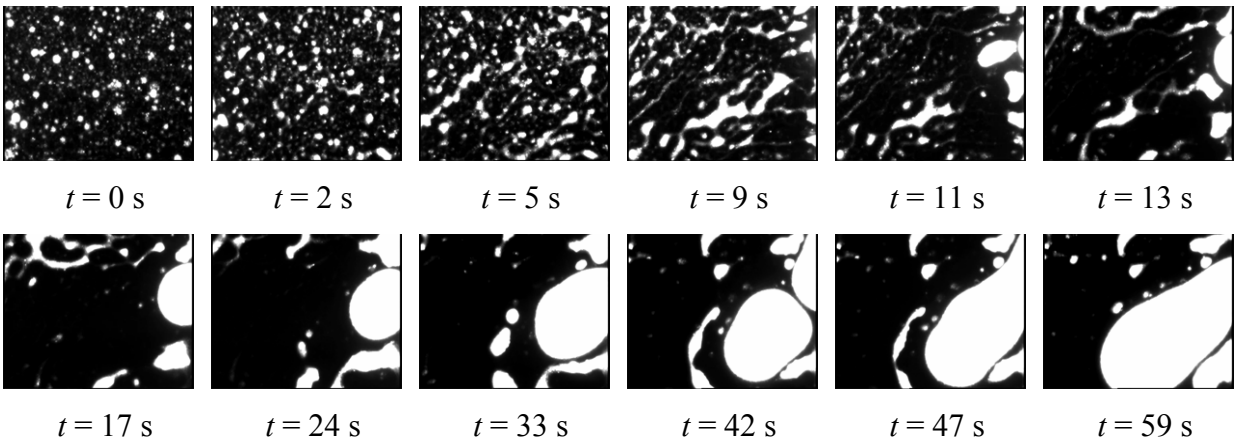

Figure 6-15. Sequence of Emulsion Dehydration

Waste Oil emulsion from Fosa Acema 100, E = 1000 V/cm for 1 min

Once the electric field is applied, the number of droplets is reduced and the water forms big drops that are accumulated in one electrode. The process is faster in the first 12 seconds, in which all the water moves to one side; nevertheless, the growth process persists up to approximately 75 seconds. After that, the sample does not experience more changes and it continues being an emulsion in the positive electrode side. The drops have a big size and can be observed without microscope, they are very close to each other, even in apparent contact, but coalescence does not occur. In the sample center and in the neighborhood of the negative electrode no water drops are seen.

At the beginning, most of the droplets are spherical, but as they grow they tend to become deformed, basically as a result of the interactions between drops. In Figure 6-16 it can be observed how macro drops are accumulated on the positive electrode, and are highly

deformed. The coalescence process could continue if the electric field is increased, but this is limited by the high crude oil conductivity, water salinity and water content.

Figure 6-16. Water accumulation on the Positive Electrode after Emulsion Dehydration Waste Oil emulsion from Fosa Acema 100, E = 1000 V/cm for 135 s

Probably coalescence does not occurs due to a steric stabilization that comes from the bulky hydrophobic groups of the asphaltenes or resin materials that are the natural surfactants of the emulsion, thus the actual distance between the drop or particle surface can never reach the minimum required for the cohesion/adhesion force to take over. The steric barrier deal with a situation in which forces or potentials oppose each other until equilibrium is reached and no consideration is made of the time scale nor the way the changes are occurring, because only physic chemical or thermodynamics phenomena are involved. But there are also situations where the kinetics is responsible for the phenomena of interest.

Since the neighborhood of the interface is a non homogeneous region, a convective fluid flow can drain away some substances, and produce a physic chemical unbalance. It is known that a system tends spontaneously to oppose any change, so the unbalance generally generates some potential that induces some motion to re-establish an equilibrium situation. These effects, that tend to restrain the thin liquid film drainage and result in an apparent increase of the liquid phase viscosity, are expected to take place when the film thickness is extremely small, say in the 100 - 500 Å range, (Salager 1994).

By the other hand, the great rigidity of the film, evidenced by the irregular shape of the water droplets, could also prevent coalescence of the droplets (Rosen 2004).

Image Analysis of Coalescence for Water in Crude Oil Emulsions in 100 mL Cell

Characterization Results from the collected data by means of the cell shown in the Figure 6-3 and the image analysis system were not satisfactory because they were not repeatable. Standard deviations up to 80% were obtained. It is presumed that at a microscopic and scale, a precision cell is required in which the position of the electrodes and the amount of sample can perfectly be controlled, and these parameters could not be kept constant since the cell was not designed for such aim.

In order to characterize the coalescence by means of microscopy, the 100 mL cell with the electrodes described as type *A* in table 6-1 was used. The cell was filled with 100 mL of sample from Fosa Merey 31, which has a water content of fw = 0.221 and a particle average size of x_s = 10.3 μm. The cell was submerged in a thermostatic bath and warmed up to 80 °C. After that, 4000 V/cm electric field was applied for 3 hours at constant temperature. At this time there was no water on the cell bottom but on the walls. For this reason it was necessary to centrifuge the sample at 2600 rpm during 30 min after which 21 % water was separated.

Before centrifugation, samples were taken from the top, center and bottom of the cell hourly and they were analyzed with the microscope. Under these conditions, the results were reproducible and the average of 4 measurements is reported. Also the influence of the number of photos in the characterization was evaluated. It depends on the used magnification. Characterization was made as described in chapter 4.

Electric field effect on particle number is shown on Figure 6-17. In the ordinate the particle number factor is shown, defined as the number of particles per unit of area measured at time t divided by the number of particles per unit of area measured at time t_0 before applying the electric field.

As it is observed, a considerable reduction in the number of particles occurs once the electric field is applied. Although the first sample was taken after one hour, it is probable that this reduction in the number of particles takes place much more early. In the subsequent measurements, appreciable changes are not observed.

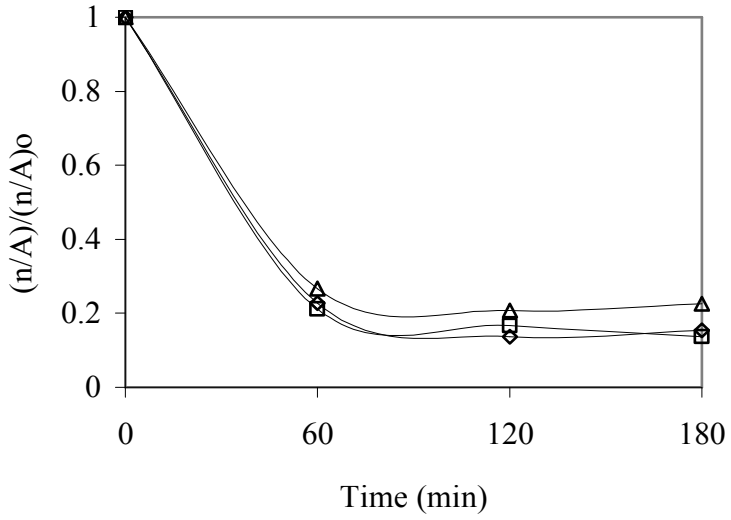

Figure 6-17. Electric Field Effect on Particle Number

Waste Oil emulsion from Fosa Merey 31, E = 4000 V/cm. 100 mL Electrostatic Cell. Particle Number (△) bottom, (◇) top, (□) center

Figure 6-18 shows the electric field effect on particle size. x_{50} of the surface distribution appears on the left and the equivalent diameter x_s on the right. The calculation corresponds to the same experiments described in Figure 6-17. In general, we find a growth of particles as a result of the electric field. A size profile, product of the combined effect of coalescence and sedimentation is developed during the process; nevertheless, after 3 hours the sample tends to be homogenous.

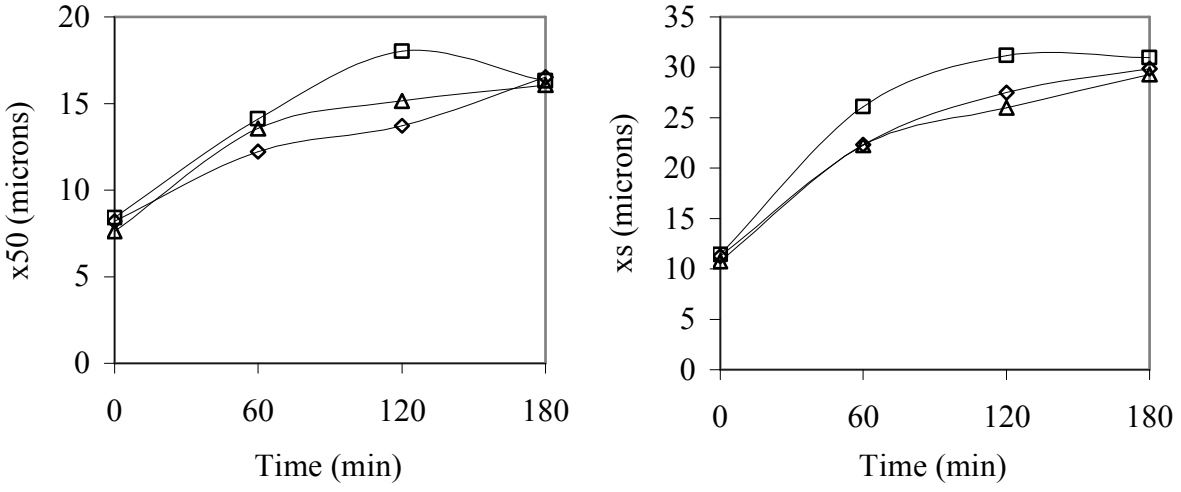

Figure 6-18. Electric Field Effect on Particle Size

Waste Oil emulsion from Fosa Merey 31, E = 4000 V/cm. 100 mL Electrostatic Cell. Particle Number (△) bottom, (◇) top, (□) center

Although the equivalent diameter x_s is tripled, this value is still small for a high viscosity emulsion with a small density difference, which explains that water does not settle and the emulsion is not broken.

Image Analysis of Coalescence for Water in Paraffin Emulsions in 20 mL Cell

Microscopy results of Merey 31 sample can be compared with what occurs with water in paraffin emulsion which is destabilized by an electric field. Three cases of water in paraffin emulsions are microscopically analyzed: the original emulsion stabilized by a Span 80 and Arkopal N 040 mixture with HLB = 5.5 and fw = 0.5, the residual emulsion after 1 hour of 1000 V voltage, and the residual emulsion after 1 hour of 1500 V voltage. In cases 2 and 3, the 20 mL glass cell described in Figure 6-1 was used. The results are shown in table 6-2. The volume of residual emulsion or unresolved emulsion Vr, the number of particles per unit of area n/A, and the equivalent diameter x_s are described as dimensionless parameters using the original emulsion data.

Table 6-2. Microscopic analysis results for a water in paraffin emulsion sample Separated by the electric field

Parameter	**0 kV original emulsion**	**1.0 kV for 1 h residual emulsion**	**1.5 kV for 1h residual emulsion**
$V_r/V_{r,0}$	1	0.449	0.399
$(n/A)/(n/A)_0$	1	2.475	3.401
$x_s/x_{s,0}$	1	0.687	0.602

At the end of the process, two fundamental differences exist in comparison with the case of the crude emulsion, where water separation was not observed. For water in paraffin emulsion, the number of particles increases instead of decreasing, and the equivalent diameter is smaller. Water drops grow sufficiently to settle, and water is accumulated at the cell bottom; also water movement generates a paraffin displacement forming a clear layer on the top. At the center of the cell there is a residual emulsion that is more concentrated than the original one, which contains all the small droplets that could not settle from the total emulsion volume.

6.3 Conclusions and Recommendations

- *DC* electric field can be used to break *W/O* emulsions, but when the emulsions are concentrated and/or the conductivity of the continuous phase is high, bridging and short circuits can happen disturbing the process.
- When a *DC* electric field is applied to a *W/O* emulsion, the drops tend to be accumulated in the positive electrode of the cell. If the emulsion is very viscous, chains of drops between the electrodes are formed and bridging occurs. In this situation, a hydrophobic coating can prevent short-circuiting, but also affect the coalescence rate.
- By a *DC* electric field, water recovery increases with the applied potential in a non-linear function. Therefore, an optimal electric field implies a compromise between the obtained separation and the operative costs.
- *DC* electric field efficiency depends considerably on emulsion water content in combination with others factors like the properties of the phase and the formulation.
- Paraffin and water recovery was higher when plate electrodes were used, even though the cylindrical electrodes cell constant was higher. In all cases, the applied electric field was more efficient to promote paraffin clarification than water coalescence.
- To destabilize highly stable emulsions, processes integration is required. For water in paraffin emulsions, an appropriate combination of electrostatic field, collector material and centrifugation increases both water and paraffin recovery. The optimum conditions depend on the emulsion formulation.
- It is recommended to evaluate a continuous system formed by a pair of “on line” electrodes, a packed bed of collector material and a centrifuge. It is presumed that the fluid movement can diminish the problems of accumulation in the electrodes.
- For waste oil emulsions at a constant *DC* electric field coalescence occurs, but once the drops reach certain size, the film thinning is stopped and settling does not take place. The process can only continue if the electric field is increased; however, the electric field strength is limited by the high crude oil conductivity, water salinity and water content.
- Emulsion separation can be characterized microscopically by the so called particle number factor and the particle size factor. The simple coalescence is detected by a growth in drop size and a reduction in the particle number; but when the emulsion is separated, the drop size of the residual emulsion is smaller than the original one and the number of drops increases proportionally to the obtained separation.

- It is recommended to include solid particles as well as asphaltenes in water in paraffin emulsions. Thus, the relative contributions of these variables to the stability could be studied.

7 General Conclusions and Perspectives

7.1 General Conclusions

In this work, knowledge on emulsion is developed in the following aspects:

A protocol to prepare stable emulsions of water in paraffin in a wide range of water content was proposed. The protocol is the result of a systematic evaluation of the influence of surfactant content, *HLB* value, emulsion batch volume, octanol content, water salinity and mixing conditions on the emulsion stability. A model to determine the emulsion viscosity of water in paraffin emulsions as a function of both water content and shear rate with 4% standard deviation is also included.

A new method to characterize water in crude oil emulsions is developed using the *ASTM* standards for water and solids estimation and the characterization by microscopy. Characterization by microscopy is improved by considering some corrections of the information obtained from the image analysis system. As an additional benefit, characterization by microscopy is made without the traditional dilution that can drastically change in some cases the original particle size distribution. The obtained information can also be used to characterize in a microscopic way the coalescence and emulsion separation by comparing changes in particle size and particle number, introducing an innovative procedure in comparison with the traditional stability estimation by measuring the separate volume.

This work introduces the collector material concept: the use of a material to help and promote emulsion separation. Several materials were tested and the best results were reached with peanut shell. Process conditions should be optimized according with the material particle size and content. Separation by centrifugation, a technique commonly used to destabilize emulsions, was significantly improved by combining with *DC* electric field and the collector material.

7.2 Perspectives

Although this research does not show a definitive and unique solution to the problem of the waste oil lagoons in Venezuela, it serves as a base providing a research methodology, techniques and first results in order to develop new projects, testing new ideas, and optimize the results.

Actually, the Chemical Engineering School of the Central University of Venezuela has the financing from the government to continue studying the problem of waste oil handling, using the more appropriate resources to generate concrete solutions from the laboratory scale, to pilot plants and also treatment in field.

Basic Research should be continued with the formulation of highly stable synthetic emulsions, including complex emulsions closer to crude oil emulsions. Three things are recommended: first including asphaltenes in the water in paraffin emulsion formula. Asphaltenes play a significant role on emulsion stability (Yang et al., 2001). They can be precipitated from clean crude oils with n-heptane and filtrated. The separation procedure is explained by Marfisi (2004). Some preliminary tests developed the last year demonstrate that the presence of asphaltenes increases considerably the emulsion stability: the higher the asphaltenes content the higher the stability.

The tests were made with an emulsion with 30% of water, 50% of paraffin and 20% of toluene in which the asphaltenes were previously dissolved. The emulsifier was a mixture of Span 80® and Arkopal N100® of *HLB* = 5.92. Due to solubility, asphaltenes content can be varied from 0 to 160 mg asphaltenes/mL toluene.

Secondly, finely divided solids should be also included. They are able to act as surfactants positioning themselves in the water-oil interface. Calcium carbonate, clay and sand are recommended for such aim. Finally, other emulsifiers can also be tested, including the ionic ones and natural surfactants extracted from crude oil.

It is also important to characterize the new emulsions: density, viscosity, conductivity and particle size distribution should be studied regularly. When asphaltenes are added, the emulsion becomes dark; therefore, the presence of asphaltenes could help on the characterization of water in paraffin emulsion by means of microscopy where some problems were observed, due to the weak contrast between the two phases.

Monitoring stability of such emulsions could require a long time. The application of an electric field can be used to evaluate more rapidly emulsion stability of different formulas when the electric field conditions remain constant. In this case, the stability will be defined by the electric field effect on particle number and average particle size (as shown in Fig. 6-17 and 6-18) and by the phase separation, reported as paraffin and water recovery.

Emulsion destabilization should be evaluated by means of process intensification. Centrifugation, electric field and the collector material concept can continue being tested. For synthetic emulsions with asphaltenes as well as for waste oil emulsions, commercial emulsifiers and temperature should also be used. Even though chemical demulsification is

very expensive, and it is considered as the last option to solve the environmental problem of the wastes, a combined process could reduce the chemical requirements.

It is probable that the cellular character and porosity of the peanut shell is the reason for which peanut shell is a good collector material, while *PVC* is not. In this work, also brown coal was tested as collector material (see Fig. 5-19). The results might be improved by using charcoal because it has a more porous structure. The collector material should also be tested in a continuous process. Thus, the material life time and the replacement time could be evaluated, indicating its applicability on a larger scale.

The oil wastes problem is not only the treatment of the production pitch. If all the waste pools were cleaned, but no actions are taken in the production process, the pools would fill again within some years. The technologies and procedures to eliminate the wastes must also be oriented to implement a clean production process where products out of specification are returned and treated.

8 References

Bailes, P., E. Stitt, Column Liquid Contacting with Vigorous Agitation Balanced by Electrostatic Coalescence, *Chem. Eng. Res. Des*. **1987**, *65*, 514–523.

Bailes, P., Electrically Augmented Settlers and Coalescers for Solvent Extraction, *Hydrometallurgy*. **1992**, *30 (1–3)*, 417–430.

Bailes, P., S. Larkai, An Experimental Investigation into the Use of High Voltage D.C. Fields for Liquid Phase Separation, *Trans. IChemE*. **1981**, *59 (4)*, 229–237.

Bailes, P., S. Larkai, Liquid Phase Separation in Pulsed D.C. Fields, *Trans. IChemE*. **1982**, *60 (2),* 115–121.

Becher, P., Emulsions: Theory and Practice. Reprint, R. Krieger, Huntington NY, **1977**.

Boyd, J., C. Parkinson, P. Sherman, Factors Affecting Emulsion Stability, and the HLB Concept, *Colloid Interface Sci*. **1972**, *41 (2)*, 359-370.

Bradbury, S., Linear Measurement with the Light Microscope, *Microsc. Anal*. **1990**, *17*, 7-12.

Caldwell, K., J. Li, Emulsion Characterization by the Combined Sedimentation Field-Flow Fractionation-Photon Correlation Spectroscopy Methods, *Colloid Interface Sci*. **1989**, *132*, 256-268.

Chen, C., J. Maa, Y. Yang, C. Chang, Effects of Electrolytes and Polarity of Organic Liquids on the Coalescence of Droplets at Aqueous–Organic Interfaces, *Surf. Sci.* **1998**, *406*, 167–177.

Chen, T., R. Mohammed, A. Bailey, P. Luckham, S. Taylor. Dewatering of Crude Oil Emulsions 4. Emulsion Resolution by the Application of an Electric Field, *Colloids Surf. A*. **1994**, *83*, 273–284.

Chesters, A., The Modelling of Coalescence Processes in Fluid–Liquid Dispersions: a Review of Current Understanding, *Trans. IChemE.* **1991**. *A*69, 259–270.

Cottrell, F., J. Speed, *Separating and collecting particles of one liquid suspended in another liquid*, US Patent 987, 115, **1911**.

Cross, J., *Electrostatics: Principles, Problems and Applications*. Adam Hilger, Bristol, **1987**.

Dezhi, S., J. Chung, D. Xiaodong, Z. Ding, Demulsification of Water in Oil Emulsion by Wetting Coalescence Materials in Stirred and Packed Columns, *Colloids and Surfaces A: Physicochemical and Engineering Aspects.* **1999**, *150*, 69-75.

Draxler, J., R. Marr, , Design Criteria for Electrostatic Deemulsifiers, International Chemical Engineering, Austria, **1993**, *33*, *1*.

Drelich, J., G. Bryll, J. Kapczynski, J. Hupka, J. Miller, F. Hanson, The Effect of Electric Field Pulsation Frequency on Breaking Water-in-Oil Emulsions, *Fuel Process. Technol*. **1992**, *31*, 105-113.

Eberth, K., J. Merry, A Comparative Study of Emulsions Prepared by Ultrasound and by a Conventional Method. Droplet Size Measurements by Means of a Coulter Counter and Microscopy, *Int. J. Pharm*. **1983**, *14*, 349-353.

Eow, J., M. Ghadiri, A. Sharif, T. Williams. Electrostatic Enhancement of the Coalescence of Water Droplets in Oil: a Review of the Current Understanding, *Chem. Eng. J*. **2001**, *84 (3)*, 173–192.

Eow, J., M. Ghadiri. Electrostatic Enhancement of the Coalescence of Water Droplets in Oil: a Review of the Technology, *Chem. Eng. J*. **2002**, *85*, 357–368.

Ford, R. , C. Furmidge, Study at Phase Interfaces II: The Stabilization of Water-in -Oil Emulsions Using Oil -Soluble Emulsifiers, *J. Colloid Interface Sci*. **1966**, *22 (4)*, 331-341.

Fox, R., A. McDonald, *Introduction to Fluid Mechanics*. John Wiley & Sons Inc, New York, **2003**, p. 752.

Freshwater, D., B. Scarlett, M. J Groves. *Am. Cosmet. Perfum*. **1966,** *81*, 43.

Friberg, S., S. Jones. Emulsions, in *Kirk-Othmer Encyclopedia of Chemical Technology*, John Wiley & Sons, Inc. Vol. 9, 4th Edition, **1996**, pp. 393–413.

Galvin, C. Design Principles for Electrical Coalescers, *IChemE Symp. Ser*. **1986**, *88*, 101–113.

Garti, N., Double Emulsions-Scope, Limitations and New Achievements, *Colloids Surf. A: Physicochemical and Engineering Aspects*. **1997**, *123-124*, 233-246.

Gossen, P., J. MacGregor, R. Pelton, Composition and Particle Diameter for Styrene Methyl Methacrylate Copolymer Latex Using UV and NIR Spectroscopy. *Appl. Spectrosc*. **1993**, *47*, 1852-1870.

Goto, M., J. Irie, K. Kondo, F. Nakashio, Electrical Demulsification of W/O Emulsion by Continuous Tubular Coalescer, *J. Chem. Eng. Jpn*. **1989**, *22 (4)*, 401–406.

Graciaa, A, J. Lachaise, M. Bourrel, I. Osborne-Lee, I. Schechter, W. Wade, Partitioning of Nonionic and Anionic Surfactant Mixtures Between Oil/Microemulsion/Water Phases. *SPE Reservoir Eng*. **1984**, *2*, 305-314.

Griffin, W.C., Classification of Surface Active Agents by HLB, *J. Soc. Cosm. Chem*. **1949**, *1*, 311-326.

Groves, M. J., B. Kaye, B. Scarlett, Size Analysis of Sub-sieve Powders using a Centrifugal Photo Sedimentometer, *Br. Chem. Eng*. **1964**, *9*, 742-744.

Hirato, T., K. Koyama, T. Tanaka, Y. Awakura, H. Majima, Demulsification of Water-in-Oil Emulsion by an Electrostatic Coalescence Method, *Mater. Trans. JIM*. **1991**, *32 (3)*, 257–263.

Hsu, E., N. Li, T. Hucal, Electrodes for Electrical Coalescence of Liquid Emulsions, *US Patent* 4 415 426, **1983**.

Isaacs, E., R. Chow, Practical Aspects of Emulsion Stability, *Adv. Chem. Ser*. **1992**, *231*, 251–277.

Ito, H., H. Hayashi, H. Sasaki, Rapid Separation of Oil Particles from Low-Concentrated O/W Emulsions in the Presence of Anionic Surfactants Using Fibrous Slag**,** *Journal of Colloid and Interface Science.* **2002***, 252*, 214-221.

Kabalnov, Thermodynamic and theoretical aspects of emulsions and their stability, *Curr. Opin. Colloid Interf. Sci.* **1998**, *3*, 270–275.

Kaler, E., K. Bennet, H. Davis, L. Scriven, Toward Understanding Microemulsion Microstructure: A Small-Angle X-Ray Scattering Study, *J. Chem. Phys*. **1983**, *79*, 5673-5684.

Kallevik, H., S. Hansen, ∅. Saether, O. Kvalheim, J. Sjöblom, Crude Oil Model Emulsion Characterised by means of Near Infrared Spectroscopy and Multivariate Techniques, *J. Disp. Sci. Technol.* **2000**, *21*, 245-262.

Kano, k., T. Yamaguchi, T. Ogawa, Fluorescense Studies on Morphological Change of Oil-in-Water Microemulsions upon Dilution with Water, *J. Phys. Chem*. **1984**, *88*, 793-796.

Kapilashrami, A., K. Eskilsson, L, Bergström, M. Malmsten, Drying of Oil in Water Emulsions on Hydrophobic and Hydrophilic Substrates, *Colloids and Surfaces A: Physicochemical and Engineering Aspects*. **2004**, *233*, 155-161.

Man, C., A. Pacek, A. Nienow, Coalescence in Dilute Non-Viscous Liquid/Liquid Dispersions: Numerical Simulation and Experimental Results, *IChemE Jubilee Res. Event,* **1997**, *22 (7)*, 356–375.

Marfisi, S., *Estabilidad de Emulsiones Relacionada con el Proceso de Deshidratación de Crudos,* Doctoral Thesis, Universidad de los Andes, Laboratorio FIRP, Venezuela, **2004**.

Mason, S., K. May, S. Hartland, Drop Size and Concentration Profile Determination in Petroleum Emulsion Separation, *Colloids Surf. A: Physicochemical and Engineering Aspects*. **1995**, *96*, 85-92.

Mikula, R., Emulsion Characterization, in *Emulsions: Fundamentals and Applications in the Petroleum Industry* (Ed.: L. Schramm), American Chemical Society, Washington, **1992**, pp. 79.

Mohammed, R., Bailey, P. Luckham, S. Taylor. Dewatering of crude oil emulsions 2. Interfacial properties of the asphaltic constituents of crude oil, *Colloids Surf. A,* **1993**, *80*, 237–242.

Morrison, I., Ross, S., *Colloidal Dispersions: Suspensions, Emulsions, and Foams*. John Wiley & Sons, inc., New Jork, **2002**, p. 616.

Münch, Ch., H. Hoffmann, K. Ibel, J. Kalus, G. Neubauer, U. Schmelzer, J. Selbach, Transient Small-Angle Neutron Scattering Experiments on Micellar Solutions with a shear-Induced Structural Transition, *J. Phys. Chem*. **1993**, *97*, 4514-4522.

Orr, C., Determination of Particle Size. in *Encyclopedia of Emulsion Technology Volume 3* (Ed.: P. Becher), Marcel Dekker, Inc., New York, **1988**, pp. 137-170.

Pohl, H., Nonuniform Field Effects: Dielectrophoresis, in *Electrostatics and its Applications* (Ed.: A. D. Moore), John Wiley, New York, **1973**, p. 336.

Rommel, W., W. Meon, E. Blass. Review: hydrodynamic modeling of droplet coalescence at liquid–liquid interfaces, *Sep. Sci. Technol*. **1992**, *27 (2)*, 129–159.

Rosen, M., *Surfactants and Interfacial Phenomena*. John Wiley & Sons, inc., New Jersey, **2004**, p. 444.

Salager, J-L., *Formulación, Composición y Fabricación de Emulsiones para Obtener las Propiedades Deseadas. Estado del Arte. Parte B. Propiedades de las Emulsiones y su Medición*, Laboratorio FIRP, Mérida, **1999**, p. 40.

Salager, J-L., Formulation Concepts for the Emulsion Maker, in *Pharmaceutical Emulsions and Suspensions* (Ed.: F. Nielloud, G. Marti-Mestres), Marcel Dekker, Inc., New York - Basel, **2000**, pp. 19-125.

Salager, J-L., *Interfacial phenomena in Dispersed Systems*, Laboratorio Firp, Mérida, **1994**, p. 26.

Salager, J-L., *Surfactantes en Solución Acuosa*, Laboratorio Firp. Mérida, **1993**, p. 26.

Santos, A., E. Lima, J. Pinto, In-Line Evaluation of Average Particle Size in Styrene Suspension Polymerization Using Near Infrared Spectroscopy, *J. Appl. Polym. Sci.* **1998**, *70*, 1737-1745.

Schulman, J., E. Cockbain, Molecular Interactions at Oil/Water Interfaces. Part I: Molecular Complex Formation and the Stability of Oil in Water Emulsions, *Trans. Faraday Soc*. **1940**, *36*, 661-668.

Sherman, P. (Ed.), *Emulsion Science*, Academic Press, Inc. New York, **1968**. p 496.

Shin, C., G. Chase, The Effect of Wettability on Drop Attachment to Glass Rods, *Journal of Colloid and Interface Science*. **2004**, *272*, 186-190.

Shinoda, K., M. Fukuda, A. Carlsson, Characteristic Solution Properties of mono-, di- and Triglyceryl Alkyl Ethers: Lipophobicity of Hydrophilic Groups**,** *Langmuir*. **1990**, *6*, 334-337.

Sun, D., S. Jong, X. Duan, D. Zhou. Demulsification of Water-in-Oil Emulsion by Wetting Coalescence Materials in Stirred- and Packed-Columns, *Colloids Surf. A*. **1999**, 150, 69–75.

Sun, D., X. Duan, W. Li, D. Zhou. Demulsification of Water-in-Oil Emulsion by Using Porous Glass Membrane, *J. Membrane Sci.* **1998**, *146*, 65–72.

Taylor, S., Conductivity and Coalescence of Water-in-Crude Oil Emulsions under High Electric Fields, *Inst. Phys. Conf. Ser*. **1991**, *118 (3),* 185–190.

Taylor, S., Investigations into the Electrical and Coalescence Behaviour of Water-in-Crude Oil Emulsions in High Voltage Gradients, *Colloids Surf.* **1988***, 29*, 29–51.

Taylor, S., Theory and Practice of Electrically Enhanced Phase Separation of Water-in-Oil Emulsions, *Trans. IChemE.* **1996**, *74 (A),* 526–540.

Vrij, Possible Mechanism for the Spontaneous Rupture of Thin Free Liquid Films, *Discuss. Faraday Soc*. **1966**, *42*, 23–33.

Warren, K., G. Sams, T. Nakayama. Electrostatic Fields: Essential Tools for Desalting, *AIChE Spring Meeting*, **1998**.

Waterman, L., Electrical coalescers, *Chem. Eng. Prog*. **1965**, *61 (10),* 51–57.

Williams, T., A. Bailey, Changes in the Size Distribution of a Water-in-Oil Emulsion due to Electric Field Induced Coalescence, *IEEE Trans. Ind. Appl*. **1986**, *1A–22 (3),* 536–541.

Yang, X. et al., Film Properties of Asphaltenes and Resins in *Encyclopedic Handbook of Emulsion Technology* (Ed.: J. Sjöblom), Marcel Dekker, Inc., New York, **2001**.

Zavarce, L., *Utilización del Concepto de Materiales Colectores para Mejorar la Cinética de la Separación del Agua en Emulsiones de Agua en Aceite*, Chemical Engineering Thesis, Universidad Central de Venezuela, **2006.**

Appendix A1. Experimental Plan for Emulsion Formulation

Table A1-1. Formulation. Determine Surfactant Content Effect on Emulsion Stability

Variable	Value
Surfactant Content (% v/v)	0.5, 1.0, 1.5, 2.0, 4.0, 8.0, 10
Water Content (% v/v)	50
Co-Surfactant Content (%v/v)	0.0
Salinity (g/dL Water)	0.0
HLB	5.5
Mixing Type	continuous
Mixing Time (min)	5
Mixing Velocity (rpm)	13400

Table A1-2. Formulation Variables. HLB Effect on Emulsion Stability

Variable	Value
Surfactant Content (% v/v)	2.0
Water Content (% v/v)	25, 50, 75
Co-Surfactant Content (%v/v)	0.0
Salinity (g/dL Water)	0.0
HLB	4.5, 5.0, 5.5, 6.0, 6.5
Mixing Type	continuous
Mixing Time (min)	5
Mixing Velocity (rpm)	13400

Table A1-3. Formulation Variables. Co-Surfactant Content Effect on Emulsion Stability

Variable	Value
Surfactant Content (% v/v)	2.0
Water Content (% v/v)	25, 50, 75
Co-Surfactant Content (%v/v)	0.0, 2.0, 4.0
Salinity (g/dL Water)	0.0
HLB	4.5, 5.0, 5.5, 6.0, 6.5
Mixing Type	continuous
Mixing Time (min)	5
Mixing Velocity (rpm)	13400

Table A1-4. Formulation Variables. Water Salinity Effect on Emulsion Stability

Variable	Value
Surfactant Content (% v/v)	2.0
Water Content (% v/v)	25
Co-Surfactant Content (%v/v)	0.0
Salinity (g/dL Water)	0.0, 4.0, 8.0, 12.0, 16.0
HLB	5.5
Mixing Type	continuous
Mixing Time (min)	5
Mixing Velocity (rpm)	13400

Table A1-5. Formulation Variables. Mixing Velocity Effect on Emulsion Stability

Variable	Value
Surfactant Content (% v/v)	2.0
Water Content (% v/v)	50
Co-Surfactant Content (%v/v)	0.0
Salinity (g/dL Water)	0.0
HLB	5.5
Mixing Type	continuous
Mixing Time (min)	5
Mixing Velocity (rpm)	6100, 9500, 13400

Table A1-6. Formulation Variables. Mixing Time Effect on Emulsion Stability

Variable	Value
Surfactant Content (% v/v)	2.0
Water Content (% v/v)	50
Co-Surfactant Content (%v/v)	0.0
Salinity (g/dL Water)	0.0
HLB	5.5
Mixing Type	continuous
Mixing Time (min)	5, 10, 20
Mixing Velocity (rpm)	13400

Table A1-7. Formulation. Mixing Type Effect on Emulsion Stability. Intermittent I: with 5 min pause. Intermittent II: 5 min at 8000 rpm, 5 min pause, 5 min at 13400 rpm

Variable	Value
Surfactant Content (% v/v)	2.0
Water Content (% v/v)	50
Co-Surfactant Content (%v/v)	0.0
Salinity (g/dL Water)	0.0
HLB	5.5
Mixing Type	Continuous, Intermittent I, Intermittent II
Mixing Time (min)	10
Mixing Velocity (rpm)	(8000 only Intermittent II) 13400

Table A1-8. Formulation Variables. Emulsion Volume Effect on Emulsion Stability

Variable	Value
Surfactant Content (% v/v)	2.0
Water Content (% v/v)	50
Co-Surfactant Content (%v/v)	0.0
Emulsion Volume (Water + Paraffin) (mL)	50, 100, 250, 500
Salinity (g/dL Water)	0.0
HLB	5.5
Mixing Type	Continuous, Intermittent I, Intermittent II
Mixing Time (min)	10
Mixing Velocity (rpm)	(8000 only Intermittent II) 13400

Appendix A2. Particle Size Distribution for Waste Oil Emulsions

Note: droplets in contact with the borders of the pictures were always excluded.

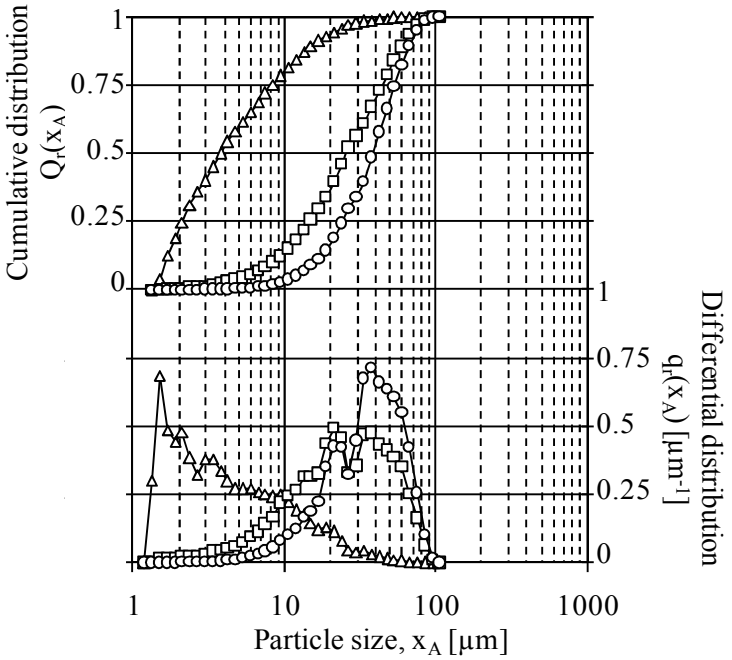

Figure A2-1. Sample Acema 100. Cumulative (top) $Q_r(x_A)$ and density size distribution (bottom) $q_r(x_A)$ for droplets determined by optical microscopy. Number of particles counted: 35074 ± 5042. Combined magnification 5X+10X+20X. Sample thickness: 27.25 ± 7.12 μm. (△) number: r = 0, (□) area: r = 2, (○) volume: r = 3

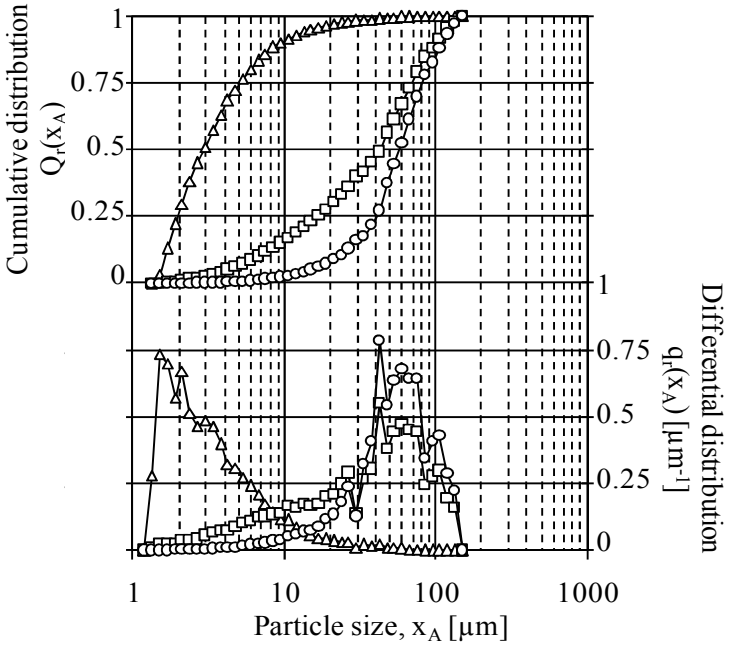

Figure A2-2. Sample Merey 31. Cumulative (top) $Q_r(x_A)$ and density size distribution (bottom) $q_r(x_A)$ for droplets determined by optical microscopy. Number of particles counted: 17737 ± 14385. Combined magnification 5X+10X+20X. Sample thickness: 36.38 ± 4.94 μm. (△) number: r = 0, (□) area: r = 2, (○) volume: r = 3

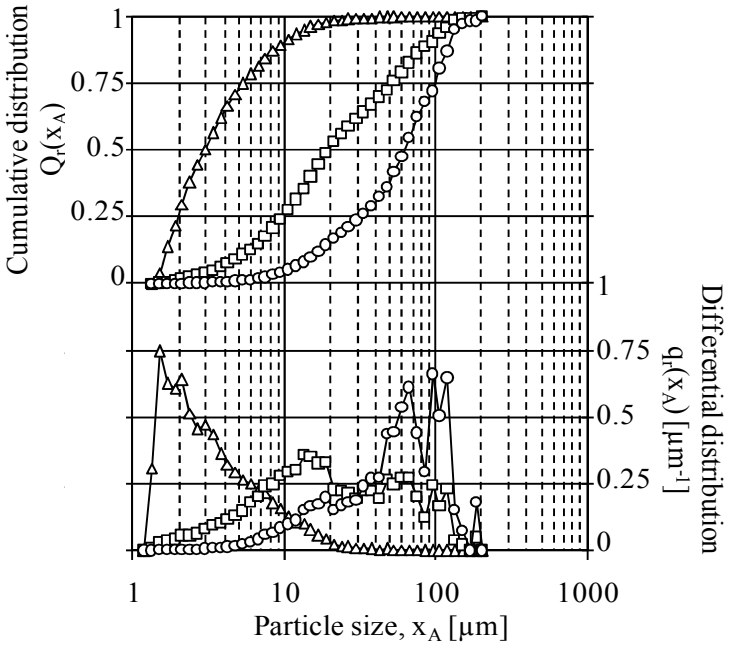

Figure A2-3. Sample Guara 2. Cumulative (top) $Q_r(x_A)$ and density size distribution (bottom) $q_r(x_A)$ for droplets determined by optical microscopy. Number of particles counted: 53843 ± 30288. Combined magnification 5X+10X+20X. Sample thickness: 61.38 ± 18.44 μm. (△) number: r = 0, (□) area: r = 2, (○) volume: r = 3

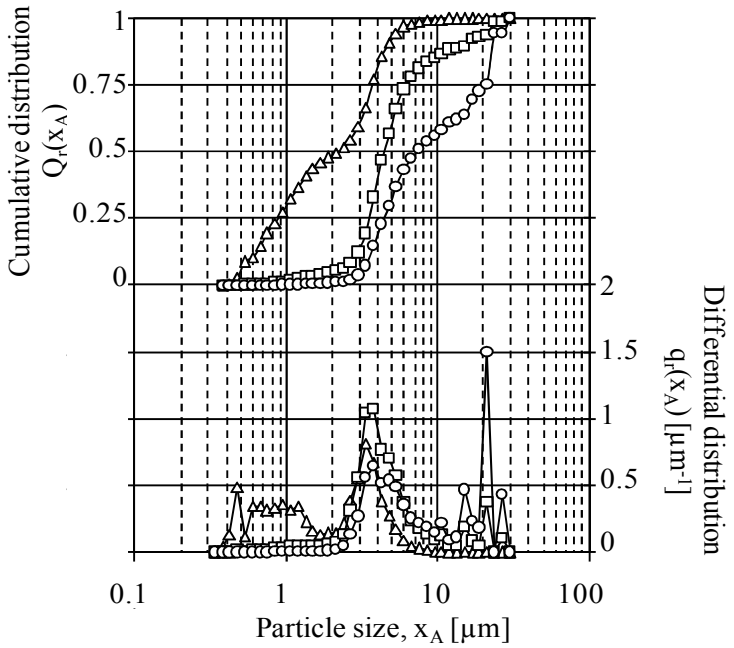

Figure A2-4. Sample Fosa 1. Cumulative (top) $Q_r(x_A)$ and density size distribution (bottom) $q_r(x_A)$ for droplets determined by optical microscopy. Number of particles counted: 5344. Combined magnification 5X+10X+20X. Sample thickness: 18.7 μm. (△) number: r = 0, (□) area: r = 2, (○) volume: r = 3

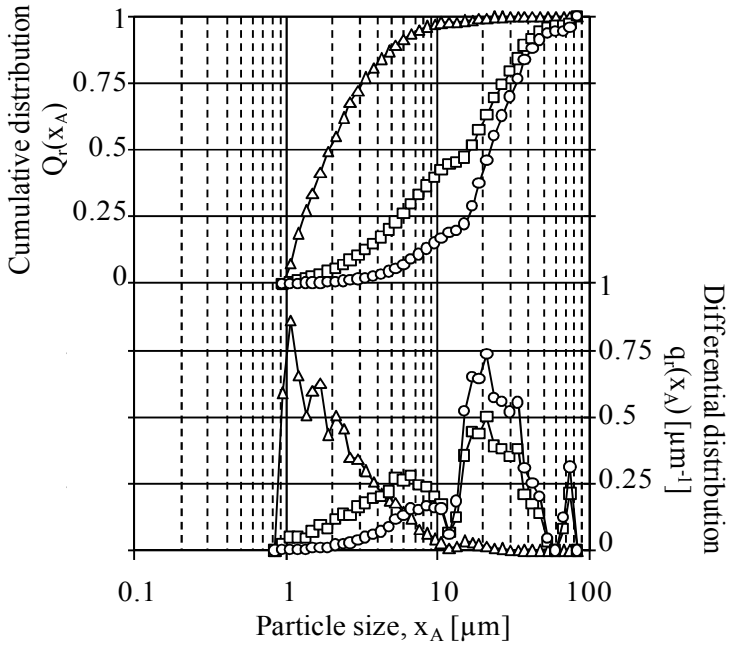

Figure A2-5. Sample Fosa 2. Cumulative (top) $Q_r(x_A)$ and density size distribution (bottom) $q_r(x_A)$ for droplets determined by optical microscopy. Number of particles counted: 92634. Combined magnification 5X+10X+20X. Sample thickness: 13.2 μm. (△) number: r = 0, (□) area: r = 2, (○) volume: r = 3

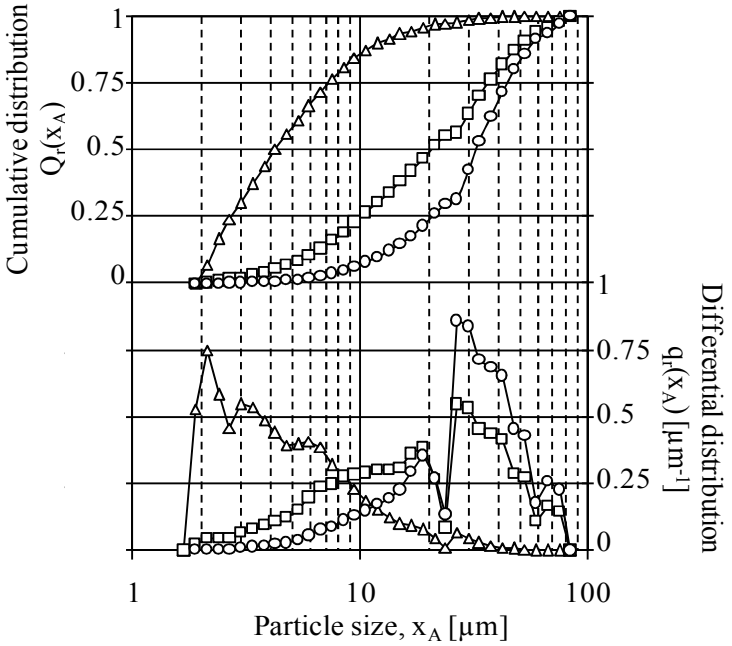

Figure A2-6. Sample Orocual. Cumulative (top) $Q_r(x_A)$ and density size distribution (bottom) $q_r(x_A)$ for droplets determined by optical microscopy. Number of particles counted: 28791. Combined magnification 5X+10X+20X. Sample thickness: 24.2 µm. (△) number: r = 0, (□) area: r = 2, (○) volume: r = 3

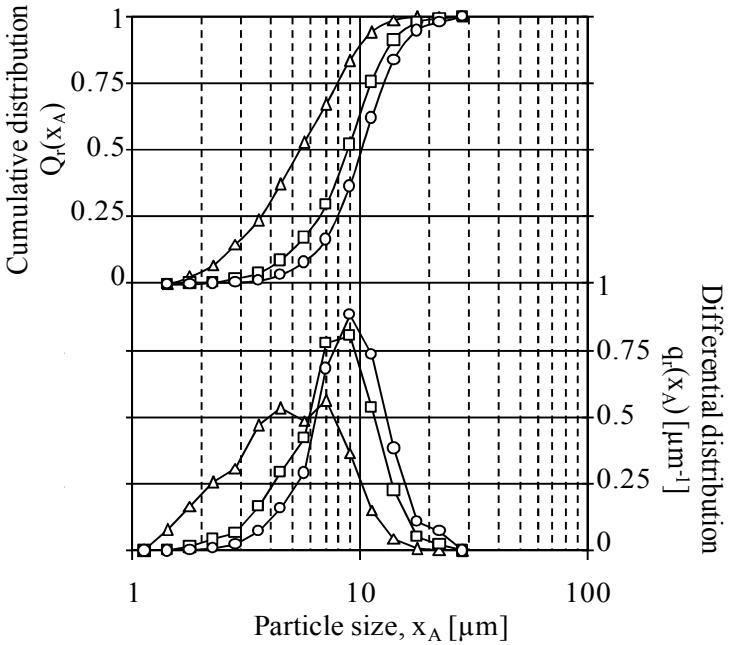

Figure A2-7. Sample Merey 31. Cumulative (top) $Q_r(x_A)$ and density size distribution (bottom) $q_r(x_A)$ for solids determined by optical microscopy. Number of particles counted: 2020. Combined magnification 5X+10X+20X. Sample thickness: 36.38 ± 4.94 µm. (△) number: r = 0, (□) area: r = 2, (○) volume: r = 3

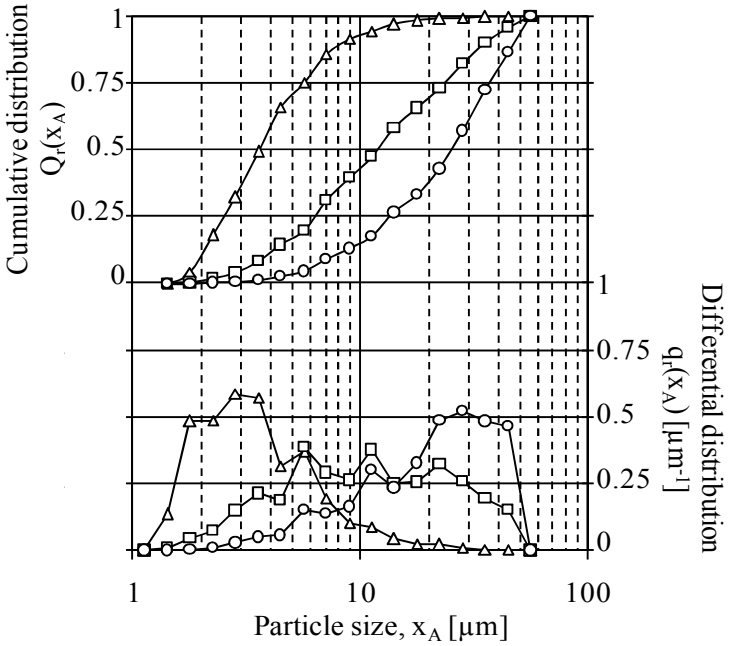

Figure A2-8. Sample Guara 2. Cumulative (top) $Q_r(x_A)$ and density size distribution (bottom) $q_r(x_A)$ for solids determined by optical microscopy. Number of particles counted: 1459. Combined magnification 5X+10X+20X. Sample thickness: 61.38 ± 18.44 µm. (△) number: r = 0, (□) area: r = 2, (○) volume: r = 3

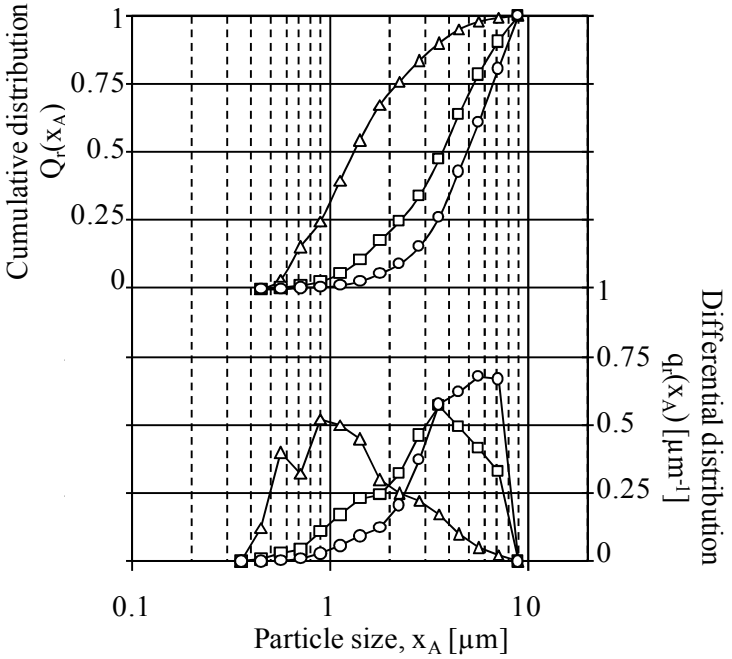

Figure A2-9. Sample Fosa 1. Cumulative (top) $Q_r(x_A)$ and density size distribution (bottom) $q_r(x_A)$ for solids determined by optical microscopy. Number of particles counted: 148. Combined magnification 5X+10X+20X. Sample thickness: 18.7 µm. (△) number: r = 0, (□) area: r = 2, (○) volume: r = 3

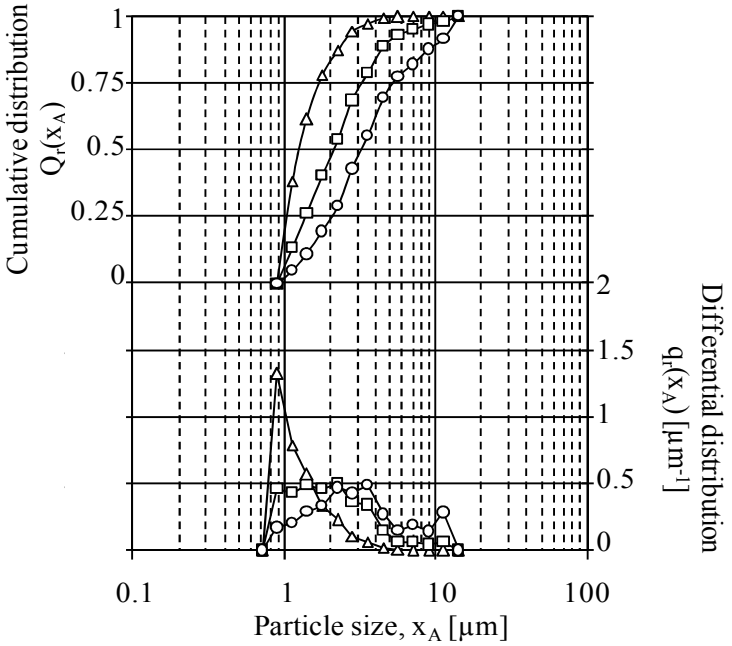

Figure A2-10. Sample Fosa 2. Cumulative (top) $Q_r(x_A)$ and density size distribution (bottom) $q_r(x_A)$ for solids determined by optical microscopy. Number of particles counted: 5162. Combined magnification 5X+10X+20X. Sample thickness: 13.2 μm. (△) number: r = 0, (□) area: r = 2, (○) volume: r = 3

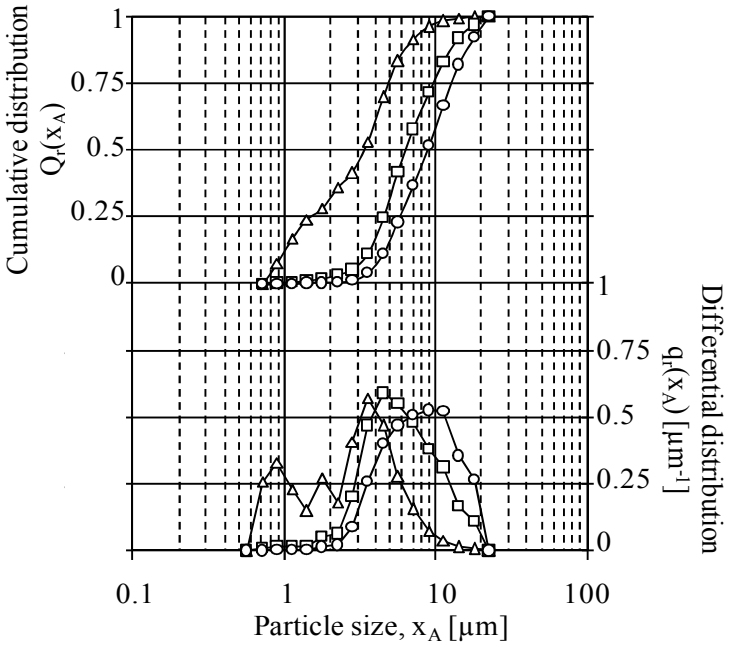

Figure A2-11. Sample Orocual. Cumulative (top) $Q_r(x_A)$ and density size distribution (bottom) $q_r(x_A)$ for solids determined by optical microscopy. Number of particles counted: 507. Combined magnification 5X+10X+20X. Sample thickness: 24.2 μm. (△) number: r = 0, (□) area: r = 2, (○) volume: r = 3

Appendix A3. Waste Oil Emulsions Water and Solids Content

Note 1: ASTM: water content by distillation ASTM D-4006 and solids content by extraction ASTM D-473.

Note 2: Droplets and solids in contact with the borders of the pictures were included.

Note 3: Water content determination include agglomerate discrimination and thickness correction.

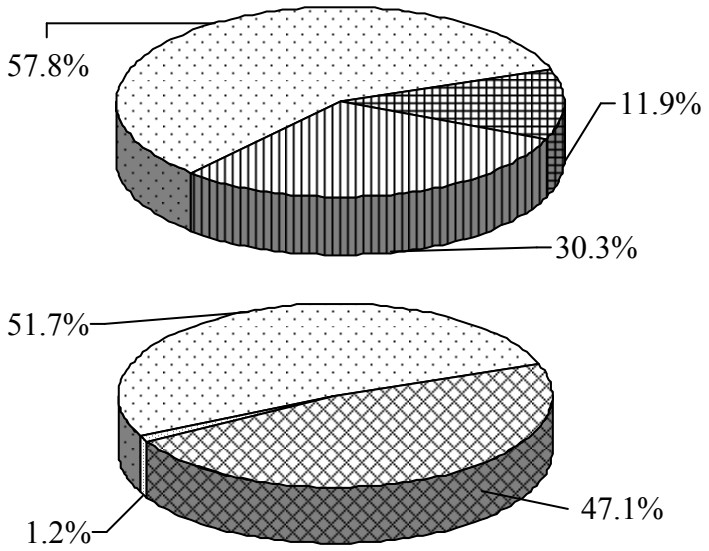

Figure A3-1. Sample Acema 100. Water and solids content (%) determination: comparison between ASTM (bottom) and microscopy (top) results. Microscopy: combined magnification 5X+10X+20X, sample thickness: 27.25 ± 7.12 μm. (▨) total water, (▮) solids, (□) crude oil, (▦) non agglomerated water, (▥) agglomerated water

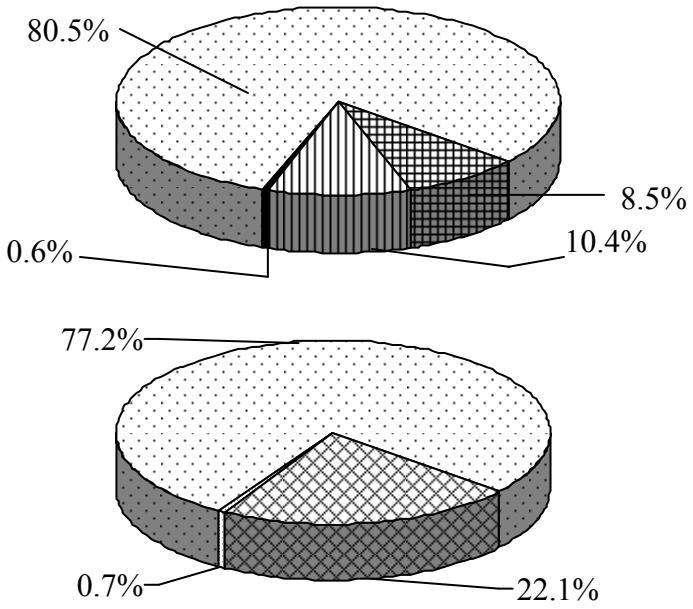

Figure A3-2. Sample Merey 31. Water and solids content (%) determination: comparison between ASTM (bottom) and microscopy (top) results. Microscopy: combined magnification 5X+10X+20X, sample thickness: 36.38 ± 4.94 μm. (▨) total water, (■) solids, (□) crude oil, (▦) non agglomerated water, (▥) agglomerated water

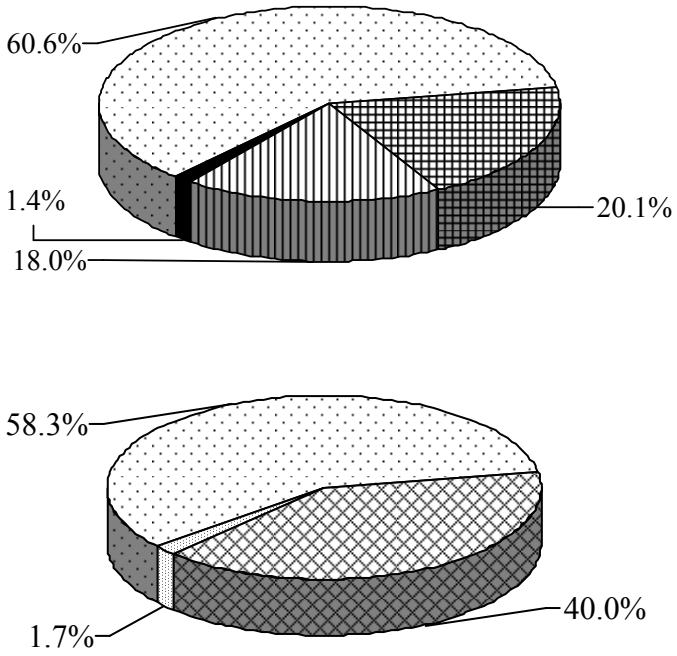

Figure A3-3. Sample Guara 2. Water and solids content (%) determination: comparison between ASTM (bottom) and microscopy (top) results. Microscopy: combined magnification 5X+10X+20X, sample thickness: 61.38 ± 18.44 μm. (▨) total water, (■) solids, (□) crude oil, (▦) non agglomerated water, (▥) agglomerated water

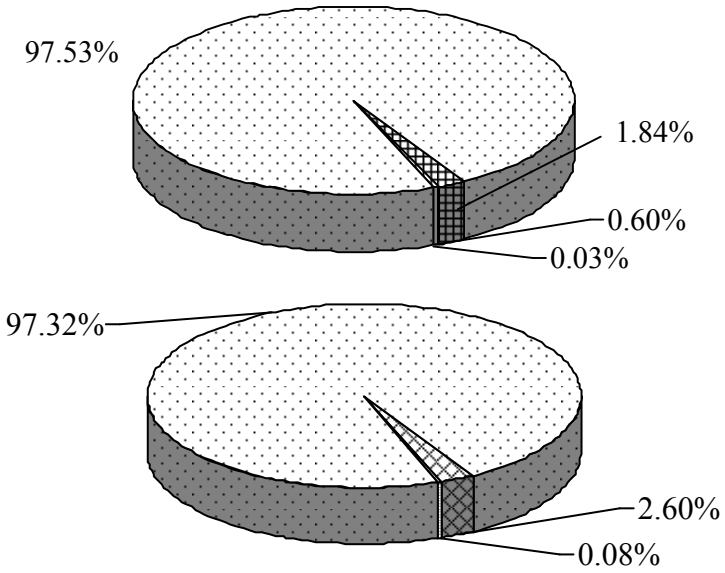

Figure A3-4. Sample Fosa 1. Water and solids content (%) determination: comparison between ASTM (bottom) and microscopy (top) results. Microscopy: combined magnification 5X+10X+20X, sample thickness: 18.7 μm. (▨) total water, (▮) solids, (□) crude oil, (▦) non agglomerated water, (▥) agglomerated water

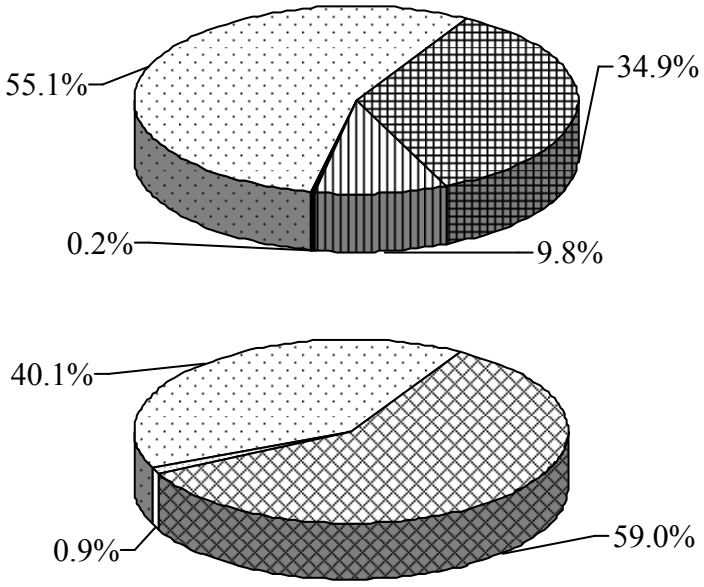

Figure A3-5. Sample Fosa 2. Water and solids content (%) determination: comparison between ASTM (bottom) and microscopy (top) results. Microscopy: combined magnification 5X+10X+20X, sample thickness: 13.2 μm. (▨) total water, (▮) solids, (□) crude oil, (▦) non agglomerated water, (▥) agglomerated water

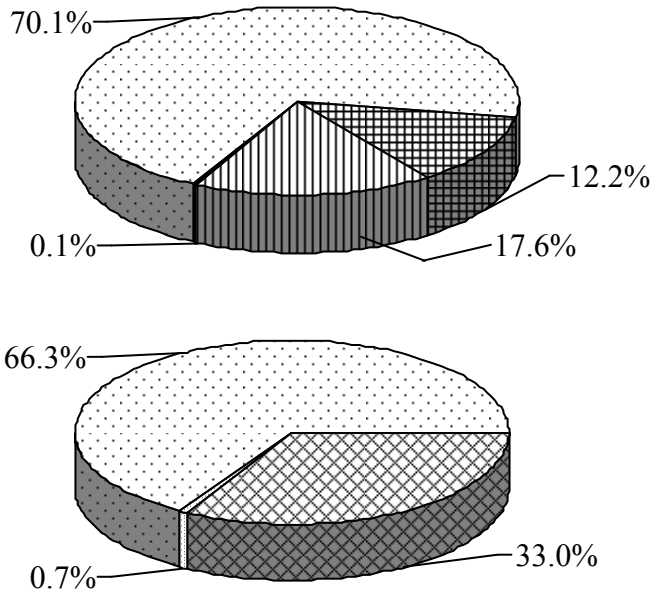

Figure A3-6. Sample Orocual. Water and solids content (%) determination: comparison between ASTM (bottom) and microscopy (top) results. Microscopy: combined magnification 5X+10X+20X, sample thickness: 24.2 μm. (▨) total water, (▮) solids, (□) crude oil, (▦) non agglomerated water, (▥) agglomerated water

Appendix A4. Cross-Linked Method Results

Note 1: Droplets and solids in contact with the borders of the pictures were included.

Note 2: Water content determination include agglomerate discrimination and thickness correction.

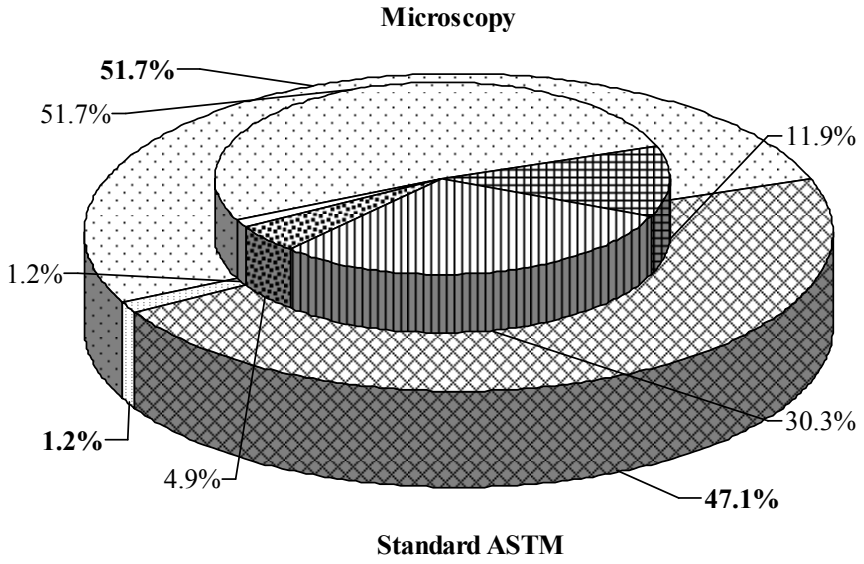

Figure A4-1. Sample Acema 100. Water, oil and solid phase volume ratio determined by cross-linked method. Microscopy (top): combined magnification 5X+10X+20X, sample thickness: 27.25 ± 7.12 μm, ASTM (bottom): water content by distillation ASTM D-4006 and solids content by extraction ASTM D-473. (▨) total water, (▮) solids, (□) crude oil, (▦) non agglomerated water, (▥) agglomerated water, (▩) non detected water, (□) non detected solids.

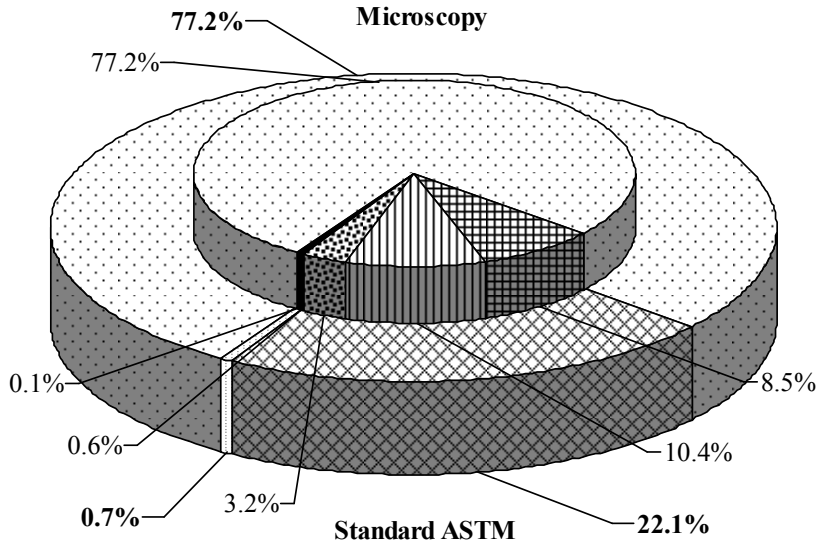

Figure A4-2. Sample Merey 31. Water, oil and solid phase volume ratio determined by cross-linked method. Microscopy (top): combined magnification 5X+10X+20X, sample thickness: 36.38 ± 4.94 μm. ASTM (bottom): water content by distillation ASTM D-4006 and solids content by extraction ASTM D-473. (▨) total water, (■) solids, (□) crude oil, (▦) non agglomerated water, (▥) agglomerated water, (▩) non detected water, (□) non detected solids

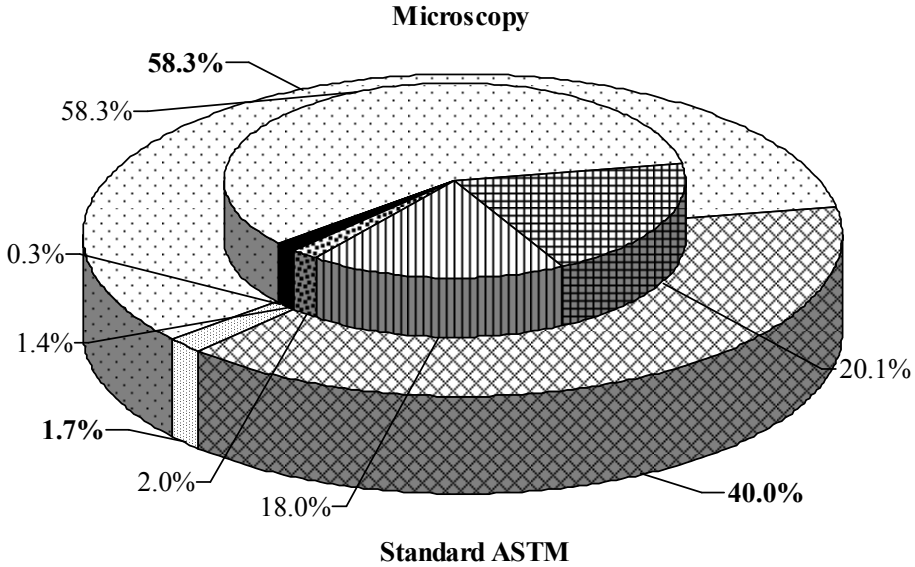

Figure A4-3. Sample Guara 2. Water, oil and solid phase volume ratio determined by cross-linked method. Microscopy (top): combined magnification 5X+10X+20X, sample thickness: 61.38 ± 18.44 μm. ASTM (bottom): water content by distillation ASTM D-4006 and solids content by extraction ASTM D-473. (▨) total water, (■) solids, (□) crude oil, (▦) non agglomerated water, (▥) agglomerated water, (▩) non detected water, (□) non detected solids

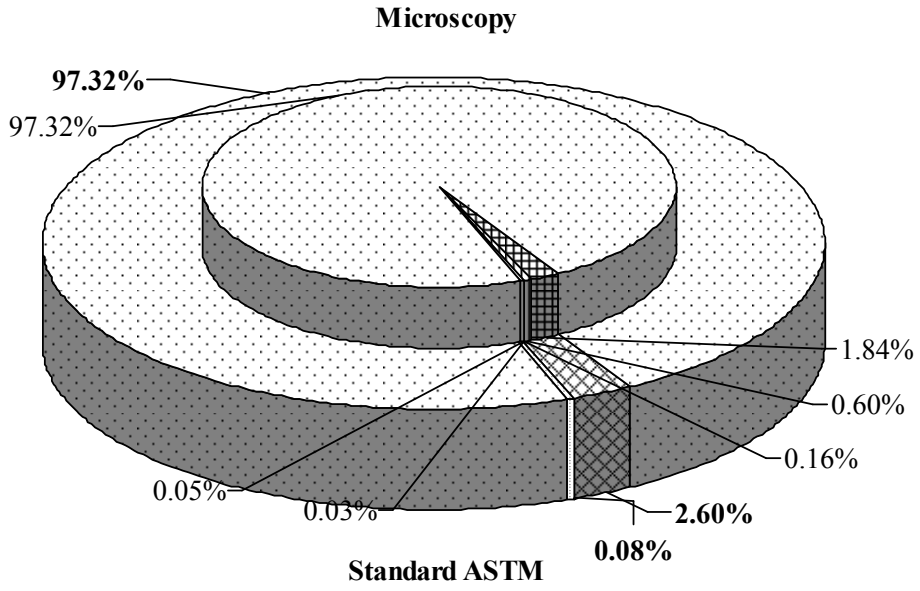

Figure A4-4. Sample Fosa 1. Water, oil and solid phase volume ratio determined by cross-linked method. Microscopy (top): combined magnification 5X+10X+20X, sample thickness: 18.7 μm. ASTM (bottom): water content by distillation ASTM D-4006 and solids content by extraction ASTM D-473. (▨) total water, (▮) solids, (□) crude oil, (▦) non agglomerated water, (▥) agglomerated water, (▩) non detected water, (□) non detected solids.

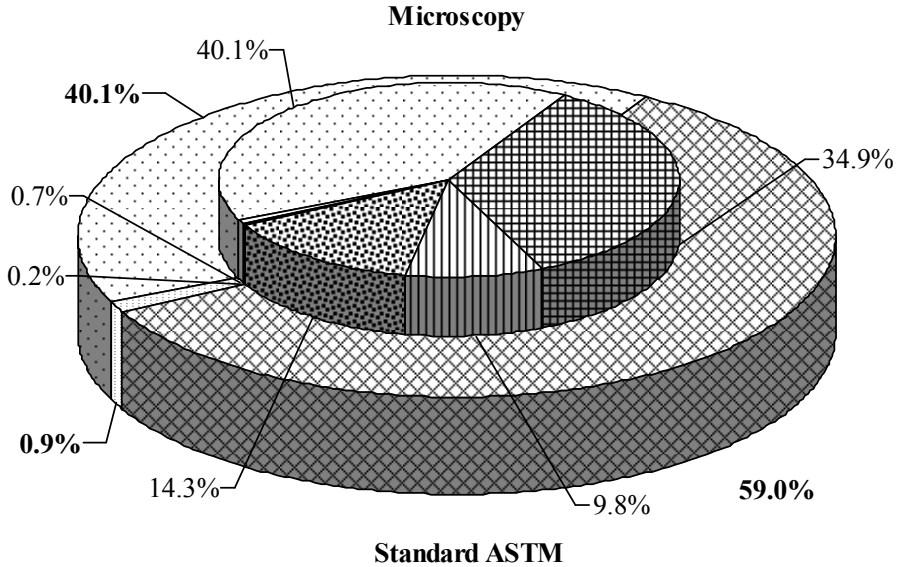

Figure A4-5. Sample Fosa 2. Water, oil and solid phase volume ratio determined by cross-linked method. Microscopy (top): combined magnification 5X+10X+20X, sample thickness: 13.2 μm. ASTM (bottom): water content by distillation ASTM D-4006 and solids content by extraction ASTM D-473. (▨) total water, (▮) solids, (□) crude oil, (▦) non agglomerated water, (▥) agglomerated water, (▩) non detected water, (□) non detected solids

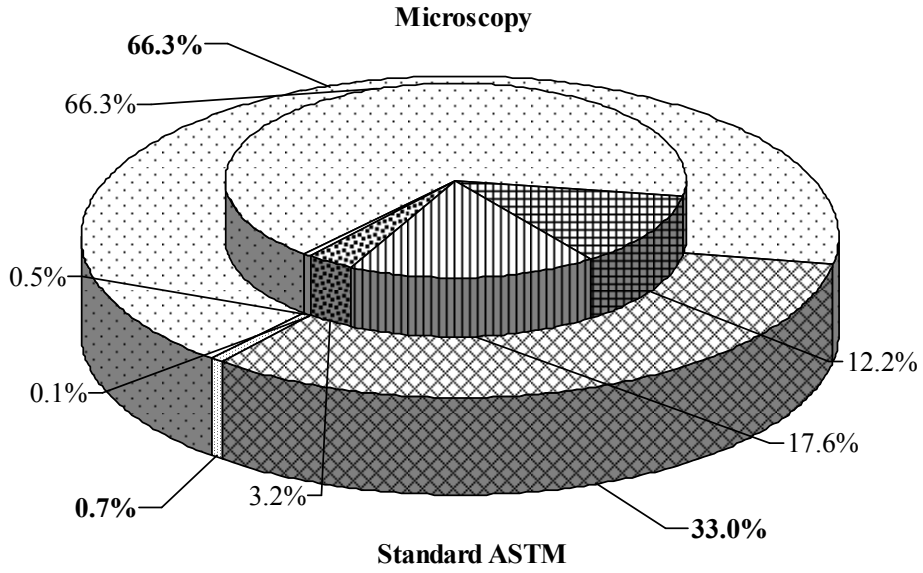

Figure A4-6. Sample Orocual. Water, oil and solid phase volume ratio determined by cross-linked method. Microscopy (top): combined magnification 5X+10X+20X, sample thickness: 24.2 μm. ASTM (bottom): water content by distillation ASTM D-4006 and solids content by extraction ASTM D-473. (▨) total water, (▮) solids, (□) crude oil, (▦) non agglomerated water, (▥) agglomerated water, (▩) non detected water, (□) non detected solids